LBL--32892

DE93 002551

The Synthesis and Structural Characterization of Novel Transition Metal Fluorides

William Jack Casteel, Jr.

Ph.D. Thesis

Lawrence Berkeley Laboratory

and

Department of Chemistry

University of California

Berkeley, California 94720 USA

September 1992

This work was supported by the Director, Office of Energy Research, Office of Basic Energy Sciences, Chemical Sciences Division of the U.S. Department of Energy under Contract No. DE - AC03 - 76SF00098

The Synthesis and Structural Characterization of Novel Transition Metal Fluorides

by

William Jack Casteel, Jr.

Abstract

High purity KMF_6 and K_2MF_6 salts (M = Mo, Re, Ru, Os, Ir, Pt) are obtained from reduction of the hexafluorides. A novel rhombohedral unit cell is observed for $KReF_6$, a_o = 5.021(3) Å, α = 97.16 °and a trigonal cell for K_2MoF_6, free of impurity phases for the first time, is observed with a_o = 5.860(2) Å, c_o = 4.634(3) Å.

Fluoride ion capture by Lewis acids from the hexafluorometallate (IV) salts affords high purity tetrafluorides for M = Mo, Re, Ru, Os, and Pd. The structure of RuF_4 is determined from a combination of X - ray synchrotron and neutron powder data. The structure is related to the layered SnF_4 type, however, a puckering of the sheets occurs in the monoclinic RuF_4 unit cell, a_o = 5.6068(6) Å, b_o = 4.9456(5) Å, c_o = 5.413(2) Å, β = 121.27(2) Å. Unit cells based on the orthorhombic PdF_4 type cell are derived from X - ray powder data for ReF_4; a_o = 9.61(2) Å, b_o = 9.61(2) Å, c = 5.66(1) Å and OsF_4; a_o = 9.89(1) Å, b_o = 9.36(1) Å, c_o = 5.70(1) Å.

Fluoride ion capture from $KAgF_4$ provides the thermally unstable trifluoride as a bright, red, diamagnetic solid. The structure solution of AgF_3 and the redetermination of the AuF_3 structure from X - ray synchrotron and neutron powder data demonstrate that the two are isostructural: AgF_3, a_o = 5.0782(2) Å, c = 15.4524(8) Å; AuF_3, a_o = 5.1508(1) Å, c_o = 16.2637(7) Å. The thermal decomposition product of AgF_3 is the mixed valence compound $Ag^{II}Ag_2^{III}F_8$.

Several new salts containing the $(Ag - F)_n^{n+}$ chain cation are prepared. The first linear $(Ag - F)_n^{n+}$ chain is observed in $AgF^+BF_4^-$ which crystallizes in a tetragonal unit cell with $a_o = 6.693(3)$ Å, $c_o = 4.004(3)$ Å. $AgFAuF_4$ has a triclinic unit cell with $a_o = 5.906(6)$ Å, $b_o = 4.769(5)$ Å, $c_o = 3.933(5)$ Å, $\alpha = 107.01(5)$ °, $\beta = 99.46(4)$ °, $\gamma = 90.75(4)$ ° and is isostructural with $CuFAuF_4$. $AgFAuF_6$ has an orthorhombic unit cell with $a_o = 7.600(4)$ Å, $b_o = 7.156(4)$ Å, $c_o = 10.137(5)$ Å and appears to be isostructural with $AgFAsF_6$. A second mixed valence silver fluoride, $Ag^{II}Ag^{III}F_5$, is prepared, which magnetic measurements indicate is probably an AgF^+ salt. Magnetic data for all of the AgF^+ salts exhibit low magnitude, temperature independent paramagnetism characteristic of metallic systems.

Cationic Ag(II) in acidic AHF solutions is demonstrated to be an exceedingly powerful oxidizer, capable of oxidizing Xe to Xe(II) and O_2 to O_2^+. Reactions with C_6F_6 and C_3F_6 suggest an electron capture mechanism for cationic Ag(II) oxidations.

To Mom and Dad

I love you

The Synthesis and Structural Characterization of Novel Transition Metal Fluorides

Table of Contents

List of Tables

List of Figures

Acknowledgements

I would like to thank Professor Neil Bartlett for his warm and patient guidance throughout the course of this work. I certainly have appreciated his genuine enthusiasm for chemistry, the creative insight and clarity that he brings to the untangling of difficult problems, as well as the good humor and grace that he has shown to me.

This work could not have been completed without the friendship and help of many gifted scientists and good people. I am indebted to Professor Boris Zemva for his creative input and technical assistance on the synthetic portion of this thesis, Dr. Angus Wilkinson for the structure determination of AgF_3 and RuF_4, and Dr. Horst Bormann for the structure determination of RuF_5 (Special thanks go to Angus and Horst for helping pass the time during a slow week at Los Alamos).

Because I have been here awhile, I must thank two "generations" of Bartlett students and post - docs. To Steve Mayorga, Mike Lerner, and Rika Hagiwara, who have since gone on: thank you for "showing me the ropes." To Byron Shen: thanks for your friendship and thoughtfulness throughout the entire time. To the youngsters, George Lucier and Lisa Chacon: Thanks for learning so quickly and being patient with a highly "entropic" senior grad student.

Additional thanks go to these people and to rest of the 5th floor Latimer family who provided many of the fond memories I'll take from this place. Truly, we had some "BIG" times.

A very special thanks goes to my friends in the Graduate and International Fellowship, particularly my housemates, for praying for me, building me up, and bringing me to the One who can help.

This work was supported by the U.S. Dept. of Energy under contract No. DE-AC03-76-SF00098 and supplemented over the last year by an IBM Fellowship.

Chapter 1

General Introduction

A broad range of simple binary and ternary transition metal fluorides have been synthesized in an effort to obtain structural data of sufficiently high quality to draw meaningful correlations between electronic configuration and molecular structure. Some of the materials of interest were of intermediate oxidation state and presented the synthetic problem of obtaining them free of other oxidation states. The synthetic schemes were also designed to ensure freedom from oxide since the similarity in size and X - Ray scattering power of O^{-2} and F^- has often in the past led to confusion of oxyfluorides with fluorides.[1] Chapter 2 describes a general anhydrous route to high purity hexafluorometallate salts. These salts, each containing the transition metal in a particular oxidation state and free of oxygen ligation were used as precursors in high purity binary fluoride synthesis. Higher precision unit cell data obtained from these salts provide also for the assessment of cation and anion effective volumes. Chapter 3 begins to compare structural data for the +3,4,5, and 6 oxidation state binary fluorides from groupV through VII, focusing, however, on the Ru - fluorides describing their high purity synthesis and details of their structure. Chapter 4 descibes structure types of the poorly characterized tetrafluorides and a general route to their synthesis exemplified by that of RuF_4.

The remainder of this work focuses on the high oxidation state chemistry of Ag(III) and Ag(II). Chapter 5 describes the synthesis and structural characterization of neutral AgF_3. The details of the structure are compared with AuF_3 and the oxidizing properties of the two are discussed. In Chapter 6, the synthesis of a variety of cationic Ag (II) materials including two mixed valence Ag(II)/Ag(III) fluorides is described and their

magnetic properties are discussed. Chapter 7 evaluates the oxidizing power of Ag(III) and cationic Ag(II).

General Experimental.

Apparatus: Vacuum Lines and Reactors. Reactions involving volatile materials were carried out in a stainless steel vacuum line constructed from 3/8 in. O.D. 316 stainless steel tubing, connected by Autoclave Engineers fittings and 30 VM series valves with vee stems rated to 30,000 psi (Autoclave Engineers, Corp, Erie, PA). A small teflon vacuum manifold consisting of teflon valves and 1/4" O.D. FEP Tubing(AIN plastics, Concord,CA) was attached to the main vacuum line for the manipulation of strongly acidic materials. The teflon valves were made in the college of chemistry machine shop to a design described below. The pressure was monitored with an Acco - Helicoid guage(Con Val, Fremont, CA) which has a range of 0-1500 Torr ± 0.25% and a Varian 801 Thermocouple guage (College of Chemistry Stores) for 0 -2000mTorr readings. A cylinder of F_2 (Air Products, Allentown, PA) was attached to the main vacuum line through Monel high pressure tubing and Monel Autocalve Engineers fittings and 30 VM valves rated to hangle 30,000 psi. A high pressure Helicoid guage (600psi) was fixed to this F_2 handling portion of the line to monitor pressures therein. A mechanical forepump was connected to the vacuum line through a Pyrex cold trap cooled to -196°C. The manifold could be evacuated directly, or through a soda-lime scrubber to dispose of F_2 and other volatile oxidative fluorinators, as well as fluoroacids such as anhydrous hydrogen fluoride (AHF) and BF_3. After passivation of the vacuum line with 2 atm F_2 for several hours, pressures of 10 - 50 mTorr were generally achieved upon evacuation.

The reaction vessels routinely used were of three types. Single armed reaction vessels consisting of a FEP tube sealed at one end and joined to a teflon valve and two

armed reactors consisting of two such FEP tubes, joined to a teflon valve by means of a teflon tee piece (Oakland Valve and Fitting, Concord, CA), were used for reactions involving liq AHF in which pressures would not exceed 2atm. FEP tubes were sealed by heating one end over a flame, pinching it shut with pliers when it had softened as signaled by increased transluscence. Teflon valves, Fig 1.1, consisted of a teflon valve body, a Kel - F stem containing an inserted teflon stem tip, and teflon packing washers, were designed so that the seat side of the valve which would be exposed to vapors from highly acidic oxidizing solutions could only come in contact with the teflon tip of the stem, while closed. The teflon packing nuts were pressed against the stem and valve body, to make a seal, by means of an additional aluminum packing washer and nut which could be screw tightened. Connections could be made to the inlet and outlet of the valve by means of 1/4" Swagelok fittings, or through 1/4" FEP tubing which could be sweated on to the knurled opening at the seat side of the valve.

For reactions at elevated temperatures, involving pressures of 5 to 20 atm Monel cans (100 and 250ml) equipped with SS 1KS4 Whitey valves (Oakland Valve and Fitting, Concord, CA) were employed. Copper gasketed Monel Parr bombs equipped with Autoclave Engineers VM30 valves were used when pressures greater than 20 atm were required.

Involatile, air - sensitive materials were handled in the dry Ar atmosphere of a Vacuum Atmospheres Corp. DRILAB. The atmosphere therein was kept rigorously dry by circulation through drying trains which were regenerated frequently. Freedom of the atmosphere from significant oxygen, or water contamination was judged by the burning of an incandescent filament for at least several days.

Reagents.

Anhydrous Hydrogen Fluoride (AHF): Anhydrous HF 98%, as obtained from Matheson, (Newark, CA) was reported to contain as much as 2% water. Rigorous drying of the HF was effected by condensing it on to dioxygenyl salts ($O_2^+SbF_6^-$, or $O_2^+Sb_2F_{11}^-$),[2] or K_2NiF_6 (Ozark - Mahoning - Pennwalt). These reagents oxidize water to ozone which was removed from the AHF by successive freeze - pump - thaw cycles.

The commonly used reagent gases BF_3 (Matheson, Newark, CA), PF_5, and AsF_5 (Ozark - Mahoning - Pennwalt, Tulsa, OK) were each checked before use by I.R. spectroscopy[3] and when found to be free of major volatile impurities were used without further purification. The much less volatile liquids BrF_3 (Matheson) and SbF_5 (Ozark - Mahoning) were generally distilled out of their cylinders directly into reaction vessels. Bromine usually accompanied BrF_3 distillation, however, since this served as a useful diluent and was a byproduct of BrF_3 oxidations, further purification was unnecessary. When small amounts of volatile O_2SbF_6 impurity in the SbF_5 could not be tolerated, it was removed by exposing the distilled SbF_5 to C_6F_6 (PCR, Gainesville, FL) which was oxidized to $C_6F_6^+$ by any O_2^+ present.[4] At one point it was necessary to prepare our own AsF_5. This was accomplished by burning As metal in liq. F_2 at -196°C in a high pressure Monel bomb.

Characterization:

Powder Diffraction: Debye - Scherrer photographs were taken on General Electric Precision Powder cameras (45cm circumference) using Ni filtered, CuK<α> radiation. Powder samples for X - Ray photographs were loaded into 0.3 or 0.5 mm diameter quartz capillaries (Charles Supper Co., Natick, MA) inside the DRILAB and temporarily sealed

with KEL - F grease (Halocarbon Product Corp., N. Augusta, SC). The capillaries were finally sealed outside the DRILAB by drawing down using a micro-torch.

Refinement of Debye - Scherrer data was accomplished using the program, CELLREF.[5]

Vibrational Spectroscopy: Infrared Spectra were measured on a Nicolet 5DX Fourier Transform Spectrophotometer. Volatile materials were expanded into a 10cm length Monel cell fitted with AgCl windows and a Whitey valve. Usually pressures of 10 - 25 Torr were employed.

Magnetic Measurements: Variable temperature magnetic susceptibility data were collected on SQUID magnetometers manufactured by S.H.E. Corp. and Quantum Dynamics. Samples were held in cylindrical containers made in the College of Chemistry machine shop. These containers consisted of two Kel - F halves, one fitting inside the other. Usually the seperate halves were passivated with 2 atm of a F_2/AsF_5, or F_2/BF_3 mixture overnight before use. Inside the DRILAB a known quantitiy of material was packed into the smaller half of the container using a Kel - F packing tool which had been through the same passivation as the container. The two halves of the container were pressed together, being sealed with a small amount of Kel - F grease. Typically measurements were taken at 5 and 40 kG between 6 K and 280 K.

References

1. Chamberland, B.L. "Crystal Chemistry of Oxyfluorides," *Inorganic Solid Fluorides,* p. 208, P.Hagenmuller, ed., Academic Press, Orlando, FL, 1985.
2. McKee, D.E.; Bartlett, N. *Inorg. Chem.* **1973**, *12*, 2738.
3. Nakamoto, K. "Infrared Spectra of Inorganic and Coordination Compounds," Wiley, New York, 1963.
4. Richardson, T.J.; Tanzella, F.L.; Bartlett, N. *J. Am. Chem. Soc.* **1986**, *108*, 4937.
5. CELLREF - "A least squares program to refine unit cell parameters from hkl, 2θ."

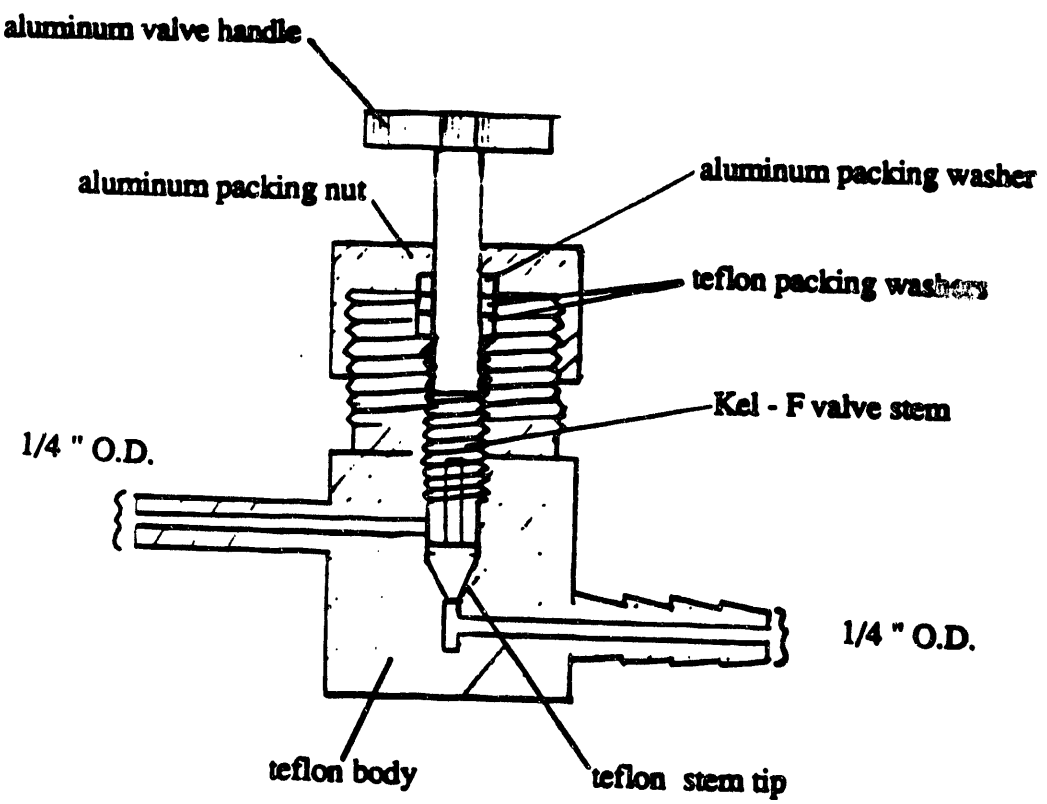

Figure 1.1 Teflon valve schematic

Chapter 2

The Preparation of Second and Third Transition Series KMF_6 and K_2MF_6 Salts from the Hexafluorides

Introduction.

A new, general method for synthesizing binary fluorides from fluorometallate precursors was discovered recently in these laboratories.[1] Some consequences of this discovery will be discussed in chapters 3,4, and 5. The successful synthesis of high purity binary fluorides by this method requires high purity fluorometallate salts which are free of oxide contamination as well as contamination by other oxidation states. This is particularly true for the synthesis of a binary fluoride in an intermediate oxidation state and this is commonly the case for tetrafluorides of second and third transition series elements from group V through VIII. In addition previous syntheses have not rigorously avoided oxygen. Instances of this are the preparation of K_2RuF_6 [2], K_2OsF_6,[3] and K_2IrF_6[3] by the reduction of the KMF_6 salt with water, or hydroxide. In all cases, some hydrolysis was observed. Furthermore,the precursor KMF_6 salts, as well as K_2PtF_6,[4] have often been made using BrF_3 in glass vessels. This has been shown to lead to oxide contamination.[5]

A non aqueous route[6] to K_2MoF_6 involved reduction of the hexafluoride with excess KI in SO_2, but the products were acknowledged to contain a mixture of oxidation states. Therefore, a new approach to the synthesis of K_2MoF_6 was also required. This and several other MF_6^- and MF_6^{-2} salts have been prepared in high purity.

Experimental.

Reagents: Prior to use KBr and KI(Fisher, Fair Lawn, NJ) were dried by heating to 200°C under a vacuum of 10^{-8} Torr. Hexafluorides were prepared by direct interaction of the

metal(previously reduced with hydrogen at 450°C) with an excess of fluorine at 250° in a monel can.

Preparation of KMF_6 Salts (M = Mo, Re, Os, and Ir). In the DRILAB, KBr(usually 1.5g, 13mmol) was loaded into a 1/2" O.D. FEP tube equipped with a KS4 Whitey valve. The reactor was degassed under dynamic vacuum(better than 0.05 Torr) and a slight excess of the hexafluoride, MF_6, was condensed on to the KBr, followed by 7ml AHF. As the HF began to melt Br_2 evolution and vigorous gas evolution were observed. Agitation of the reaction mixture was begun to help insure contact between the hexafluoride in solution and any HBr gas which may have formed on interaction of the HF with KBr, and was continued for 30min until all gas evolution had ceased and the mixture, which had become slightly warm, had cooled to room temperature. Bromine and HF were removed from the voluminous precipitate under dynamic vacuum leaving, the KMF_6 salt in quantitative yield. X - Ray powder data of each salt were indexed.That for $KReF_6$ revealed a novel rhombohedral unit cell and is given in Table 2.1. The unit cells for the other salts were roughly in accord with earlier reports.[7,8]

Table 2.1. X - Ray powder data (CuK<α> radiation, Ni filter) for $KReF_6$ with a rhombohedral cell: $a_o = 5.021(3)$Å; $\alpha = 97.16(4)°$; $V = 122.7(3)$Å^3.

	$1/d^2 \times 10^4$ Å^{-2}		
I/I_o[a]	**obsd**	**calc**	**hkl**
9	414	413	010
9	718	708	$0\bar{1}0$
8	937	943	110
7	1130	1121	$1\bar{1}1$
7	1657	1651	$0\bar{2}0$
4	1843	1829	$1\bar{2}0$
6	2146	2124	$1\bar{2}1$
6	2289	2298	210
10	2370	2359	$2\bar{1}1$

Table 2.1. cont.

	$1/d^2 \times 10^4$		
I/I	**obsd**	**calc**	**hkl**
6	2860	2832	$2\bar{2}0$
6	3045	3063	211
6.5	3266	3245	$2\bar{2}1$
7	3724	3714	$0\bar{3}0$
7	3793	3771	220
		3775	$1\bar{3}0$
--	----	4422	$3\bar{1}1$
9	4470	4479	310
		4483	$2\bar{2}2$
3	4690	4653	221
		4661	$2\bar{3}0$
5	5000	4956	$2\bar{3}1$
4	5207	5191	$3\bar{2}1$
2	5329	5361	311
4	5890	5895	$3\bar{1}2$
3	6423	6360	222
		6372	$3\bar{3}0$
4	6565	6546	$1\bar{4}0$
4	6640	6603	$0\bar{4}0$
		6607	$1\bar{4}1$
3	6818	6785	$3\bar{3}1$
4	7014	7068	321

[a] intensities estimated visually

Preparation of K_2MF_6 Salts (M = Mo, Re, Os, and Ir). In the DRILAB 1:1 mixtures (usually 5mmol) of KMF_6 and KI were loaded into one arm of a two armed teflon-FEP reactor. A red discoloration due to the formation of a small amount of I_2 was observed upon contact of the solid reagents. The reactor was degassed in a dynamic vacuum , the arm containing the reactants being cooled to avoid transferring I_2 into the stainless steel vacuum line. AHF (10ml) was condensed on to the reactants. On melting of the HF copious I_2 formation was observed, along with some gas evolution. Agitation of the reactor was maintained until the mixture had warmed to room temperature and was continued intermittantly over the next hour. At this time a solid precipitate of I_2 was

observed in a colored solution, the color being dependent upon the MF_6^{2-} anion in solution. The readily soluble K_2MF_6 salt was easily separated from the insoluble I_2 by decantation of the HF solution into the free arm of the reactor. Back distillation of the HF into the original reaction arm followed by decantation was repeated (usually 5 times) until a colorless solution remained above the I_2. After the last back distillation , the HF over the I_2 was frozen at -196°C. The reactor was filled with dry N_2 (1atm), and the arm containing the K_2MF_6 was sealed with a screw clamp. This arm was removed from the reactor, fitted to a Whitey valve, and attatched to the stainless steel vacuum line for final drying under dynamic vacuum. Quantitative yields of K_2MF_6 salts were obtained. The X-Ray powder data for each salt was indexed completely on the basis of a trigonal K_2GeF_6 type cell,[9] that for the K_2MoF_6 salt being observed for the first time, Table 2.2

Preparation of K_2RuF_6 and K_2PtF_6. In the DRILAB 1:1 mixtures of KMF_6 (made from the pentafluoride and KF in AHF) and KBr were loaded into a one armed FEP reactor fitted with a Whitey valve. The reactor was degassed under dynamic vacuum, and 5ml AHF was condensed on to the solid reagents. Immediately upon melting, Br_2 evolution and vigorous gas evolution were observed. The reactor was agitated intermittantly as the reaction warmed to room temperature and for 30min thereafter. A dark brown solution and red Br_2 vapor resulted. Removing the HF and Br_2 under dynamic vacuum gave quantitative yields of K_2RuF_6 and K_2PtF_6. X - Ray powder data for each material was indexed completely on the basis of a trigonal K_2GeF_6 type cell.

Reaction of WF_6 with KBr. The reaction was performed identically to the general KMF_6 salt preparation, however only 0.5576g (4.69mmol) KBr was used with an excess of WF_6. After degassing under dynamic vacuum 5ml AHF was condensed on to the reactants. On melting, vigorous gas evolution and Br_2 evolution were observed as with

other KMF_6 preparations. However, on cessation of gas evolution, the increase in the volume of solid product was considerably less than expected for KWF_6 formation. After removing the HF and Br_2 only 0.7487g products were obtained. X - Ray powder photographs revealed the presence of KHF_2 in addition to KWF_6.

Table 2.2. X - Ray powder data (CuK<α>, Ni filtered radiation) for K_2MoF_6 with a trigonal cell; a_o = 5.860(2)Å, c_o = 4.634(3)Å.

	$1/d^2 \times 10^4$		
I/I_0	**obsd**	**calc**	**hkl**
6	388	388	100
4	464	466	001
9	852	854	101
7	1159	1165	110
-	-	1553	200
2	1627	1631	111
-	-	1863	002
10	2015	2019	201
6	2253	2251	102
-	-	2718	210
-	-	3028	112
6	3169	3184	211
7	3402	3416	202
3	3482	3495	300
-	-	4191	003
4	4580	4580	103,212
4	4654	4659	220
-	-	5048	310
-	-	5125	221
4	5366	5357	113,302
4	5525	5513	311
2	5730	5744	203
-	-	6212	400
-	-	6522	222
2	6673	6678	401
3	6920	6910	213,312
-	-	7377	320
2	7687	7686	303
3	7851	7843	321

Preparation of KWF_6. In the DRILAB usually 800mg (5mmol) KI was loaded into one arm of a two armed teflon reactor. After evacuation on the vacuum line,an excess of WF_6, usually 10mmol, was condensed onto the KI. On warming to room temperature the liquid WF_6 took on a blood red color. AHF (5ml) was condensed on to this reaction mixture. As the reactor was warmed to room temperature, vigorous gas evolution ensued. During this time and for thirty minutes after all gas evolution had ceased, the reactor was intermittantly agitated. On standing, dark red insoluble I_2 remained in a colorless solution. A soluble colorless product was washed into the other arm of the reactor by decantation. The process of back distillating the AHF into the original reaction arm at -196°C, followed by decantation into the second arm was repeated 10 times to effect complete separation of the product from I_2. Finally all AHF was condensed into the reaction arm containing the I_2. The arm containing the colorless product was sealed with a screw clamp and fitted to a Whitey valve on the vacuum line for thorough removal of AHF under dynamic vacuum. The colorless KWF_6, obtained quantitatively, gave X - Ray powder data which was indexed completely on the basis of a tetragonal unit cell appropriate for KWF_6.[10]

Results and Discussion.

Synthesis of K_2MF_6 salts from hexafluorides, MF_6, has been achieved by the two step reduction process in AHF:

$$MF_6 + KBr \xrightarrow{AHF} KMF_6 + 1/2Br_2 \qquad (1)$$

$$KMF_6 + KI \xrightarrow{AHF} K_2MF_6 + 1/2\, I_2 \qquad (2)$$

The use of iodide alone as the reducing agent for the preparation MF_6^{-2} had been shown to produce mixtures of oxidation states by Edwards in the synthesis of K_2MoF_6 even when a 1:2 stoichiometry of hexafluoride to iodide was rigorously maintained. The source of the problem probably lies in the ability of the hexafluorides, all aggressive oxidizing agents, to oxidize I^- beyond I_2 to iodine fluorides, thus complicating the reaction and making the determination of stoichiometry difficult. The MF_6^- salts do not appear to oxidize I^- beyond I_2 thereby avoiding the difficulties of a complex reaction.

A hexafluoride, in slight excess, was reduced by KBr in AHF to give a high purity, microcrystalline KMF_6 salt. The isolated salt was then reduced in a separate step by one equivalent of KI, also in HF. KMF_6(M = Mo, Re, Os, and Ir) have been prepared by reaction 1. The rhombohedral form $KReF_6$ (Table 2.1), observed here for the first time, indicates a close structural relationship to the later elements of the third transition series. A tetragonal cell was previously reported.[11] A rhombohedral cell is adopted by all later third row transition series KMF_6 salts. However, a transition to a tetragonal cell, in which the fluorine and potassium atoms are no longer close packed, is observed in KWF_6 and $KMoF_6$; therefore it is possible that $KReF_6$ is dimorphic.

Because of the difficulty in obtaining the thermally unstable hexafluorides, RuF_6 and PtF_6, their KMF_6 salts were obtained by interaction of the pentafluorides with KF. The preparation of K_2MF_6 (M = Mo, Re, Os, and Ir) has been achieved by reaction 2. X-ray powder data for K_2MoF_6, which has been obtained in crystallographically pure form for the first time, are given in Table 2.2.

The oxidizing power of the hexafluorides, the MF_6^- salts, and the MF_6^{-2} salts is expected to increase across each transition series as the effective nuclear charge increases. This is clearly seen in the synthetic work. In general bromide ion reduces M(VI) fluorides to M(V), eq.1, with the more powerfully reducing iodide ion being required to reduce M(V) completely to M(IV). However, there are exceptions. Bromide will not completely

reduce W(VI) to W(V) as judged by the formation of KHF_2 in the WF_6/KBr reaction and the resulting poor yield of KWF_6. Iodide was required to bring about the complete reduction. Among the later transition metals, Ru(V) and Pt(V) reduction to M(IV) fluorides is easily affected by Br^- ion. This increase in oxidizing power across a transition series is the result of the increasing electronegativity of the metal center arising from the ineffective shielding of increasing nuclear charge by antibonding π electrons. A similar increase in shielding of the nucleus down a group, on moving to higher d shells, results in the decreasing oxidizing power and increased difficulty in reduction observed.

Interaction of AHF with alkali-metal halides produces the alkali-metal fluoride and the corresponding hydrogen halide according to the solvolysis reaction[12]

$$AX + HF \longrightarrow HX + AF \qquad (3)$$

A sharp increase in pressure above the vapor pressure of HF was observed when reactions 1 and 2 were run without agitation, indicating that some solvolysis to volatile, HF insoluble HBr and HI was occuring. Furthermore, if the pressure was reduced to the HF vapor pressure by evacuation, reactions 1 and 2 failed to go to completion, instead producing large quantities of KHF_2 along with the intended product. Thus the sparingly soluble HBr and HI are important reducing species in these reactions along with Br^- and I^-. A two step process, involving a one electron reduction followed by the attack of the fluorobase KF, must therefore complement reactions 1 and 2

$$MF_6 + HBr \xrightarrow{AHF} MF_5 + 1/2\,Br_2 + HF \qquad (4)$$

$$MF_6^- + HI \xrightarrow{AHF} MF_5^- + 1/2I_2 + HF \qquad (5)$$

$$K_nMF_5^{n-} + KF \xrightarrow{AHF} K_{n+1}MF_6^{(n+1)-} \qquad (6)$$

where n = 0 or 1

The low solubility of Br_2 and I_2 in AHF lowers their activity and contributes to the effectiveness of the reduction. The reducing capability of HBr and HI in AHF as expressed in equations 5 and 6 suggests that they may be useful in the synthesis of lower oxidation state binary fluorides.

The ready synthesis of high purity, microcrystalline KMF_6 and K_2MF_6 salts has afforded the opportunity of evaluating the lattice constants and formula unit volumes of these salts to higher precision (Table 2.3). As expected, a decrease in formula unit volumes from early to late transition metals is observed. Again this can be accounted for on the basis of the increasing electronegativity of the metal center. This effect must counter that of filling the t_{2g}^*, antibonding π orbitals, which increase electron density on the F ligand away from the nucleus. It is apparent, however, that this decrease in volume is not monotonic, but is itself, decreasing. Evidently, as the effective volume of the metal center decreases, F ligand - F ligand repulsion becomes more important.

Because the rhombohedral KMF_6 salts and the trigonal K_2MF_6 salts both consist of close packed layers of fluorine and potassium atoms with the metal occupying octahedral holes, it is anticipated that the difference in formula unit volumes will roughly measure the volume of the potassium cation. However such an estimate assumes no volume difference between the MF_6^- and the MF_6^{2-} anions. Due to the increased electron density on the fluorine atoms of the MF_6^{2-} anion, this anion must be larger than MF_6^-. The difference in volume, ΔV, of the M(V) and M(IV) salts of $\approx 14.7 Å^3$ (shown in Table 2.3) is contant within experimental error across the third transition series, and is signicantly larger than the volume of $13.3 Å^3$ calculated from Pauling's radii.[13] This difference, perhaps signifies the difference in anion sizes and indicates that the dianion is probably no more than 1.5 $Å^3$ larger than the monoanion.

Table 2.3. A Comparison of Lattice Parameters and Unit Cell Volumes for Some Close-packed Hexafluorometallate Salts

	Re	Os	Ir	Pt[14,15]	Ru
KMF_6 a_o(Å)	5.012(4)	4.987(1)	4.9744(7)	4.96	4.968(1)
KMF_6 α(°)	97.15(4)	97.18(1)	97.399(9)	97.4	97.40(1)
KMF_6 V(Å^3)	122.7(3)	120.8(1)	119.72(5)	118.7	119.3(1)
K_2MF_6 a_o(Å)	5.852(2)	5.824(2)	5.798(2)	5.76	5.755(2)
K_2MF_6 c_o(Å)	4.594(3)	4.617(2)	4.617(2)	4.64	4.657(4)
K_2MF_6 V(Å^3)	137.4(2)	135.6(2)	134.4(2)	133.3	133.6(2)
ΔV(Å^3)	14.7	14.8	14.7	14.7	14.3

References

1. Žemva, B; Lutar, K.; Jesih, A.; Casteel, W.J.; Bartlett, N. *J. Chem. Soc., Chem. Commun.* **1989**, 346.
2. Hepworth, M.A.; Peacock, R.D.; Robinson, P.L. *J. Chem. Soc.* **1954**, 4835.
3. Hepworth, M.A.; Robinson, P.L.; Westland, G.J. *J. Chem. Soc.* **1958,** 611.
4. Sharpe, A.G.; *J. Chem. Soc.* **1950**, 3444.
5. Holloway, J.H.; Peacock, R.D. *J. Chem. Soc.* **1963**, 527.
6. Edwards, A.J.; Steventon, B.R. *J. Chem. Soc., Dalton Trans.* **1977**, 1860.
7. Hargreaves, R.; Peacock, R.D. *J. Chem. Soc.* **1957**, 4212.
8. Hepworth, M.A.; Jack, K.H.; Westland, G.J. *J. Inorg. Nucl. Chem.* **1956,** *2*, 79.
9. Hoard, J.L.; Vincent, W.B. *J. Am. Chem. Soc.* **1939**, *61*, 2849.
10. Kemmitt, R.D.; Russell, D.R.; Sharp, D.W.A. *J. Chem. Soc.*, **1956,**
11. Peacock, R.D.; *J. Chem. Soc.* **1957**, 407.
12. Glemser, O. *J. Fluorine Chem.* **1986**, *33*, 50.
13. Pauling, L. "The Nature of the Chemical Bond," p.514, Cornell University Press, Ithaca, NY, **1960**.
14. Bartlett, N.; Lohmann, D.H. *J. Chem. Soc.* **1964**, 619.
15. Mellor, D.P.; Stephenson, N.C. *Australian J. Sci. Res.* **1951**, *4A*, 406

Chapter 3

Preparation and Structure of Ruthenium Tetrafluoride and a Structural Comparison with Ruthenium Trifluoride and Ruthenium Pentafluoride

Introduction.

A large body of structural information exists for the transition metal binary fluorides and a number of generalizations can be made.[1,2] With the exception of seven coordinate ReF_7 and the group III and IV transition metals which prefer eight coordination, the binary fluorides maintain at least roughly octahedral coordination of six fluorine ligands. This octahedron can be distorted quite severely if e^*_g σ antibonding orbitals are populated, and d^8 systems such as AuF_3 are more often thought of as square planer complexes.[3] However, when these orbitals are left vacant as they are in the second and third transition series from group V through VIII distortions from octahedral symmetry are relatively minor. Those distortions that do occur, result because all systems in these series with oxidation state lower than the +6 of the monomeric hexafluorides must involve F ligands in M - F - M bridging to maintain 6 coordination. The pentafluorides involve 2 fluorine ligands in bridging and form either tetramers, or chain polymers. Tetrafluorides must involve 4 F ligands in bridging to remain 6 - coordinate and are known to form 2 - D and 3 - D polymers. Regular octahedral geometry is again observed for the trifluorides which involve all 6 F ligands in bridging. Only symmetric M - F - M bridges have been observed, indicating that the shared F ligands in bridging systems are equivalently held by the two involved metal centers.

A remarkable feature of the structural data is the apparent uniformity of metal fluorine interatomic distances from group V through VIII in the second and third transition series. The interatomic distance in the M-F_{unique} bond is always ≈1.80Å, while M - $F_{bridging}$ interatomic distances are ≈2.00Å regardless of the metal center and oxidation state. Subtle differences show up when more precise structures can be compared, but even these differences are surprising. In the rhodium fluorides precise M - $F_{bridging}$ interatomic bond distances are known for the pentafluoride[4] and trifluoride[5], averaging 2.000(3)Å and 1.961(2)Å respectively. The lower oxidation state which contains more t_{2g}^* antibonding electrons appears to make shorter M - F bonds! Data for NbF_5 and NbF_3, while of lower precision,[6,7] indicate nearly identical M - $F_{bridging}$ interatomic distances , as well. Unfortunately a complete set of high precision data for all the oxidation states of a given metal has not been available to allow firm conclusions to be drawn. An effort was made, therefore, to acquire such a data base.

The binary fluorides of ruthenium suggested themselves as a good set for further evaluation. As a second row transition metal, the possibility of obtaining high precision bond lengths from X-ray data was much greater than for one of the heavier third row metals. A high precision strucure of RuF_3 had already been obtained.[8] It appeared that the pentafluoride structure,[9] although of low quality, could readily be redetermined to high precision and would offer valuable comparisons with the well defined RhF_5 structure. Existing structural information on impure samples of the tetrafluoride suggested that it exhibited a new structure type for the tetrafluorides. In addition, the hexafluoride of Ru is also known and although it is of limited thermal stability, it is known to be octahedral.[10] Gas electron diffraction studies could give a highly precise M - F_{unique} interatomic distance.

The repeated failures[9,11] to achieve a highly precise structure for RuF_5 calls attention to a significant problem in undertaking such a structural study, that being the possibility of oxide contamination. The oxide ligand is practically indistinguishable from F^- by X-rays, or neutrons, but its presence can result in dramatically altered "M - F" bond distances. Even the third structure determination of RuF_5 is unacceptably imprecise. It is nearly certain that the first crystal to be examined contained some dissolved $RuOF_4$, this being subsequently shown as a co-product with RuF_5 in the BrF_3 oxidation of Ru in glass containers.[12] Jack and his coworkers[8] reported variable lattice parameters, for different samples of RuF_3 and this, being prepared from reduction of RuF_5 made in the above manner, is likewise probably a consequence of oxide contamination. Therefore a reinvestigation of the RuF_3 structure was also warranted.

An even greater challenge was involved in the synthesis of pure RuF_4. Previous attempts at its synthesis by the reduction of higher fluorides have resulted in inseparable mixtures of the tetrafluoride, trifluoride, and Ru metal.[13] This is a common problem in the synthesis of polymeric binary fluorides of intermediate oxidation state. It was expected that a structure determination of RuF_4 would require powder diffraction methods, the likelihood of obtaining single crystals being small. Therefore, a high purity synthesis of RuF_4 was essential.

Experimental.

Reagents. Powdered ruthenium, supplied by Alfa Products, Thiokol, Danvers, MA 01923, was reduced in hydrogen at 450°C for 6h and stored in the DRILAB prior to use.

RuF_5 Preparation. In the DRILAB 300mg of Ru powder was loaded into a small nickel vessel and placed into a 250ml Monel can reactor which had been passivated with 4atm of F_2 at 250°C for 24h. The can was fitted with a valved lid, which could be cooled during the experiment, and evacuated to better than 10^{-2} Torr on a stainless steel vacuum line. After pressurizing the can to 4atm with F_2, the can was heated to 250°C and held at this temperature for 24h, the lid being cooled with cold water. On cooling the can to room temperature, the remaining F_2 was evacuated through a glass U-trap, cooled to -196°C, into a soda-lime scrubber. A small amount of red-brown RuF_6 was collected in the U-trap. The can was opened in the DRILAB. revealing waxy, lime-green RuF_5 on the lid and cooler portions of the can. For crystal growth, the RuF_5 was loaded into a flame-dried, 0.25 in o.d. Pyrex tube, which was cooled in liquid N_2 and then sealed off under a vacuum of 10^{-8} Torr. The tube containing the RuF_5 was set up vertically and the bottom heated to 65°C. Crystals suitable for X-ray studies were grown by Dr. Horst Bormann by sublimation over several days. Selected crystals were inserted into nominally 0.3 mm capillaries which had been drawn down further to provide for the tight fit of such small crystals. The structure refinement was performed by Dr. Horst Bormann and details of the refinement are given in ref. 14.

RuF_5 Structure. The structure is no different, qualitatively, from that derived originally by Holloway and his coworkers.[9] It consists of tetrameric units closely-packed such that the F ligand arrangement is almost that of a hexagonal-close-packed array. The greater precision now attained clearly differentiates the bridge Ru-F interatomic distances from the non-bridging and accurately defines the coordination sphere about each Ru atom. The distances and angles of chemical interest are given in Table 3.1. Fig. 3.1 illustrates the

tetramer geometry, with Ru-F interatomic distances and Ru-F-Ru bridging angles specified.

Table 3.1. Interatomic Distances and Bond Angles in $(RuF_5)_4$

Interatomic Distances (in Angstrom Units)

Atom 1	Atom 2	Distance	Atom 1	Atom 2	Distance
Ru1	F1	1.798(1)	Ru2	F5	2.007(1)
Ru1	F2	1.793(1)	Ru2	F6	2.003(1)
Ru1	F3	1.821(1)	Ru2	F7	1.795(1)
Ru1	F4	1.817(1)	Ru2	F8	1.823(1)
Ru1	F5	1.995(1)	Ru2	F9	1.796(1)
Ru1	F6	1.999(1)	Ru2	F10	1.824(1)

Angles (in Degrees)

F1 - Ru1 - F2	93.99(6)	F5 - Ru2 - F6	86.20(4)
F1 - Ru1 - F3	92.36(6)	F5 - Ru2 - F7	175.67(5)
F1 - Ru1 - F4	92.04(6)	F5 - Ru2 - F8	87.83(5)
F1 - Ru1 - F5	175.50(6)	F5 - Ru2 - F9	90.21(5)
F1 - Ru1 - F6'	89.08(5)	F5 - Ru2 - F10	87.30(6)
F2 - Ru1 - F3	92.12(6)	F6 - Ru2 - F7	89.51(5)
F2 - Ru1 - F4	92.47(6)	F6 - Ru2 - F8	88.00(5)
F2 - Ru1 - F5	90.51(5)	F6 - Ru2 - F9	176.41(5)
F2 - Ru1 - F6'	176.93(5)	F6 - Ru2 - F10	87.54(5)
F3 - Ru1 - F4	173.40(6)	F7 - Ru2 - F8	92.62(6)
F3 - Ru1 - F5	87.54(5)	F7 - Ru2 - F9	94.08(6)
F3 - Ru1 - F6'	87.61(5)	F7 - Ru2 - F10	91.93(6)
F4 - Ru1 - F5	87.68(5)	F8 - Ru2 - F9	92.00(6)
F4 - Ru1 - F6'	87.55(5)	F8 - Ru2 - F10	173.60(5)
F5 - Ru1 - F6'	86.42(4)	F9 - Ru2 - F10	92.16(6)
Ru1 - F5 - Ru2	140.83(6)	Ru2 - F6 - Ru1'	136.80(6)

It is seen that the six F ligands about each Ru atom are in approximately octahedral array a *cis* pair of F atoms being each shared with another Ru atom, such linkages forming the tetrameric ring. The bridging Ru-F distances range from 1.995(1) to 2.007(1)Å, these

being barely significantly different from 2.000Å. The Ru - F - Ru bridges are bent, as in the other ideally hcp pentafluorides, creating the puckered ring shown. The symmetry of the cell allows for two the different bridging angles of 136.80(6)° for the bridges which point into the tetrameric unit and 140.83(6)° for those pointing away from this unit.

The non-bridging Ru-F distances are geometrically classified into two significantly different sets. Those non-bridging Ru-F *trans* to the bridges are shorter than those perpendicular to the plane containing each Ru atom and its bridging F ligands. The distances for the former range from 1.793(1) to 1.798(1)Å, whereas the latter values span 1.817(1) to 1.824(1)Å. There are slight but significant departures from an octahedral framework, the non-bridging Ru-F *trans* to the bridges subtending an angle at the Ru atom significantly greater than 90°, the pair of bridging F atoms subtending an angle correspondingly less than 90°. In addition the non-bridging F atoms normal to the plane, defined by the Ru atom and its bridging F ligands, are displaced slightly along the bisector of the angle subtended by the Ru-F bridging atoms. These angle deformations and displacements are consistent with ligand-ligand repulsive interactions, those associated with the shortest Ru-F being strongest and those with the longest Ru-F (the bridging distances) being weakest.

Preparation of RuF_4. In the DRILAB 600mg(2mmol) was loaded into one arm of a teflon tee apparatus. The reactor was evacuated through a teflon manifold connected to the main stainless steel vacuum line and 5ml AHF was condensed on to the solid K_2RuF_6. The solid completely dissolved at room temperature giving a golden solution. To the solution, AsF_5 was slowly admitted (slow addition giving a more crystalline product) resulting in the immediate formation of a deep-pink precipitate, and was continued until the precipitate in a colorless solution remained. To facilitate removal of the $KAsF_6$

formed as a side product in the reaction, the AsF_5 rich AHF was removed under vacuum and 5ml of pure were condensed back on to the solid mixture. The insoluble RuF_4 was washed free of $KAsF_6$ by decantation into the free arm of the reactor, followed by back distillation, under static vacuum, into the arm of the reactor containing the RuF_4. This process was repeated 10 times, a cloudiness of the AHF above the RuF_4 usually signalling that the material was free of $KAsF_6$.

Although PF_5 proved to be ineffective in forming RuF_4, it giving rise to a dark brown solution (probably of RuF_5^-) and KPF_6, it was useful in combination with AsF_5, the product being somewhat more crystalline than with AsF_5 alone. For this procedure, the solution of K_2RuF_6 was first treated with PF_5 until no further uptake was observed, AsF_5 then being introduced with agitation for several hours. The solid was washed as above leaving on evacuation, homogeneous deep-pink RuF_4. To analyze the pink solid, it was decomposed in aqueous sodium hydroxide, F^- in the filtrate being determined as PbClF. Decomposition of of a sample in steam at 300°C followed by reduction in hydrogen at 450°C gave the metal. Anal. Found: F, 42.1; Ru, 57.7. Calcd for RuF_4 : F, 42.9; Ru, 57.1. X - Ray powder patterns of the RuF_4 prepared in this way proved to be the same as those of the RuF_4 phase present in the product of the reduction of $(RuF_5)_4$ with Ru metal or RuF_3.

Structure of RuF_4. Data Collection. Synchrotron powder X-Ray diffraction data were collected by Drs. David Cox and Angus Wilkinson on a sample of RuF_4 contained in a 0.5mm diameter quartz capillary using beam line X7A at Brookhaven National Laboratory (details in Table 3.2). Additionally, time-of-flight powder neutron diffraction data were collected on approximately 50mg of material contained in a 2-mm diameter quartz capillary using the high-intensity powder diffractometer (HIPD) at Los Alamos National

Laboratory.[15] The availability of instruments such as HIPD, with very high neutron flux and medium resolution, allows the study of small samples , such as those required for work in special environments or where there are sample handling and synthesis difficulties. The neutron data were collected for 20 hours with the source operating at a proton current of 90 mA. Normally a period of 1-2 hours would be used for the collection of data from a much larger sample (typically 5-10g of material), consequently the present data is of considerably lower statistical quality than that usually obtained.

Table 3.2. RuF_4 X-Ray Synchrotron Data Collection

Instrument Employed	Brookhaven National Laboratory National Synchrotron Light Source Beam Line X7A
Sample	RuF_4 contained in a 0.5mm Diameter Quartz Capillary
Wavelength	λ = 1.24805Å from a Si(111) channel cut monochromator
Diffraction Geometry	Debye-Scherrer, with a 0.55mm receiving slit 70cm from the sample
Data Range	13.0° to 58.4° in 0.04° steps with 64 contributing reflections

The Bragg peaks resulting from the main phase in the powder X-Ray pattern had a FWHM of at least 0.24°. The peaks due to the presence of a small amount of $KAsF_6$ were considerably sharper and were comparable with the instrumental resolution (approximately 0.09°). The first 16 peak positions in the X-Ray data excluding those from $KAsF_6$ were located precisely using a least squares fitting procedure and were used as input for the auto indexing program TREOR.[16] The best solution was a monoclinic cell with a_o = 5.614(1) Å, b_o = 4.9508(7) Å, c_o = 5.414(1) Å, ß = 121.41(2)°, M_{16} = 49 (Ref 17) giving Z = 2. The observed systematic absences were consistent with the space

group $P2_1/n$, but a space group could not be unambiguously assigned due to the small range of well resolved data. The program GSAS[18] was used for further analysis. The Ru atoms were assigned to a special position in the space group $P2_1/n$ and the fluorine atoms located in a Fourier difference map. The resulting model was then refined using the Rietveld method[19] to give a chemically plausible structure, but a poor fit to the diffraction pattern. A more crystalline RuF_4 sample containing less $KAsF_6$ impurity was prepared for the neutron diffraction work using PF_5 in combination with AsF_5 (q.v. preparation). Neutron diffraction data were collected using this sample.

The X-Ray structural model was used as a starting point for the time-of flight powder neutron diffraction data. This analysis employed the data collected on the +153°, -153° and -90° banks of the instrument HIPD, the resolution of the lower angle banks being too low to warrant inclusion in the refinement. The count rate in the +90° bank appeared to be anomalously low hence these data were excluded from the refinement. A refinement using a cosine Fourier series background was performed but did not produce a satisfactory background fit. Subsequently the background was modeled assuming that it contained a contribution due to scattering from an amorphous component, the resulting fit was improved but the refined background parameters had no physical significance. An unrestrained refinement including all positional parameters and isotropic temperature factors was initially performed. A second refinement which included restraints on the Ru - F distances (bridging Ru-F distance 2.00Å and terminal Ru-F distance 1.82Å) was then carried out. The results of both refinements are given in Table 3.3 and the interatomic distances and angles are given in Table 3.4 for comparison. The fitted neutron time of flight powder diffraction data are shown in Fig. 3.2. There is no significant difference in the quality of the fit for either of these models as judged by the profile R factors, but the R_F's (the normal crystallographic R factors) appear to be significantly lower for the

restrained model. The slightly better compatibility of the diffraction data, with the restrained model, is also evident from the lower esd's on the co-ordinates and bond lengths from that refinement.

Table 3.3. A Comparison of the Restrained (r) and Unrestrained (u) Refinements of the Structural Models for RuF_4 in Space Group $P2_1/n$

a_o =5.6068(6)Å, b_o = 4.9456(5)Å, c_o = 5.413(2)Å, ß = 121.27(2)°

R factors	R_{wp}	R_p	R_F	
-90°bank (including 233 reflections)	4.53%	2.81%	5.06%	u
	4.54%	2.81%	4.90%	r
+153°bank (including 630 reflections)	3.12%	2.14%	17.20%	u
	3.13%	2.14%	15.25%	r
-153°bank (including 629 reflections)	3.42%	2.33%	14.26%	u
	3.43%	2.34%	13.31%	r

overall X^2 = 1.388 for the free refinement and 1.397 for the restrained refinement.

	x	y	z	$100xU_{iso}$	
Ru(1)	0.0	0.0	0.0	1.98(9)	u
				2.02(9)	r
F(1)	0.8662(24)	0.1523(11)	0.2231(10)	2.0(1)	u
	0.8762(10)	0.1498(9)	0.2212(8)	1.6(1)	r
F(2)	0.3636(24)	0.1674(9)	0.2485(10)	1.7(1)	u
	0.3736(6)	0.1696(6)	0.2509(8)	1.8(1)	r

Table 3.4. Interatomic Distances (Å units) and Angles (deg.) in RuF_4

	Model	
	unrestrained	restrained
2 x Ru(1) - F(1)	1.88(2)	1.82(1)
2 x Ru(1) - F(2)	1.95(3)	2.00(3)
2 x Ru(1) - F(2)	2.02(1)	2.00(1)
F(1) - Ru(1) - F(2)	89.4(6)	89.7(6)
F(1) - Ru(1) - F(2)	88.2(4)	89.3(2)
F(2) - Ru(1) - F(2)	89.2(12)	90.3(12)
F(1) - Ru(1) - F(2)	90.6(6)	90.3(6)
F(1) - Ru(1) - F(2)	91.8(4)	90.7(2)
F(2) - Ru(1) - F(2)	90.8(12)	89.7(12)
Ru(1) - F(2) - Ru(1)	134.9(8)	133.0(6)

The observed Debye Scherrer data together with relative intensities calculated for the restrained model are given in Table 3.5 and the structure is illustrated in Fig. 3.3.

Table 3.5 X-Ray powder data (CuK<α> radiation, Ni filter) for the RuF_4 monoclinic unit cell indexed based on the unit cell parameters from the neutron diffraction data with $a_o = 5.6068(6)$, $b_o = 4.9456(5)$, $c_o = 5.413(2)$Å, $\beta = 121.27(2)°$, V=128.3Å^3, Z=2, space group $P2_1/n$.

		$1/d^2 \times 10^4$		
I/I_0	Icalc	obs	calc	h k l
vs	100	430	434	1 0 $\bar{1}$
vs	0	840	843	1 1 $\bar{1}$
	83		844	1 1 0
vs	81	877	876	0 1 1
m	22	1374	1371	1 0 1

Table 3.5. cont.

I/I_0	Icalc	obs	calc	h k l
w	7	1640	1635	0 2 0
w	11	1675	1681	2 1 $\bar{1}$
s	11	1739	1738	2 0 $\bar{2}$
	14		1741	2 0 0
ms	24	1774	1776	1 1 $\bar{2}$
	0		1779	1 1 1
vvw	1	1869	1868	0 0 2
m	19	2053	2070	1 2 $\bar{1}$
	0		2071	1 2 0
m	9	2095	2102	0 2 1
m	8	2146	2146	2 1 $\bar{2}$
	8		2150	2 1 0
---	0	---	2277	0 1 2
---	0	---	2907	2 2 $\bar{1}$
ms	0	2999	2978	3 0 $\bar{2}$
	6		2981	3 0 $\bar{1}$
	0		3003	1 2 $\bar{2}$
	13		3006	1 2 1
vvw	4	3240	3235	1 0 $\bar{3}$
s(br)	11	3391	3372	2 2 $\bar{2}$
	10		3377	2 2 0
	9		3387	3 1 $\bar{2}$
	0		3390	3 1 $\bar{1}$
m	15	3503	3504	0 2 2
s(br)	17	3656	3546	2 1 $\bar{3}$
	17		3554	2 1 1
w	0	3656	3644	1 1 $\bar{3}$
	9		3649	1 1 2

RuF_3 Structure: High purity, oxide free RuF_3 was prepared at Princeton University in 1969 by Mr.Robert Serfass from the reductive thermal decomposition of $SF_3^+RuF_6^-$. Details are given in Ref. 14. X-Ray powder diffraction photographs of this material using

LiF monochromatized CuK<α> radiation were sharp and of low background. The patterns were indexed completely on the basis of a rhombohedral cell (see Table 3.6) and refinement yielded unit cell parameters with a_o = 5.4098(4)Å, α = 54.67(1)° . Jack and his coworkers[8] had observed a range of lattice parameters in various preparations of RuF_3. Ultimately they settled on the largest cell parameters, a_o = 5.408±0.001Å, α = 54.67±0.01° as indicative of pure RuF_3. These are not significantly smaller than those obtained from the pyrolysis of $SF_3^+RuF_6^-$. The relative line intensities obtained here from the X - Ray photographs of the material prepared by Serfass, were not significantly different from those given by Jack and his coworkers. Applying the positional parameter found by Jack and his coworkers (x = -0.100, for which 3σ is ± 0.005) to their cell, the Ru-F interatomic distance is 1.981(6)Å. With the cell parameters found in this work Ru-F = 1.982(6)Å. The Ru-F-Ru bridging angle found here is 136(1)°.

Table 3.6. X-Ray powder data (CuK<α> radiation, LiF monochromator) for RuF_3 with a rhombohedral unit cell with a = 5.4098(4)Å, α = 54.68(1)°, V = 98.08Å^3, Z = 2, space group $R\bar{3}c$.

	$1/d^2 \times 10^4$		
I/I_0	obs	calc	h k l
10	757	751	1 1 0
6.5	1400	1385	2 1 1
4	1635	1620	1 0 $\bar{1}$
1	1920	1902	2 2 2
4	2114	2095	2 0 1*†
5	2389	2371	2 0 0
5	3030	3005	2 2 0
10	3545	3522	3 2 1
---	---	3833	2 0 $\bar{1}$*
4	3945	3921	3 3 2
6	4015	3991	2 1 $\bar{1}$
6	4650	4625	3 1 0

Table 3.6. cont.

I/I_0	obs	calc	h k l
6	4877	4860	2 $\bar{1}$ $\bar{1}$
---	---	5100	3 2 0*
4	5554	5541	4 2 2
4	5842	5822	4 3 3
1	5937	5898	4 3 2*†
---	---	6368	4 2 1*
3	6492	6480	2 0 $\bar{2}$
3	6778	6761	3 3 0, 4 1 1
1	6974	6955	3 1 $\bar{1}$*†
---	---	7073	2 $\bar{2}$ 1*
6	7183	7160	4 3 1
6	7240	7231	3 0 $\bar{1}$
4	7447	7442	4 4 2
3	7610	7606	4 4 4
5	7864	7865	3 2 $\bar{1}$
---	----	8340	4 1 0*
6	8384	8381	4 2 0
3	8829	8851	2 2 $\bar{2}$
4	9057	9062	5 3 2
4	9226	9226	5 4 3
3	9491	9485	4 0 0
---	---	9608	4 3 0*
---	---	10171	5 4 2*
---	---	10313	3 0 $\bar{2}$*
5	10400	10400	5 2 1
4	10479	10471	3 1 $\bar{2}$
---	---	10758	5 3 1*†
3	10900	10893	5 5 4
4	11106	11105	4 1 $\bar{1}$
4	11346	11340	3 $\bar{2}$ $\bar{1}$
---	---	11580	4 2 $\bar{1}$
1	11817	11815	3 2 $\bar{2}$, 4 0 $\bar{1}$*†
3	12030	12020	4 4 0
5	12292	12302	5 4 1
7	12475	12466	6 3 3, 5 5 2
---	---	12513	6 4 4
---	---	12707	6 4 3*

Table 3.6. cont.

I/I_0	obs	calc	h k l
---	---	12848	5 2 0*
10	13243	13241	4 3 $\bar{1}$, 5 1 0
---	---	13411	6 3 2*
---	---	13505	6 5 4*†
7	13647	13640	5 3 0
---	---	13711	$\bar{4}$ 1 1
5	13933	13922	6 2 2
6	14125	14133	6 5 3
4	14348	14345	3 3 $\bar{2}$
5	14579	14580	3 0 $\bar{3}$
---	---	15055	4 $\bar{2}$ 1*†
6	15328	15331	4 0 $\bar{2}$
6	15543	15542	6 3 1
---	---	15618	5 4 0*†
5	15697	15679	6 6 4
---	---	15947	6 5 2*
6	15964	15965	4 $\bar{2}$ 2
---	---	16440	5 $\bar{1}$ 1*
5	16477	16481	5 2 $\bar{1}$

* These are fluorine-only reflections ($h + k + l$, odd)

† Fluorine only reflections for which $h + k + l = 3(2n+1)$

Results and Discussion:

The synthesis of high purity RuF_4 has been achieved by fluoride ion capture from a hexafluorometallate (IV) salt using a strong acid:

$$K_2RuF_6 + 2AsF_5 \xrightarrow{AHF} RuF_4\downarrow + 2KAsF_6 \qquad (1)$$

The reaction, while certainly facilitated by the low solubility of RuF_4, must primarily be driven by the greater acidity of AsF_5 than RuF_4 in AHF. This is implied by rapid completion of the reaction(seconds with agitation)when using AsF_5 compared with the inability of the weaker acid, PF_5, to carry out the displacement of RuF_4. The production of KPF_6 from the interaction of PF_5 with K_2RuF_6, however, indicates that PF_5 is sufficiently strong to abstract F^- from RuF_6^{-2}. Use of PF_5 in conjunction with AsF_5:

$$2\,K_{(solv)}^{+} + RuF_6^{-2} + PF_5 \xrightarrow{AHF} \text{"}RuF_5^{-}\text{"sol'n} + KPF_6 + K^{+}_{(solv)}$$

$$+$$

$$RuF_4 + PF_5 + 2KAsF_6 \xleftarrow{AHF} 2AsF_5$$

resulted in a slower reaction and more crystalline samples of RuF_4. It may be that the less soluble PF_5 displaced from KPF_6 in step 2 simply acts as a barrier gas, slowing AsF_5 uptake.

X - ray synchrotron data from samples obtained by this two step process allowed for unambiguous determination of the unit cell. However, the final structure determination was based on a knowledge of the RuF_5 and RuF_3 structures. It is therefore useful to examine the results of these structures first.

The determination of bond lengths and angles in RuF_5 to high precision, combined with the confirmation of the RuF_3 structure enabled a meaningful comparison of the two. Both the tetrameric RuF_5 and the 3 -D polymeric RuF_3. arrange their fluorine ligands in a nearly hexagonal closed packed array, as do their rhodium counterparts. The similarities of the structures are clearly seen in Fig. 3.4. For an atom occupying an octahedral hole in an hcp network, the ideal bridging angle is 132°. The RhF_5 M - F - M bridging angles = 134.4(1)° and 135.7(1)° and those of RhF_3 = 132°. These are significantly closer to the ideal bridging angle of 132 ° for hcp than the analogous ruthenium compounds in which M - F - M ∠ = 136.80(6)°, and 140.83(6)° for the pentafluoride and 136(1)° for the trifluoride.

The angle of the M - F - M bridges can be correlated with the increased population of t_{2g}^* antibonding π orbitals. Increase in t_{2g}^* population can account for the decrease in bridging angle from Ru to Rh. In d^3 RuF_5 a single electron is in each of the t_{2g}^* orbitals (these orbitals are actually split by the slight distortion from octahedral symmetry caused by having two types of F ligands), hence a single electron fills the orbital in the plane containing the two M - $F_{bridging}$. The d^4 RhF_5 must pair electrons in one of the "t_{2g}^*" orbitals and they must do so in the orbital in the plane containing the bridging F ligands, this orbital being lowest in energy. Complete filling of this orbital effectively shuts down any π bonding interaction allowing the minimum angle for hcp to be approached. A similar situation exists for the trifluorides. The low spin d^6 configuration pertaining in RhF_3 fills each of the π antibonding orbitals, effectively quenching any π interaction and accounting for the almost ideal hexagonal close packing observed in that fluoride. One fewer electron is placed in the orbitals involved in the six bridges of RuF_3, allowing for a slightly increased bridging angle.

The greatly improved precision of the interatomic distances in RuF_5 also allows for useful comparisons. In RuF_5, the M - $F_{bridging}$ interatomic distances range from 1.995(1)Å to 2.007(1)Å. This is longer, although perhaps not significantly so, than the Ru - $F_{bridging}$ interatomic distance of 1.982(6)Å observed in RuF_3. Considering the increase in the antibonding π electron population from Ru(V) to Ru(III), this is quite remarkable. Yet this is not an isolated case. Morrell et. al.[6] found Rh - $F_{bridging}$ interatomic distances to range from 1.993(4)Å to 2.005(3)Å in their structure of RhF_5. This is significantly longer than the 1.961(2)Å Rh - $F_{bridging}$ distance observed by Grosse and Hoppe in their single crystal structure of RhF_3. There appears to be no tendency for interatomic distances of M - $F_{bridging}$ bonds to increase as the t_{2g}^* antibonding orbital population is increased on lowering the oxidation state. Apparently F ligand repulsions play an important role in determining interatomic distances in these systems and outweigh the effects of π^* orbital occupancy. The repulsive impact of short-bonded unique fluorine ligands are expected to be greater than that of the long-bonded bridging F ligands. The bridging M - F bonds in the higher oxidation state RuF_5 and RhF_5 find all their bonds somewhat stretched by the steric interaction of 4 unique F atoms. The lower oxidation state trifluorides, which contain no short bonded sterically active unique F ligands, are able to form the shortest bridging bonds.

While their impact of the t_{2g}^* electron population on M - F bond lengths is not clear in the above comparison, it appears that the orbital population is not without effect. A comparison of the highly precise Ru(V) and Rh(V) fluoride structures serves to highlight these effects. The M - $F_{bridging}$ interatomic distances in these two fluorides are not significantly different from each other, all being almost exactly 2.000Å. However, small but signicant differences are observed in the M - F_{unique} interatomic distances of the two pentafluorides. In RuF_5 (Fig. 3.1) the M - F_{unique} interatomic distances for

those F ligands *trans* to the bridging F ligands are 1.798(1)Å and 1.793(1)Å. These distances are significantly shorter than those observed for the F ligands disposed *cis* to the bridging F ligands, these being 1.821(1)Å and 1.817(1)Å respectively. The RhF_5 *cis* and *trans* counterparts might be expected, in the absence of antibonding π effects, to exhibit slightly shorter M - F_{unique} interatomic distances, because the effective nuclear charge increases as the atomic number increases in the presence of the poorly shielding antibonding π electron. This is in fact the case for the *cis* unique F ligands in which the M - F_{unique} interatomic distance are 1.802(4)Å and 1.803(4)Å respectively, these being significantly shorter than the analogous Ru - F bonds. However, the unique F ligands *trans* to the bridging F ligands in RhF_5 give rise to M - F_{unique} distances of 1.817(4)Å and 1.820(4)Å. These are decidedly longer than the comparable bonds in RuF_5. This is again, likely a consequence of going from the d^3 Ru(V) configuration to the d^4 Rh(V) configuration. As observed above, the Rh(V) system must place 2 electrons, as opposed to 1 in the Ru(V) case, in the antibonding π orbital in the plane containing the bridging F ligands and the unique F ligands *trans* to them. This increased antibonding character in the bridging plane has the effect of lengthening these M - F_{unique} bonds a small, but significant amount, with respect to their Ru counterparts and may explain why no decrease is seen in M - $F_{bridging}$ interatomic distances of RhF_5 with respect to RuF_5.

A much more perplexing difficulty, is the definite shortening of the M - F_{unique} bonds in RuF_5 of the unique F ligands *trans* to the bridging F ligands with respect to those which are *cis*. This may simply be a consequence of the unique F ligands in *trans* positions being in the same plane as the slightly lower energy antibonding orbital created by the longer bridge bonds. Hence, the antibonding effect is smaller than for the *cis* unique F ligands which feel the impact of the two singly occupied higher energy antibonding π orbitals. It is perhaps more likely that a *trans* electrostatic effect is shortening the *trans*

unique F ligands. That is, the longer bonded, more electron rich bridging F ligands may be viewed as on the ionization pathway to F^-. This pulling away of electron density from one side of the metal d_{xy} orbital results in contraction of the electron density on the opposite side, with the resultant shortening of M - F_{unique} interatomic distances.

X-Ray powder data had indicated that RuF_4 was not isostructural with the two known tetrafluoride structure types, PdF_4 and SnF_4.[20-23] This data had, however, suggested M - M distances similar to those of the PdF_4 related structures, indicating the M - F - M bridges in RuF_4 were probably similarly bent to an angle of ≈135°. The structure solution from X-Ray synchrotron and neutron powder data has confirmed these conclusions.

The unit cell parameters obtained from the synchrotron data are highly precise. Combined with the neutron data they provide for an unambiguous assignment of the space group $P2_1/n$, which places the two Ru atoms in each cell at 0,0,0 and 1/2,1/2,1/2. Hence a nearest Ru - Ru distance of 3.664(2)Å is obtained for the material. This distance is remarkably close to those observed in RuF_3, where Ru - Ru = 3.672(4)Å and RuF_5, where Ru - Ru = 3.7207(2) and 3.7705(2)Å. Hence the bridge bonding and bridging angle of the three oxidation state Ru fluorides must be very similar.

A Fourier distance map was unable to precisely place the F atoms in this structure, but does indicate a roughly octahedral arrangement of 6 F atoms about each Ru. More importantly it clearly shows that the 4 F ligands involved in bridging adjacent Ru atoms are in the same plane, the 2 unique F ligands being *trans*. This arrangement results in a sheet structure with unique F ligands from one layer nestling into holes made by unique F ligands of adjacent layers and is not too different from SnF_4, or NbF_4. This difference amounts to a puckering of the sheets in RuF_4 vs the flat sheets of NbF_4 and simply results from the nonlinearity of the M - F- M bridge.

A constrained refinement was chosen after the unrestrained refinement resulted in a structure with assymmetric M - F - M bridging. This type of bridging has not been observed in any binary fluoride system, including the isomorphous relative of RuF_4, VF_4, whose structure was reported during the course of this work.[24] The constrained refinement, which eventually gave a slightly better fit to the data than the unrestrained refinement, was based on a M - $F_{bridging}$ distance of 2.00Å and a M - F_{unique} distance of 1.82Å. These distances were dictated by the corresponding RuF_3 and RuF_5 bond lengths and the the closeness of the Ru - Ru distances in each of the fluorides.

The Ru - F - Ru bridge angle arrived at in the chosen geometry is 133°. This is nearly the ideal for an hcp system and as such is smaller than bridge angles in RuF_3 and RuF_5. By shortening the Ru - F bridging interatomic distances in RuF_4, the bridge angle can be made larger, 1.99Å resulting in a 134° angle, while the 1.98Å distance observed in RuF_3 gives to a 135° angle. However, this is perhaps unnecessary. The d^4 configuration of RuF_4 must place 2 electrons in the lowest energy orbital of the ideally t_{2g}^* set. This orbital must be the one in the plane containing the 4 bridging F ligands. Hence any π bonding interaction which would favor more linear bridges is effectively quenched in this plane, resulting in the close approach to hcp.

The geometry of RuF_4, Fig. 3.3, obtained from this refinement is particularly satisfying when compared with that of RuF_5. Indeed, the The RuF_4 structure can be built up from the RuF_5 tetramers. By taking the unique F ligands *trans* to the bridging F ligands of the pentafluorides and involving them in bridging in such a way that each new M - F - M bridge is kinked in a manner opposite to that of its *trans* partner, an ideal RuF_4 structure can be formed which is identical to that of RuF_4.

Since precise bond lengths were not obtained for RuF_4, an effort was made to obtain gas phase electron diffraction data for thermally unstable RuF_6 in the hope that

these data would allow for meaningful comparisons of M - F_{unique} interatomic differences with those of RuF_5. While the structure has not been obtained to date, the possible range for the Ru - F interatomic distance can de derived from the available MF_6 structural data. Unit cell parameters are available for all of the second and third series transition metal hexafluorides in both their orthorhombic and cubic forms.[25] As was found in the hexafluorometallate salts (chapter 2), a significant contraction is observed in formula unit volumes from early to late transition metals, as the effective nuclear charge increases. In the second transition series, only the structure of MoF_6 has been determined to high precision, having been found to contain an Mo - F distance of 1.820(3)Å.[26] Using this distance as a starting point and assuming that all of the formula unit volume contraction observed in the unit cell data is due to shortening of the M - F bonds, leads to an estimated Ru - F distance of 1.77Å. In chapter 2, however, it was suggested that part of the observed volume contraction was probably due to a greater polarization of the non-bonding electrons on the F ligands towards the metal centers of the more electronegative late transition metals. This notion is supported by electron diffraction data on the third transition series hexafluorides.[27] Here a remarkable near constancy of bond length; W - F = 1.833(4)Å, Os - F = 1.831(4)Å, and Ir - F = 1.830(4)Å, is seen in spite of the significant contraction in formula unit volumes across the series. Presumably, while the increasing effective nuclear charge is acting to contract the system, the increasing population of the t_{2g}^* π antibonding orbitals is favoring, weaker, longer bonds, thus maintaining a nearly constant bond length. A dramatic decrease in hexafluoride vibrational force constants across the series, further supports this effect of filling the antibonding π orbitals. Therefore, the Ru - F interatomic distance will almost certainly be larger than the 1.77Å value based on bond- shortening accounting for the formula unit volume decrease; and it may not be significantly smaller than the Mo - F distance of 1.820(3)Å. If this is the case,

then the Ru - F distance in the hexafluoride would not be significantly different from that observed in the pentafluoride for the unique F ligands which are *cis* to the bridging F ligands.

Conclusions:

The available data on bridging and unique M - F interatomic distances in the group V to VIII binary fluorides of the second transition series are summarized in Fig. 3.5. Clearly M - F distances, for both bridging and unique F ligands, do not vary significantly from 2.00Å and 1.80Å, respectively. This suggests, as do the third transition series hexafluoride data, that while the effect of the t_{2g}^* antibonding orbital population on M - F interatomic distances must be small, it is sufficient to nearly counter the expected decrease in interatomic distances with increased nuclear charge across the transition series.

Moreover, the trend in M - $F_{bridging}$ interatomic distances of decreasing with decreasing oxidation state observed for the Rh fluorides and nearly so for the Ru fluorides appears to hold across the entire series. Although data for NbF_5 and MoF_5 are much too imprecise to make the above conclusion a firm one, change in oxidation state certainly does not have a large effect on the bond distances in these systems. Altering the t_{2g}^* orbital population by changing oxidation state must not dramatically change the effective nuclear charge observed by the bridging F ligands, these antibonding π electrons being poorly shielding of the effective nuclear charge. Any changes observed, are apparently compensated and as suggested by the Rh - fluorides over-compensated for by steric interaction of short - bonded unique F ligands. Increasing the oxidation state, increases the number of short - bonded unique F, which must result in a stretching of the bridging bonds.

Firm conclusions about changes in M - F_{unique} interatomic distances await either more precise data on MoF_5, or a precise structure determination of RuF_6. Interestingly, the imprecise M - F_{unique} distances observed for NbF_5 and MoF_5, suggest that they, like the same distances in RuF_5 and RhF_5, are in two distinct sets; those *cis* to the bridging F ligands(referred to here as axial) and those *trans* to the bridging F ligands(referred to here as equatorial). If this is truly the case MoF_5, being the d^1 counterpart to d^4 Rh would be expected to display longer equatorial than axial unique F M - F distances. Similarly if a *trans* influence is the cause of the equatorial unique F bonds being shorter than the axial in RuF_5, a like result is expected for its d^0 analog, NbF_5. These results are suggested by the data in Fig. 3.5, but much higher quality data is needed to confirm these tentative conclusions.

References

1. Edwards, A.J.; *Advances in Inorganic and Radiochemistry* **1983**, *27*, 83.
2. Babel, D.; Tressaud, A., in "Inorganic Solid Fluorides," Hagenmüller, P., ed., Academic Press, Inc., New York, 1985, pp 78-204.
3. Einstein, F.W.B.; Rao, P.R.; Trotter, J.; Bartlett, N. *J.Chem. Soc. A* **1967**, 478.
4. Morrell, B.K.; Zalkin, A.; Tressaud, A.; Bartlett, N., *Inorg. Chem.* **1973**, *12*, 2640.
5. Grosse, L; Hoppe, R., *Z. Anorg. Allg. Chem.* **1987**, *552*, 123.
6. Edwards, A.J., *J. Chem. Soc.*, **1964**, 3714.
7. Pouchard, M., Torki, M.R., Demazeau, G., Hagenmüller, P., *C.R. Hebd. Sceances Acad. Sci. Ser.* **1971**, *C273*, 1093.
8. Hepworth, M.A.; Jack, K.H.; Peacock, R.D.; Westland, G.J., *Acta Crystallogr.* **1957**, *10*, 63.
9. Holloway, J.H.; Peacock, R.D.; and Small, R.W.H., *J. Chem. Soc.* **1964**, 644.
10. Claasen, H.H.; Selig,H.; Malm, J.G.; Chernick, C.L.; Weinstock, B. *JACS* **1961**, *83*, 2390. Weinstock, B.; Claassen, H.H.; Chernick, C.L. *J. Chem. Phys.* **1963**, *38*, 1470.
11. Mitchell, S.J.; and Holloway, J.H., *J. Chem. Soc.* **1971**, 2789.
12. Holloway, J.H; Peacock, R.D., *J. Chem. Soc.* **1963**, 527.
13. A. Tressaud, unpublished results.
14. Casteel, W.J.; Wilkinson, A.P.; Bormann, H.; Serfass, R.E.; Bartlett, N. *Inorg. Chem.* **1992**, *31*, 3124.
15. Myer, D.K., ed., Condensed Matter Research of LANSCE', Los Alamos Laboratory Report LALP 90-7, January 1990, pp 10-11.

16. Werner, P.-E.; Eriksson, L.; Westdahl, M.J.; *J. Appl. Crystallogr.* **1985**, *18*, 367.

17. De Wolff, P.M., *J. Appl. Crystallogr.* **1968**, *1*, 108.

18. Larson, A.C.; Von Dreele, R.B., Los Alamos Laboratory Report, 1990, No LAUR86-748.

19. Rietveld, H.M., *J. Appl. Crystallogr.* **1968**, *2*, 65.

20. Wright, A.F.; Fender, B.E.F.; Bartlett, N.; Leary, K., *Inorg. Chem.* **1978**, *17*, 748.

21.Gortsema, F.P.; Didchenko, R. *Inorg. Chem.* **1965**, *4*, 182.

22. Schäfer, H.; Schnering, H.G.; Niehuess, K.J.; Nieder-Varenholz, H.G., *J. Less Common Metals* **1965**, *9*, 95.

23.Hoppe, R.; Dahne, W., *Naturwiss.*, **1962**, *49*, 254.

24. Becker, S., and Müller, B.G., *Angew. Chem. Int. Ed.* **1990**, *29*, 406.

25. Siegel, S.; Northrop, D.A. *Inorg. Chem.* **1966**, *5*, 2187.

26. Seip, H.M., Seip, R., *Acta Chem. Scand.* **1966**, *20*, 2699.

27. Kimura, M.; Schomaker, V.; Smith, D.W.; Weinstock, B., *J. Chem. Phys.* **1968**, *48* 4001.

28. LaValle, D.E., Steele, R.M., Wilkinson, M.K., Yakel, H.R. Jr., *J. Am. Chem. Soc.*, **1960**, *82*, 2433.

29. Edwards, A.J., Peacock, R.D., Small, R.W.H., *J. Chem. Soc.*, **1962**, 4486.

30. Levy, J.H.; Sanger, P.L.; Taylor, J.C.; Wilson, P.W. *Acta Crystallogr.* **1974**, *B31*, 1065.

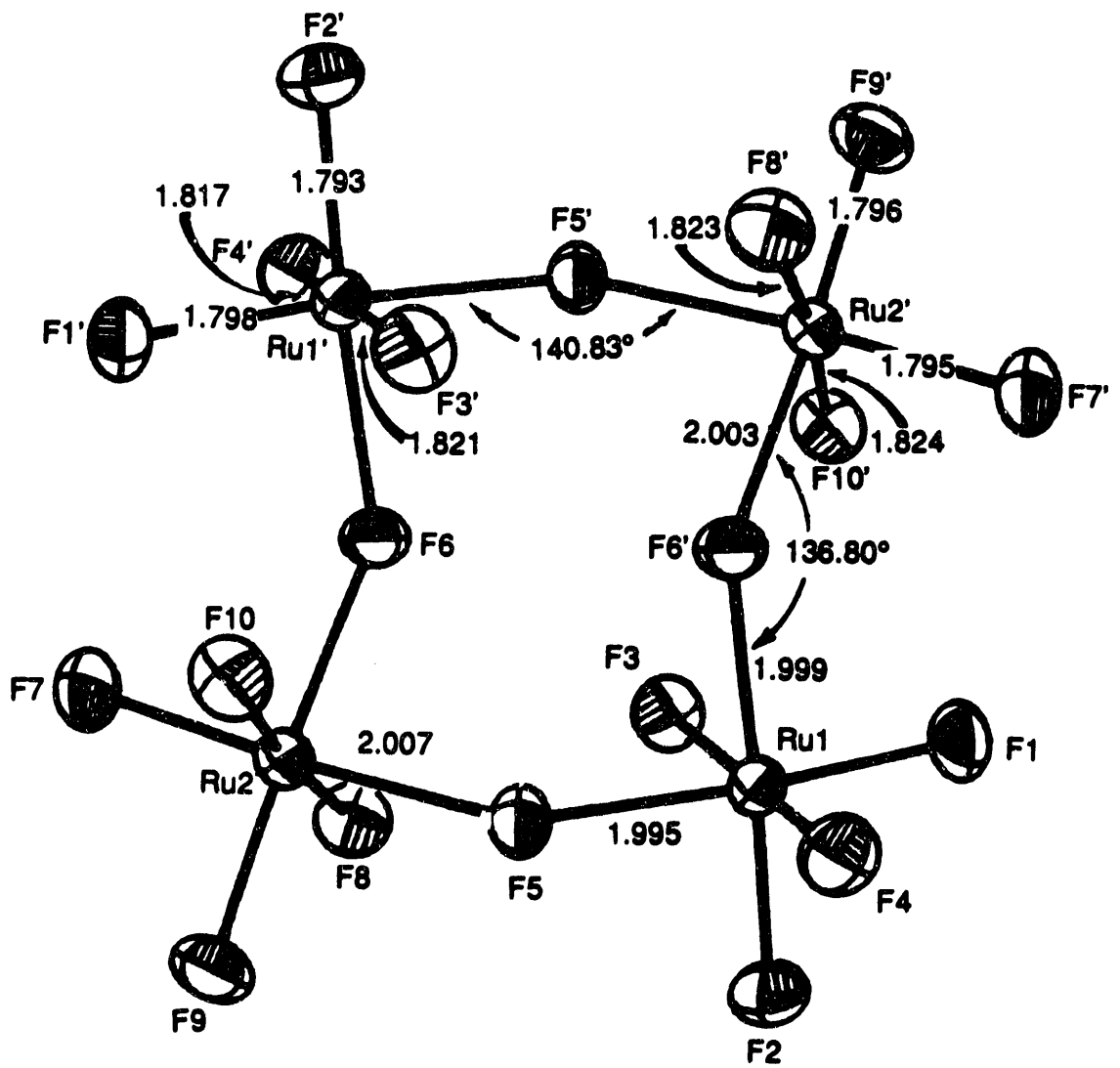

Figure 3.1. Tetrameric structural unit of $(RuF_5)_4$ (70 % probability ellipsoids) with interatomic distances (Å) and bridge - bonding angles (deg).

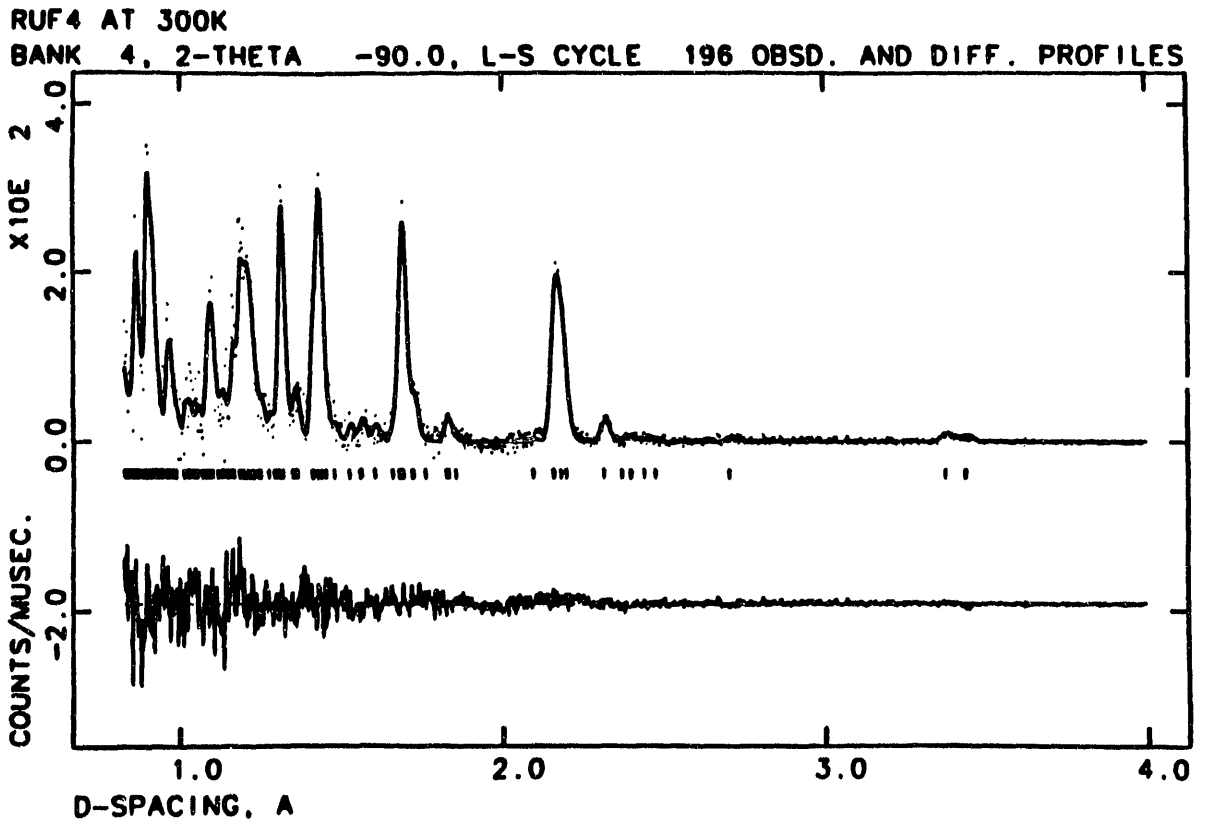

Figure 3.2. Observed neutron time - of - flight powder diffraction data minus the calculated background shown as dots. The calculated values from the constrained model with bridging M - F = 2.00 Å and nonbridging M - F = 1.82 Å are shown as a curve. A difference (I_{obs}- I_{calc}) curve and the reflection positions are also shown.

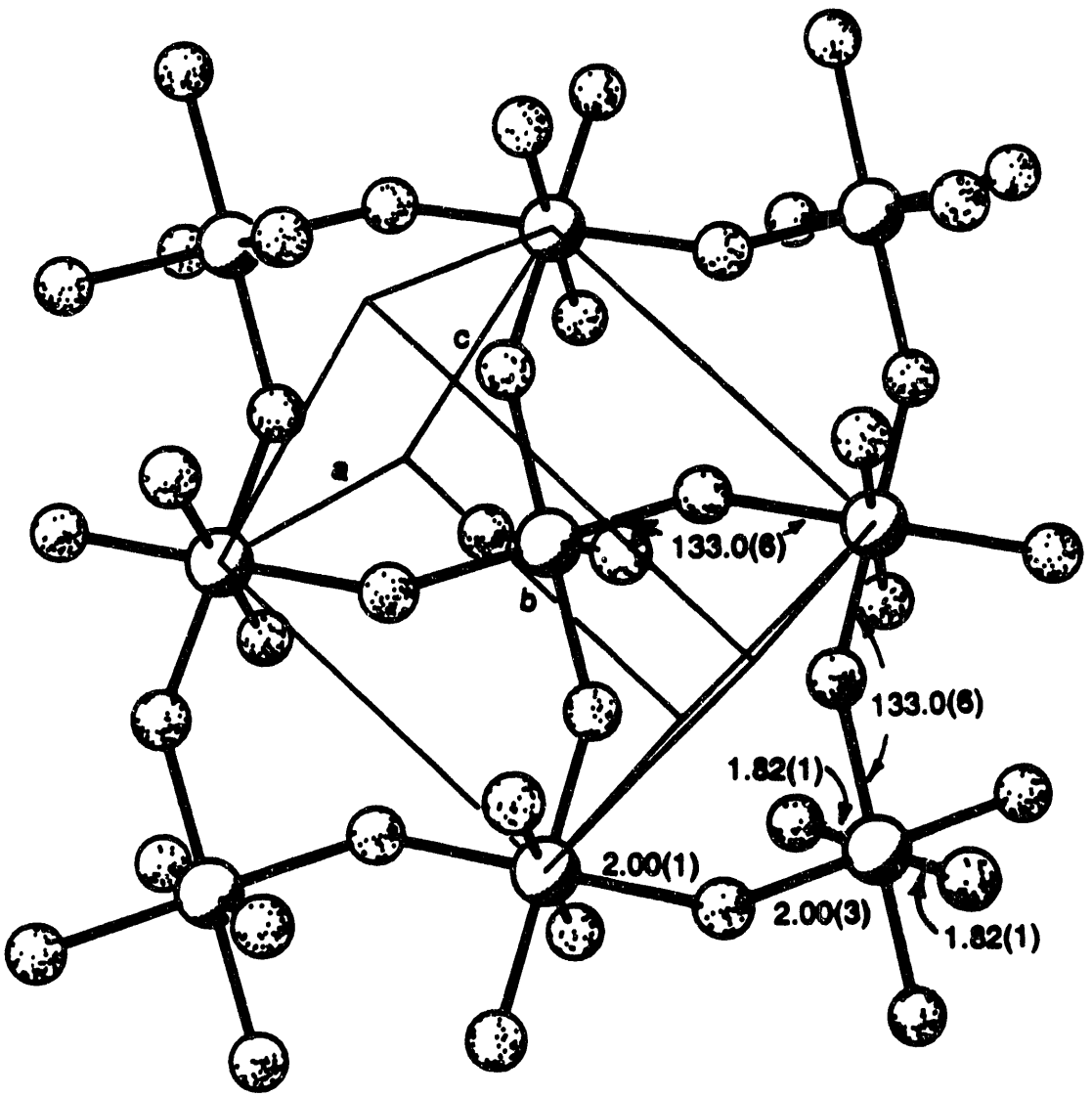

Figure 3.3. View of the puckered - sheet structure of RuF_4 with interatomic distances (Å) and bridge - bonding angles (deg.)

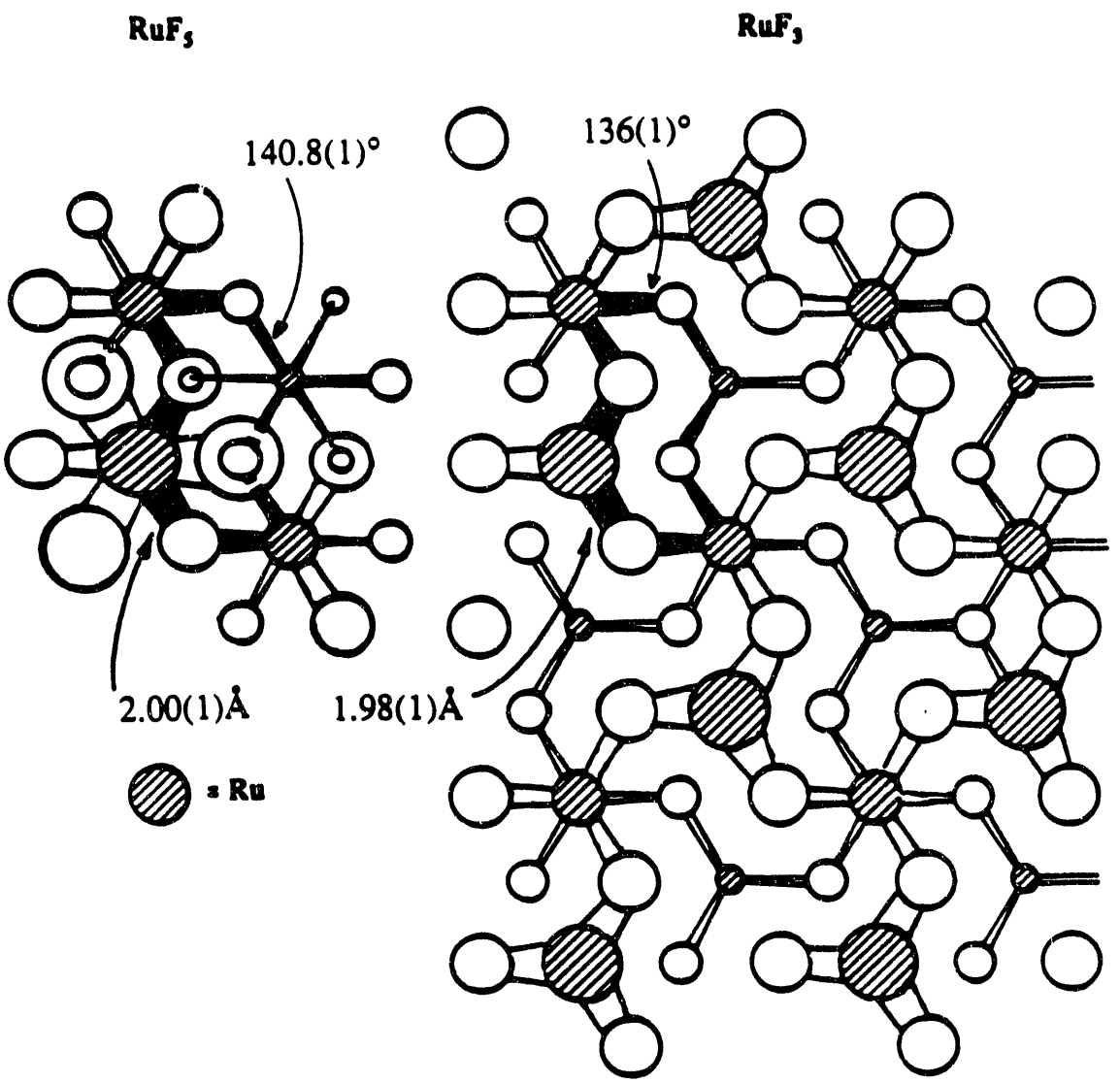

Figure 3.4. Relationship of the $(RuF_5)_4$ geometry to an element of the RuF_3 infinite hexagonal nearly - close - packed F atom array.

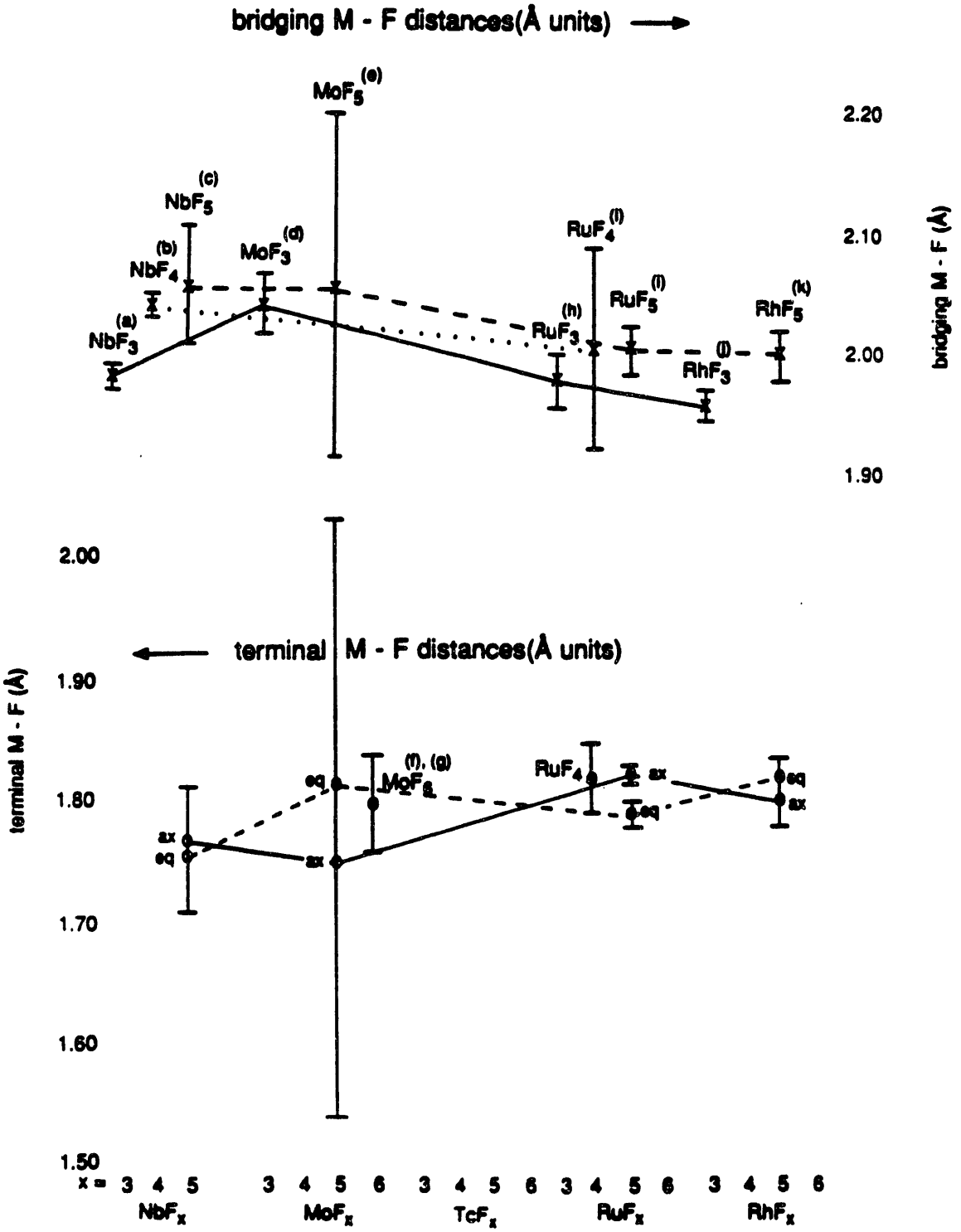

Figure 3.5. M - F interatomic distances, terminal and bridging (Å) for the binary fluorides of Nb through Rh (errors bars represent ± 3σ). Reference key for footnotes: a, 7; b, 21 and 22; c, 6; d, 28; e, 29; f, 30; g, 26; h, 8; i, present work; j, 5; k, 4.

Chapter 4

Synthesis and Structure Types of the Transition Metal Tetrafluorides

Introduction

In Chapter 3, a structural investigation of the Ru binary fluorides demonstrated remarkable constancy of M - F interatomic distances for bridging F - ligands with change in oxidation state. Comparisons were made with other metals in the second and third transition series from groups V through VIII and this constancy appeared to be general. Indeed, there appeared to be little change in M - $F_{bridging}$ bond length for different metals in this series.

Those observations are particularly remarkable given the variety of structure types observed as the bridge bonding changes rather dramatically from linear M - F - M bridging in the group V systems to ≈ 132° bridging at the end of group VIII.

The trifluorides show three types of structures (Table 4.1), depending upon this bridging angle. A ccp - ReO_3 type structure results when the bridges are linear and an hcp based distortion of this structure is observed when the bridge angle is 132°, this being the ideal M - F - M angle for hcp arrangements of fluorine atoms with regular 1/3 occupancy of the octahedral holes.[1] Intermediate bridging angles give rise to structures which may be viewed as distortions from the hcp and ccp structures.

Table 4.1. Structures of Second and Third Transition Series Trifluorides

	Nb^2	Mo^3	Ru^1	Rh^4	$PdPdF_6{}^5$
MFM∠(°)	180	141	136	132	132
				Ir^1	$PtPtF_6{}^6$
MFM∠(°)				132	132

The pentafluorides also exhibit three structure types (Table 4.2), each placing the bridging F ligands *cis* to each other. Two of these , those with linear M - F - M bridges

and those with an M - F - M angle ≈135° are based on tetramers. Interestingly these tetrameric pentafluorides again may be viewed as ccp and hcp arrangements of F atoms, for linear and 132° M - F - M bridges, respectively, with M regularly occupying 1/5 of the octahedral holes.[7] The third structural conformation is the chain polymer VF_5 structure and occurs in those pentafluorides, TcF_5 and ReF_5, for which the M - F - M bridging angle ≈150°. The fluorines in this structure are not close packed.

Table 4.2. Structures of Second and Third Transition Series Pentafluorides

V	VI	VII		VIII	
Nb^8	Mo^9	Tc^{11}	Ru^{12}	Rh^{13}	
Ta^8	W^{10}	Re^{11}	Os^{14}	Ir^{15}	Pt^{16}
ccp		not close packed	hcp		

It is among the tetrafluorides, however, that the greatest structural diversity might be expected. The available data indicate that these materials undergo similar bending of their M - F - M bridges, across the transition series as do the trifluorides and pentafluorides on going from NbF_4 which contains linear bridges[17] to PdF_4 with an M - F - M angle of 135°.[18] Moreover the two unique F ligands, in the octahedral framework about each metal atom, are observed in *trans* relationship in the NbF_4 sheet structure and *cis* in the 3-D PdF_4 structure. The finding that the VF_4, d^1 structure,[19] is like that of RuF_4, d^4 (Chapter 3), and places the unique fluorines *trans* to each other, in spite of significant bending in the bridge bonding further indicates that there is not a simple correlation with the "non - bonding" valence - electron configuration. In addition, the M - F - M bridging angles in the RuF_4 sheet structure are not significantly different from those determined in the PdF_4, IrF_4, and PtF_4 structures. Prior to this study, however, the only second and third transition series tetrafluorides known (and most of these are not

well described) were those of Zr[20], Nb, Rh[21], Pd, Ir[21], and Pt[21]. Indeed, many have never been synthesized in high purity.

The highest oxidation state fluorides can often be synthesized by direct fluorination, their volatility allowing them to be separated from lower fluorides by vacuum sublimation.[22] The lower oxidation state systems, in this series the trifluorides, can often be made in high purity by reduction of higher fluorides using an excess of reducing agent, or by interaction of the metal with AHF at elevated temperatures.[23] The intermediate oxidation state tetrafluorides, being polymeric and difficult to separate from admixtures with trifluoride, awaited a general, high purity synthesis. The latter was of particular interest for reliable magnetic data, but the lower symmetry of tetrafluorides (in contrast to the high symmetry of trifluorides) also makes high purity a precondition for successful indexing of X - Ray powder diffraction data for such materials.

The successful synthesis of RuF_4 by fluoride-ion capture from the hexafluorometallate salt, suggested a new access to high purity tetrafluorides, via:

$$K_2MF_6 + 2A \xrightarrow{AHF} MF_4\downarrow + 2KAF \qquad (1)$$

A in eq. 1 is the fluoroacid BF_3, AsF_5, or SbF_5 and M is any metal from which the hexafluorometallate(IV) salt can be synthesized in high purity(Chapter2). This was observed in this study for Os, Re, Mo, and Pd.

Experimental

Preparation of OsF_4. In the DRILAB usually 600mg (1.5 mmol) K_2OsF_6 (chapter 2) was loaded into one arm of a two armed Teflon T apparatus. The reactor was attached to a Teflon/FEP manifold of the vacuum line and evacuated. AHF (6ml) was condensed on to the K_2OsF_6 which completely dissolved on warming to room temperature. The addition of AsF_5 to the yellow solution brought about the immediate precipitation of a heavy

yellow - brown solid. On attaining a colorless supernatent solution, AsF_5 addition was ceased. It was found that the $KAsF_6$ side product in this reaction was not very soluble in the presence of dissolved AsF_5. For this reason the AsF_5 containing AHF was removed, by evacuation through a small trap containing KF, from the mixture of products. A second 6 ml aliquot of AHF was condensed on to the yellow brown solid in the reactor and the $KAsF_6$ was then removed by decantation of the supernatent solution into the free arm of the reactor. Cooling the original reaction arm distilled the AHF back on to the product for further washing. This decantation/ distillation procedure was repeated 10 times to completely remove $KAsF_6$ from the product. Finally the AHF was evacuated through a soda - lime scrubber, the solid being dried under dynamic vacuum. Nearly quantitative yields of OsF_4 were obtained, there being some loss in the decantation process. X - Ray powder data, Table 4.3 , could be indexed completely on the basis of the orthorhombic PdF_4 type cell the extinctions of which are in harmony with space group Fdd2, with is the group established for PdF_4.

Table 4.3. X-Ray powder data (Cu K<α> radiation, Ni filter) for OsF_4, orthorhombic cell with a=9.89(1) Å, b=9.36(1) Å, c=5.70(1) Å, z=8, V=528 $Å^3$, possible space group, Fdd2.

		$1/d^2x10^4$	
I/Io	Obs	Calc	hkl
w	431	409	200
		456	020
vs	523	524	111
w	1351	1341	311
w	1454	1437	131
s	1636	1635	400

Table 4.3 cont.

I/Io	Obs	Calc	hkl
		1639	202
m	1827	1826	040
m	2099	2092	420
		2095	222
w	2969	2983	113
vw	3269	3262	151
vs	3473	3461	440
		3464	242
vw	3796	3801	313
vw	3877	3896	133
w	4699	4690	442
		4714	333
ms	4940	4919	004
		5722	153
		5743	460
vw	5758	5746	262
		5785	224
m	6579	6539	353
		6555	404
m	6748	6745	044
w	7330	7304	080
m	8436	8390	444
m	8977	9027	064
w	11544	11525	026
m	12268	12223	084
m	13362	13379	175
vw	13900	13855	484

Reaction of K_2OsF_6 with BF_3. In a reaction similar to that above, BF_3 was added to a solution of 492 mg (1.3mmol) K_2OsF_6 in 5ml AHF. After washing, an orange insoluble solid (207 mg) was isolated which was completely amorphous to X - rays. Addition of

AsF_5 to this solid in AHF resulted in an immediated color change to yellow - brown. Washing as above left OsF_4 as indicated by the X- Ray powder data.

Reaction of K_2RuF_6 with BF_3. Interaction of 600mg (2.0 mmol)K_2RuF_6 with BF_3 under conditions identical to those above produced an insoluble orange solid which gave no X-ray powder pattern. Interaction of this solid with AsF_5 in AHF produced an immediate color change to the deep pink characteristic of RuF_4. The X - Ray powder data contained only lines due to RuF_4.

Reaction of K_2ReF_6 with AsF_5. K_2ReF_6 (chapter 2) dissolved in AHF to give a pale pink solution. Addition of AsF_5 as above immediately produced a light pink solid. However on standing for 5 min in AsF_5 rich AHF the pink solid dissolved giving a green solution, suggesting that oxidation of ReF_4 to green ReF_5 by AsF_5 had occured.[24]

Preparation of ReF_4: In the DRILAB 295 mg (0.78 mmol) K_2ReF_6 was loaded into one arm of a two armed Teflon reactor. A large molar excess of SbF_5 (1ml, 14 mmol) was introduced, in the DRILAB, into the other arm of the reactor. After adding AHF to both arms of the reaction vessel, the solution of SbF_5 in AHF was poured into the AHF solution of K_2ReF_6 a pink precipitate was rapidly produced. On standing for 30 min in the SbF_5 rich solution the pink solid showed signs of dissolution and gave a pale blue solution. This was washed in the usual way to leave 110 mg (0.32 mmol, 42% yield based on ReF_4 formation) of pink solid. The X-Ray powder pattern of the pink material was indexable on the basis of a tetragonal cell, akin to the orthorhombic cell of PdF_4. The data are given in Table 4.4.

Table 4.4. X-Ray powder data (Cu K<α> radiation, Ni filter) for ReF_4, orthorhombic (pseudo tetragonal) with a=b=9.61(2) Å, c=5.66(1) Å, z=8, V=522 $Å^3$, possible space group Fdd2

		$1/d^2x10^4$	
I/Io	Obs	Calc	hkl
s	537	529	111
w(br)	867	866	220
m(br)	1401	1395	311,131
s	1696	1683	202,022
---	---	1732	400,040
vw	2138	2116	222
---	---	2165	420,240
vw	2240	2261	331
w(br)	3048	3029	113
---	---	3127	511,151
vs(br)	3450	3414	422,242
		3465	440
w(br)	3920	3892	313,133
---	---	3994	531,351
---	---	4331	620,260
vvw	4723	4758	333
w(br)	4999	4994	004

Reaction of K_2ReF_6 with BF_3. When BF_3 was admitted to a solution of K_2ReF_6, an agglomerated black solid resulted. Increasing the BF_3 concentration by cooling the solution to -20 °C resulted in a small amount of pink solid forming on the black product, but this disappeared on warming to room temperature. In order to add SbF_5 by distillation under static vacuum, the black solid was evacuated to dryness and 1ml of SbF_5 was condensed into the free arm of the two armed reactor. AHF (3ml) was condensed into both arms of the reactor. On warming to room temperature, the SbF_5 solution was poured on to the black solid in AHF, completely converting it to a pink solid, which is presumed

to be ReF_4. Unfortunately this material was of insufficient crystallinity to produce an X - ray powder pattern.

Preparation of MoF_4: In a reaction similar to that for the preparation of ReF_4, 410 mg (1.4 mmol) K_2MoF_6 was loaded into one arm of a two armed teflon/FEP tee reactor. The K_2MoF_6 dissolved in AHF to give a green solution. A solution of SbF_5 in AHF in the other arm of the reactor was poured onto the green solution immediately producing a pale green insoluble precipitate. Addition of the SbF_5/AHF was stopped when the solution above the green solid became colorless. Further addition of the SbF_5/AHF solution caused some dissolution of the green solid producing a pale green supernatent solution. This product was washed in the usual way, the AHF/SbF_5 solution finally being removed through a soda - lime scrubber under dynamic vacuum. The green solid (110 mg, 0.58 mmol, 41 % yield based on MoF_4) precipitated by addition of excess SbF_5 in AHF proved to be very poorly crystalline, but the X - Ray powder data match the strongest lines in the pattern obtained by Payne and Asprey[25] for their MoF_4. Data are given in Table 4.5. This pattern showed no similarity to those of SnF_4 (NbF_4 type), RuF_4, or PdF_4 and has not been indexed.

Table 4.5. X - ray powder data for MoF_4 and Comparison with Payne and Asprey data

		Payne, Asprey data	
I/I_0	$1/d^2 \times 10^4$	I/I_0	$1/d^2 \times 10^4$
		vw	152
		vw	210
		vw	331
		mb	452
		m	516
2	625	m	625
10	706	s	692
		sbr	793
3	996	w	995
		w	1020

Table 4.5 cont.

I/I_0	$1/d^2 \times 10^4$	I/I_0	$1/d^2 \times 10^4$
		w	1445
7	2478	m	2500
		vw	2712
		vw	2890
3	3093		
3	3143	vw	3156
1	4506	vw	4565
1	5676		

Reaction of K_2MoF_6 with AsF_5: Addition of AsF_5 to a solution of K_2MoF_6 in AHF immediately produced a green solid which on standing in AsF_5/AHF solution quickly became a pale, tan color, indicative of MoF_5. [9]

Reaction of K_2MoF_6 with BF_3: Addition of BF_3 to a solution of 405 mg (1.41 mmol) K_2MoF_6 in AHF produced a heterogeneous mixture of insoluble products containing a pale green friable solid and a rubbery yellow brown solid in AHF. The finely divided green solid tended to remain suspended in the AHF solution, which complicated the washing procedure.Significant losses of the green solid during washing are probably responsible for the low final product weight (based on the production of MoF_4, or $KMoF_5$) of 138 mg X - Ray powder photographs show the strong lines seen in the SbF_5 preparation above as well as some additional lines not attributable to the Payne and Asprey material. Addition of SbF_5 to this mixture of products in AHF immediately produced a homogeneous pale green solid.

Preparation of PdF_4: K_2PdF_6 prepared by the method of Sharpe[26] was dissolved at 20°C in AHF to yield a yellow-orange solution. Addition of excess AsF_5 with rapid stirring of the solution quickly produced a brown solid. With the reactor continously agitated and a high AsF_5 concentration maintained in the AHF, the brown solid gradually

took on the pink to red color associated with PdF_4.[21] No further AsF_5 uptake was observed after 12 hours. X-ray powder photographs of the red solid were identical to those of PdF_4 prepared by high pressure fluorination.

Results and Discussion

The synthesis of several tetrafluorides, MF_4 (M = Mo, Re, Os, Ru, and Pd), in high purity has now been accomplished by fluoride ion capture from the hexafluorometallate(IV) salts via reaction (1). As with any class of complexes of a given oxidation state, the oxidizing power, and hence the stability to strong oxidizing agents, of these tetrafluorides is expected to increase, with the nuclear charge from early to late transition metals. This proved to be an important factor in the synthesis of different tetrafluorides. The tetrafluorides of Mo and Re are unstable with respect to the powerfully oxidizing acid AsF_5, being oxidized to Mo(V) and Re(V) by that reagent. However, RuF_4, OsF_4, and PdF_4 are stable with respect to oxidation by AsF_5, and no further reaction with this reagent occurred over several hours of contact. Indeed, PdF_4 is known to be a very powerful oxidizer and has been difficult to prepare, owing to its low thermal stability at temperatures usually required for the direct fluorination of lower oxidation state polymeric fluorides.[21] The low temperatures that can be used in reaction (1) are particularly favorable for thermodynamically unstable fluorides. This is best exemplified by the synthesis of AgF_3 (Chapter 5).

An increase in Lewis acidity was also observed which appears to follow the trend in oxidizing power across the series. There is some evidence that MoF_4 and ReF_4 are produced by BF_3, but that an equilibrium is set up in reaction (1) which only favors tetrafluoride production at the low temperatures where high concentrations of BF_3 can be brought into the solution. To complete the reaction, a stronger acid, which was not a powerful oxidizer was required. SbF_5 proved to be satisfactory. There was no indication

that BF_3 was able to produce any RuF_4, or OsF_4, so AsF_5 was used to bring about these reactions. The strongest fluoroacid in this tetrafluoride series ought to be PdF_4, and it may be that the formation of a low solubility PdF_5^- salt was responsible for the very slow reaction to produce PdF_4 as a homogeneous product. Increasing electronegativity of the metal center and increased Lewis acidity are expected to go hand in hand as long as the increased ligand - ligand repulsion, consequent upon shortening M - F distances, does not become too unfavorable. For the second and third series MF_6^{-2} salts, however, there is not a large decrease in M - F distance through to Pd(IV) and Pt(IV), therefore a smooth increase in fluoroacidity might be expected across each series.

Reaction(1), while producing the tetrafluorides in high purity, does not result in very crystalline materials, therefore much of the structural data obtained is of low quality. Nevertheless, a number of meaningful conclusions can be drawn. With the exception of MoF_4, which may prove to exhibit a new tetrafluoride structure, the tetrafluorides fall into three tetrafluoride structure types Fig. 4.1. The SnF_4 structure, Fig. 4.2, so far only adopted by NbF_4 among the transition metals, places the two unique F ligands of the octahedrally coordinated tetrafluoride in *trans* positions. The bridging F ligands are in a square plane, thus a sheet structure results. Because the M - F - M bridges are linear, the sheets are flat and may be thought of as two dimensional sections of the ReO_3 perovskite structure. RuF_4 exhibits a similar sheet type structure, (see Fig. 3.3) however, now the M - F - M bridges subtend an angle of 133° causing the sheets to be puckered. VF_4 is also known to adapt this structure with a larger M - F - M angle of 151°. The third structure places the two unique F ligands *cis* to each other with bridging M - F - M angles slightly greater than the hcp limit of 132°, Fig. 4.3. This structure is related to rutile[27] and can be derived from such difluoride structures by ordered removal of every other metal atom from a rutile, MF_2 - type structure (see Fig 4.4). This structure is apparently adopted by RhF_4, PdF_4, ReF_4, OsF_4, IrF_4, and PtF_4[16] all of which have the roughly isodimensional

Fdd2 orthorhombic unit cells. The X - ray powder diffraction patterns of all these tetrafluorides, except those of RhF_4, and OsF_4, resemble one another closely and support the expectation of the PdF_4 structure being common to all. RhF_4 and OsF_4 may not be exactly of this structure type even though the observed extinctions are appropriate for space group Fdd2.

As may be seen from Fig 4.3 which shows a view of this cell along the *c* axis, the metal atoms lie in the 220 planes, as is required for placing them in special positions of the Fdd2 cell. Although there are F atoms in between these planes, they are much poorer scatterers of X - rays than the second and and third row transition metals, hence significant intensities are expected for the 220 reflection in these tetrafluorides. This is, in fact observed for Re, Ir, Pd, and Pt tetrafluorides, however, in RhF_4 this reflection is very weak[21] and in OsF_4 it is not present at all. This is not yet fully understood, but does indicate that an ordered PdF_4 - type structure is not appropriate. The two fluorides have very similar powder patterns, the lines of which are broad, background heavy, and line intensity decreasing markedly with 2θ increase. All of this hints at substantial disorder in both the RhF_4 and OsF_4 structures. The view of the PdF_4 structure down the 110 plane seen in Fig. 4.4 shows the connectivity of that structure along the *c* axis arising because all the unique F ligands are on the same side of all octahedra (this is a polar space group). This connectivity can be broken by alternating the unique F ligands up and down (Fig. 4.5) thus creating a two dimensional slab. A somewhat disordered arrangement of such 2 - dimensional slabs could account for the absence of the 220 reflection. The first requirement to settle this structural problem is more crystalline RhF_4, or OsF_4. This is not a simple task, since even the high temperature synthesis[28] of RhF_4 described by Rao, resulted in poorly crystalline material which was not significantly better than that produced by the low temperature route. In any event, the apparent isomorphicity of the unit cells strongly suggests similar distances of M - M closest approach and hence similar M - F - M bridge bonding.

The change observed in the M - F - M bridge angle in the trifluorides and pentafluorides can be correlated with the t_{2g}^* antibonding orbital population across the transition series. For the most part, linear bridged fluorides exist for d^0 and d^1 configurations, d^2 systems involve bridges with ≈ 150° angles, and complexes with an electron configuration of d^3 or higher generate bridging angles closer to 135° , nearly that of ideal hcp systems. A similar trend is now partially observed for the tetrafluorides (although d^1 VF_4 contains M - F - M bridges of 151°). NbF_4 with a d^1 configuration contains linear bridges, while tetrafluorides with 3 or more t_{2g}^* electrons all adopt structures where M - F - M bridging angles close to 135° must pertain. If in fact it is antibonding π orbital filling which is causing this dramatic change in bridging angle, then only a very small energy difference between the linear bridged ccp based structures and the bent bridged hcp based structures is indicated, since antibonding π effects are expected to be small in transition metal fluorides where orbital overlap is poor.

A perplexing problem encountered during this study was the appearance of different structure types for the low spin d^4 tetrafluorides RuF_4 and OsF_4 with *trans* and *cis* dispositions of the unique F ligands, respectively. RuF_4 has a distorted SnF_4 type sheet structure with the two unique F ligands located *trans* to each other and an M - F - M bridge angle of 133°, resulting in the puckering of the sheet. The X-ray powder data for OsF_4, however, can be indexed on the basis of an orthorhombic PdF_4 type cell, suggesting a *cis* disposition of the two unique F ligands as well as a M - F - M bridge angle which must be close to 135°. Ligand - Ligand repulsions are expected to provide the primary influence in determining which conformation is preferred, *cis* interactions playing the most important role. The *cis* interactions can be ranked in descending order of their unfavorable repulsions as follows: short - bond/short - bond > short - bond/long - bond > long - bond/long - bond. This order of steric effects is indicated in the structures of the RuF_5 and RhF_5 tetramers(chapter 4). In the tetrafluorides the conformation placing the two unique

F ligands in *trans* positions allows for no *cis* short - bond/short - bond F interactions and 8 cis short - bond/long - bond interactions. The *cis* conformation contains 1 *cis* short - bond/short - bond interaction, but only 6 *cis* short/long - bonded interactions. Since RuF_4 and OsF_4 involve similar d^4 electron configurations and have similar formula unit volumes (indicative of similar atom sizes) it can only be supposed that changes in the polarity of the M - F bonds (RuF_4 is likely to have lower bond polarity) favors one arrangement over the other. The energy difference must be subtle, yet decisive, since there has never been any hint of RuF_4 adopting the PdF_4 - type structure.

Among the third row transition metals only the *cis* conformation has been observed thus far (although the OsF_4 structure is not known in detail), the PdF_4 structure maintained for d^3 ReF_4 through d^6 PtF_4. Only a slight increase is expected in all M - F interatomic distances over those of the second transition series based on larger M(IV) cores for the third series transition metals, but this may serve to weaken the single *cis* short - bond/short - bond repulsive interaction enough that the *cis* conformation, which is already probably slightly lower in energy in the second transition series, is favored exclusively in the third series, perhaps even for d^4 OsF_4. Unfortunately, no data are available for TaF_4 and WF_4.

References

1. Hepworth, M.A.; Jack, K.H.; Peacock, R.D.; Westland, G.J. *Acta Crystallogr.* **1957**, *10*, 63.

2.Pouchard, M., Torki, M.R., Demazeau, G., Hagenmüller, P., *C.R. Hebd. Sceances Acad. Sci. Ser.* **1971**, *C273*, 1093.

3. LaValle, D.E., Steele, R.M., Wilkinson, M.K., Yakel, H.R. Jr., *J. Am. Chem. Soc.*, **1960**, *82*, 2433.

4. Grosse, L; Hoppe, R., *Z. Anorg. Allg. Chem.* **1987**, *552*, 123.

5. Bartlett, N.; Rao, P.R. *Proc. Chem. Soc.* **1964**, 393.

6. Tressaud, A.; Pintchovski, F.; Lozano, L.; Wold, A.; Hagenmuller, P. *Mater. Res. Bull.* **1976**, *11*, 689.

7. Edwards, A.J. *Adv. in Inorg. Chem. and Radiochem.* **1983**, *27*, 83.

8. Edwards, A.J., *J. Chem. Soc.* **1964**, 3714.

9. Edwards, A.J.; Peacock, R.D., Small, R.W.H., *J. Chem. Soc.*, **1962**, 4486.

10. Edwards, A.J.; *J. Chem. Soc. A* **1969**, 909.

11. Edwards, A.J.; Jones, G.R.; *J. Chem. Soc. A* **1969**, 1651.

12. Chapter 3 of this work.

13. Morrell, B.K.; Zalkin, A.; Tressaud, A.; Bartlett, N., *Inorg. Chem.* **1973**, *12*, 2640.

14. Mitchell, S.J.; Holloway, J.H. *J. Chem. Soc. A* **1971**, 2789.

15. P. R. Rao, Ph.D. Thesis, University of British Columbia, 1964.

16. Müller, B.G.; Serafin, M. *Eur. J. Solid State Inorg. Chem.* **1992**, *29*, 625.

17. Gortsema, F.P.; Didchenko, R. *Inorg. Chem.* **1965**, *4*, 182.

18. Wright, A.F.; Fender, B.E.F.; Bartlett, N.; Leary, K. *Inorg. Chem.* **1978**, *17*, 749.

19. Becker, S., and Müller, B.G., *Angew. Chem. Int. Ed.* **1990**, *29*, 406.

20. Burbank, R.D.; Bensey, F.N. *U.S. At. Energy Comm. Rep.* **1956**, K - 1280.

21. Rao, P.R.; Tressaud, A.; Bartlett, N. *Inorg. Nucl. Chem. Lett.* **1976**, 23.

22. Colton, R.; Canterford, J.R. "Halides of the Second and Third Transition Metals," p. 3, Wiley, London, 1968.

23. Muetterties, E.L.; Castle, J.E. *J. Inorg. Nucl. Chem.* **1961**, *18*, 148.

24. Hargreaves, G.B.; Peacock, R.D. *J. Chem. Soc.* **1960**, 1099.

25. Payne, R.T; Asprey, L.B. *Inorg. Chem.* **1974**, *13*, 1529.

26. Sharpe, A.G. *J. Chem. Soc.* **1953**, 197.

27. Bartlett, N.; Tressaud, A. *C.R. Hebd. Seances Acad. Sci., Ser. C,* **1974**, *278*, 1501.

28. Rao, P.R. Ph.D. Thesis, University of British Columbia, 1964.

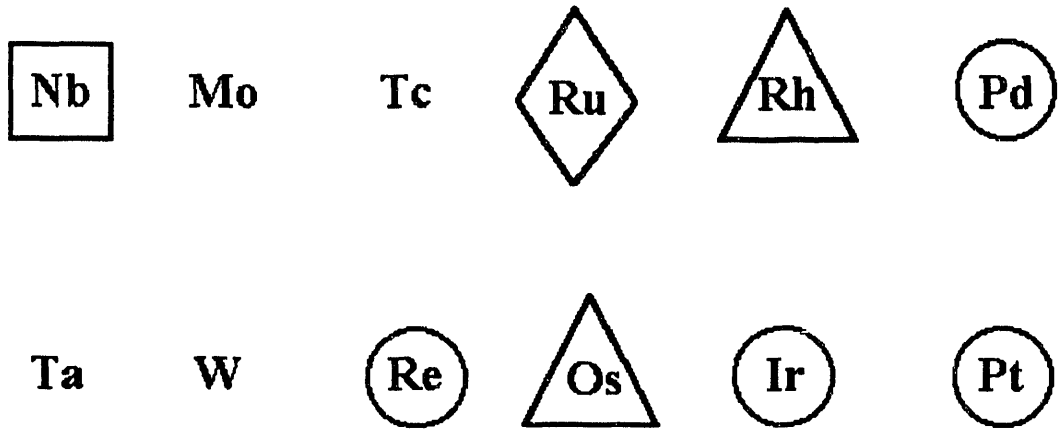

Figure 4.1. Observed structure types of the second and third transition series tetrafluorides. SnF_4 type, (□), ref. 15; RuF_4 type, (◊), this work; PdF_4 type, (○), ref. 16,22, and this work; possible PdF_4 type, Δ, ref. 22 and this work.

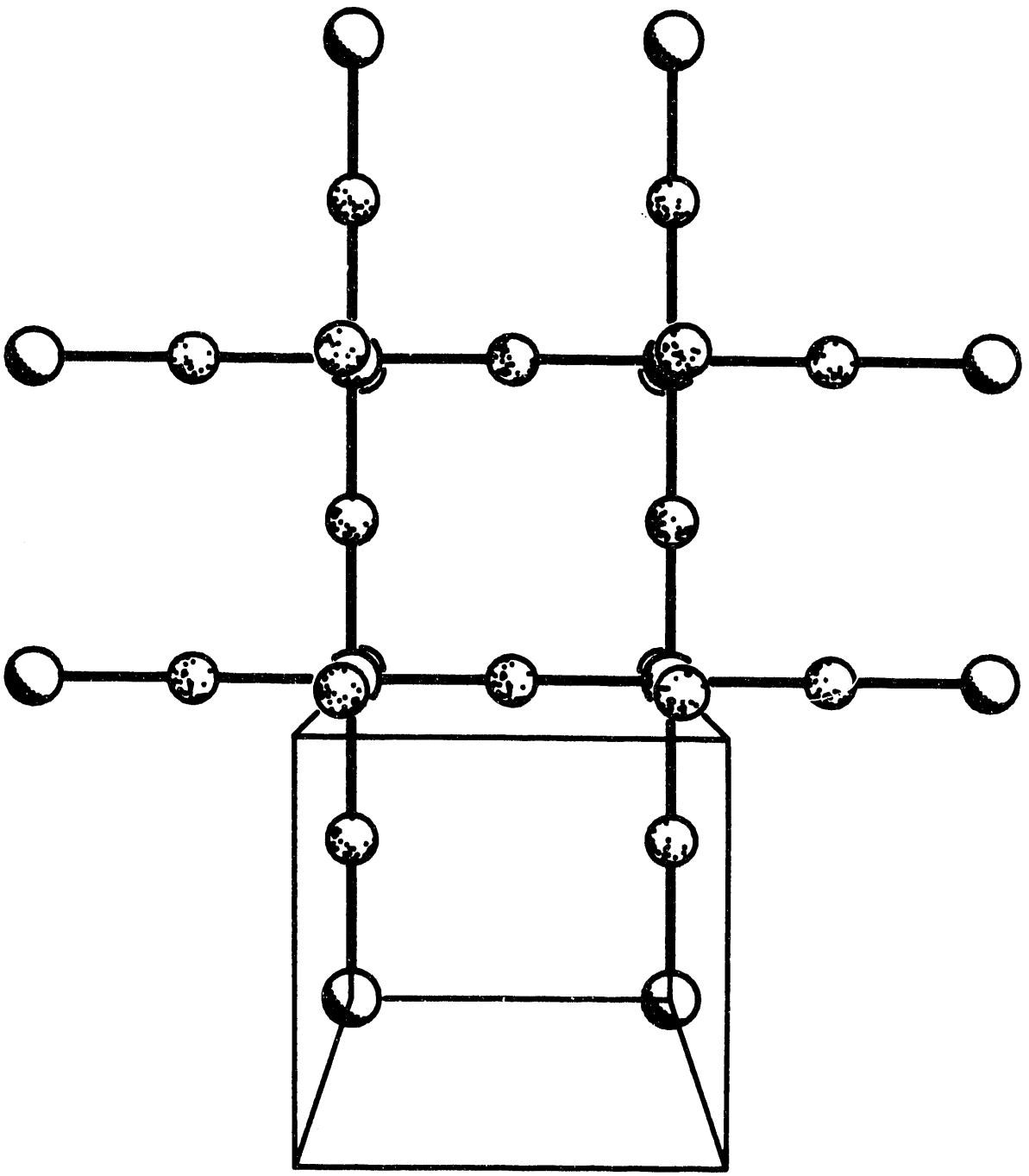

Figure 4.2 . The SnF_4 type structure.

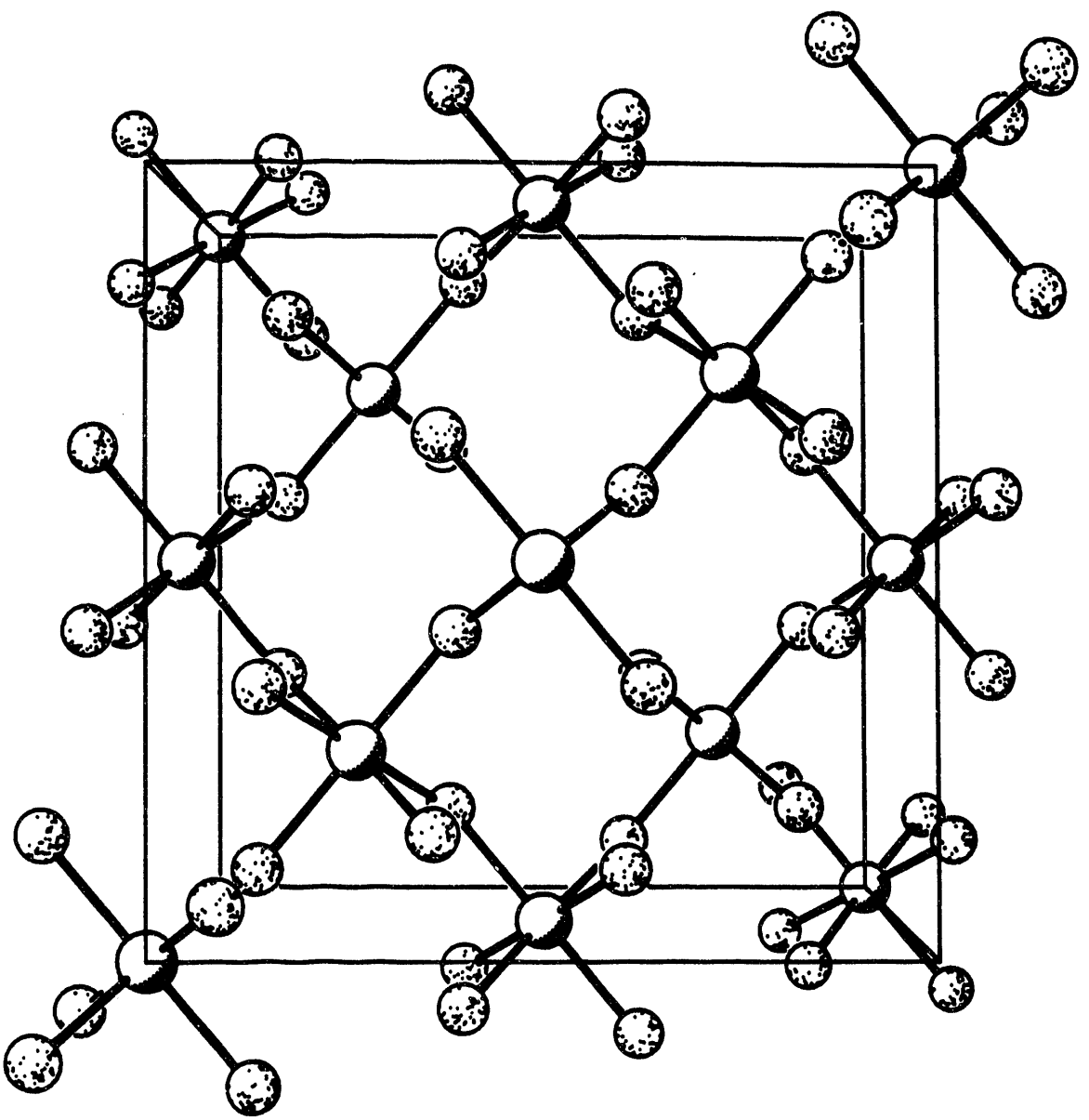

Figure 4.3. The PdF_4 structure viewed along the *c* axis.

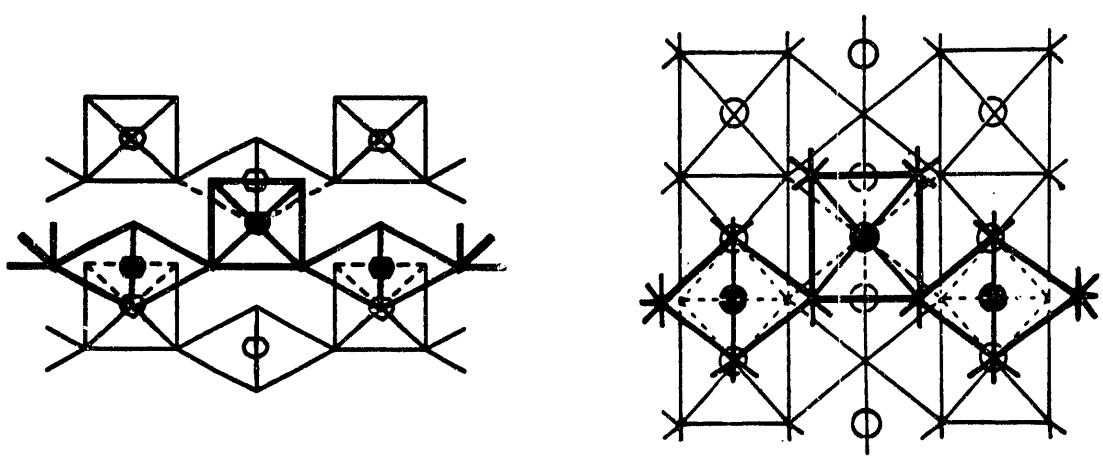

a b

Figure 4.4. View along the 110 plane of the PdF_4 type structure (a) and a comparison with the rutile structure (b).

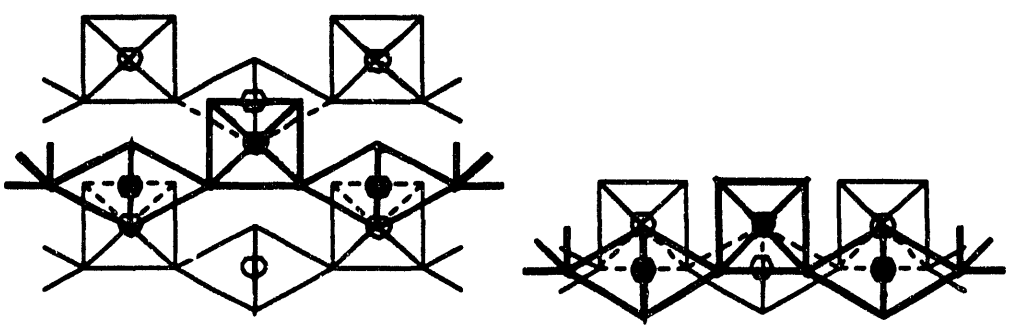

a b

Figure 4.5. The PdF_4 structure (a) in which all unique F ligands are pointed up with respect to the 110 plane and a section of 2 -D sheet (b) which would result if the placement of the unique F ligands was alternated up and down with respect to the 110 plane.

Chapter 5

Silver Trifluoride: Preparation, Crystal Structure, Some Properties, and Comparison with AuF_3

Introduction

Some interesting differences are observed in the high oxidation state chemistry of the coinage metals, silver and gold. Gold is easily oxidized to Au(III) and several complex ternary fluorides as well as neutral AuF_3 are known.[1] Under more rigorously oxidizing conditions, Au(V) can be obtained as the hexafluoroaurate(V), AuF_6^- anion.[2] Thermal decomposition of the dioxygenyl salt containing this anion, $O_2^+AuF_6^-$, has even afforded small quantities of neutral AuF_5.[3] Obtaining similar levels of oxidation in silver has proven much more difficult. Conditions similar to those which produce Au(V) salts were employed by Hoppe to produce the first Ag(III) salts.[4] The majority of such salts contained Ag(III) as the square tetrafluoroargentate ion, AgF_4^- and were found to be isomorphous with the analogous AuF_4^- salts and similarly diamagnetic, but Hoppe and Homann[5] have described Cs_2KAgF_6 which has the elpasolite structure with octahedrally coordinated Ag(III) and a ground state triplet d^8 electron configuration.

X - ray powder data had indicated significantly smaller formula unit volumes in the Ag(III) compunds with respect to the Au(III) compounds. Subsequent structure determinations by Hoppe and Homann indicated that at least a portion of this volume decrease could be attributed to M - F bond shortening in the square planer MF_4^- units of the silver compounds; Ag - F = 1.90Å; Au - F = 2.00Å.[6] Such bond shortening can only account for roughly 1/3 of the volume decrease, however. It is likely that the greater electronegativity of the Ag(III) metal center which results in shorter more covalent M - F bonds is also reducing the spacial extension of the remaining Ag(III) valence electrons,

principally that of greatest steric effect, d_z^2.

Compounds containing Ag(V) have been claimed by Hagenmuller et al.,[7] however Žemva et al. have shown that even the most powerful oxidizing agents known, the krypton fluoride oxidizers, give no further oxidation of Ag(III) even though Au(V) is readily produced by these reagents.[8]

As F ligands (non - bridging) are added to a central atom, the electronegativity of that atom must increase. Probably as a consequence of strong F - F repulsions, the coordination rarely exceeds six and octahedral coordination is commonly encountered, particularly with the less electropositive transition elements. Very high oxidation states are much more stable as anions, the additional electron density effectively reducing the electronegativity of the coordination center. Neutral systems of the same high oxidation state are consequently more difficult to obtain and can be thermodynamically unstable, yet preparable.

In 1983 Bougon reported that AgF_3 could be obtained from the room temperature fluorination of silver or lower silver fluorides using KrF_2 in AHF.[9] The material obtained, however, was not isomorphous with AuF_3. Furthermore, it was paramagnetic,[10] indicating that it could not be a low spin d^8 system as is AuF_3. Hoppe and Homann had demonstrated the existence of high spin Ag(III) in Cs_2KAgF_6, indicating that the high spin octahedral conformation of Ag(III) is close energetically to that of low spin, square planer Ag(III). Kiselev et al. subsequently reported a similar preparation of AgF_3 from the fluorination of AgF_2 with O_2F_2, which is comparable to KrF_2 as a F atom source. A hexagonal unit cell, not isomorphous with AuF_3 was reported for this material, but no magnetic data were given.[11] The Kiselev et al. diffraction data indeed bore a close resemblance to those given by Bougon and his coworkers.

In an effort to test the validity of a radically different structure for AgF_3 from that already established[12] for AuF_3 an independent synthesis was sought. The ability of strong

fluoroacids to displace binary fluorides from their parent fluoroanions, Chapter 4, suggested that similar removal of F^- from AgF_4^- salts, which are readily characterized and obtainable in high purity, would afford high purity AgF_3. This has proved to be so.

Experimental

Materials. KNO_3, $AgNO_3$ (Fisher Scientific, Fair Lawn, NJ) and Au powder (LBL stores)were used as supplied. $PdBr_2$ [13] and AgF_2 [14] were prepared by literature methods. The preparation of $AgFAsF_6$ will be described in Chapter 6.

Preparation of $KAgF_4$: Roughly 1:1 mixtures of KNO_3 (1.81g, 17.9mmol) and $AgNO_3$ (2.86g, 16.8mmol) were ground together with a mortar and pestle before being loaded into the nickel insert of a high pressure Monel Parr bomb equipped with an Autoclave Engineering valve. The nitrate salts were heated above their eutectic melting point to ≈150 °C for thirty minutes. On cooling, the Ni insert was placed inside the Parr bomb which was then sealed with a copper gasket and shown to be leak free with a He leak detector prior to the fluorination step. It was evacuated on a stainless steel vacuum line and cooled in liquid N_2 to condense in 33mmol of F_2 which resulted in a pressure of 30 atm at room temperature. The bomb was heated in a sand bath to between 350 and 400 °C for 24 h. At this time the reactor was cooled to to room temperature and volatile materials were evacuated through the soda - lime scrubber. A second aliquot of F_2 was added followed by a second heating cycle. After similar cooling and removal of the volatiles the bomb was opened in the DRILAB to reveal a bright orange solid admixed with a small amount of brown solid. The crude product was loaded into one arm of a two armed teflon tee reactor and removed to a vacuum line where 7 ml AHF was condensed in at -196 °C. On warming a deep orange solution formed over the brown solid. Successive washings by decantation

of the orange solution freed bright orange $KAgF_4$ (2.1g, 9.4 mmol; 56 % yield)from the brown insoluble solid which proved, by X - ray powder diffraction, to be largely AgF_2. Usually X-Ray powder photographs of the washed material could be indexed completely on the basis of the tetragonal $KAgF_4$ pattern.[6] However small amounts of KHF_2 were present as a consequence of AgF_2 formation. Some of the KHF_2, being much more soluble than $KAgF_4$, could be removed by washing the contaminated $KAgF_4$ with successive small amounts of AHF at ≈ 0 °C. However, when the F^- concentration became too low in the AHF, partial solvolysis of the $KAgF_4$ to AgF_3 and KF was observed to occur, so KHF_2 could not be completely removed in this manner.

Preparation of AgF_3: In the DRILAB $KAgF_4$, usually 600mg (? 7 mmol) was loaded into one arm of a two armed teflon tee reactor which had been passivated with 2 atm F_2 for several hours. The reactor was attached to an all Teflon - FEP manifold of the vacuum line and evacuated. AHF, 6ml, was condensed on to the $KAgF_4$ by cooling to -196 °C. On warming to room temperature, a small amount of red brown precipitate (presumed to be AgF_3 formed by solvolysis) formed in an orange solution. When this material had settled, the orange solution was decanted into the free arm of the reactor. BF_3 was slowly admitted and immediately a bright red precipitate began to form. Addition of BF_3 was continued until the supernatant solution was colorless. Even in the presence of excess BF_3, no further reaction with the AgF_3 was observed. The AgF_3 was washed free of KBF_4 by decantation of the supernatant AHF solution into the other arm of the reactor. This AHF was distilled back on to the AgF_3 by cooling it to -196°. This decantation and back distillation procedure was done 8 times, quickly to minimize decomposition of the AgF_3 in AHF at room temperature. AHF was removed through the soda - lime scrubber under dynamic vacuum, the AgF_3 product being finally dried by evacuation through the main trap. Usually 400mg (2.4 mmol) AgF_3 was obtained, some being lost in the

decantation process. X - Ray powder patterns showed no KBF_4 and indicated that AgF_3 was isomorphous with AuF_3. The analysis of AgF_3 was performed in the laboratories of Žemva et al.[15] They measured, by tensimetry, the quantity of F_2 liberated by AgF_3 as it decomposed in AHF over 19 h and found it to correspond to: $3AgF_3 \rightarrow Ag_3F_8 + 1/2F_2$. The composition of Ag_3F_8 for the thermal decomposition product was determined directly by their analysis and from its synthesis by other routes in this work(q.v.). The diamagnetism of the material freshly precipitated (with BF_3) was measured in these laboratories and its close structural relationship with AuF_3 (q.v.) combined with these other observations settled the composition as AgF_3.

Synchrotron X-ray Powder Diffraction Data Collection and Structure Analysis for AgF_3. X - Ray synchrotron powder diffraction data were collected at Brookhaven National Laboratory by Dr. David Cox and Dr. Angus Wilkinson who also analyzed the data. A wavelength of 1.24805 Å was employed as a compromise between the conflicting requirements of minimizing the sample absorption, maintaining reasonable pattern resolution and operating at an energy where the X-ray source had a high output. The data collected showed Bragg peaks with FWHM's greater than 0.18° which is considerably in excess of instrumental resolution. All the peaks in the pattern, with the exception of a single weak line, were indexed on a hexagonal unit cell, a = 5.0753(3) Å, c = 15.448(1) Å, (see Table 5.1) similar to that of AuF_3.[12] The unindexed diffraction maximum at d ~ 3.7 Å is attributable to the strongest Bragg reflection of a small amount of Ag_3F_8 impurity, this particular AgF_3 sample having been prepared (q.v.) using AsF_5.

Table 5.1. X-Ray Powder Data for AgF_3[a] (Synchrotron Radiation, λ = 1.24805 Å)

h, k, l	I/I_o	$1/d^2 \times 10^4$ obsd	$1/d^2 \times 10^4$ calcd
100	31	518	518
101	21	560	560
102	19	685	685
103	100	895	895
104	6	1187	1188
006	5	1508	1509
110	10	1550	1553
105	10	1565	1565
111	5	1596	1595
112	12	1720	1720
113	2	1928	1930
106	10	2026	2026
200	5	2070	2070
114	1	2213	2223
202	19	2239	2238
203	3	2447	2448
107	4	2575	2571
115	25	2602	2600
204	16	2742	2741
116	12	3061	3062
108	3	3200	3200

[a] Hexagonal unit cell with (20°C) a_o = 5.0753(3)Å, c_o 15.448(1) Å, V = 344.62(7) $Å^3$; z = 6; space group $P6_122$ - D_6^2 or $P6_522$ - D_6^2.

Neutron Powder Diffraction Data Collection and Structure Analyses for AgF_3 and AuF_3. Drs. Horst Bormann, Angus Wilkinson, and Robert Von Dreele were involved in the data collection and analysis with this worker. Details of the data collection are given in Table 5.2. The High Intensity Powder Diffractometer (HIPD) was chosen because the extremely high incident neutron intensity afforded the possibility of using small samples of these very reactive fluorides. The success of this approach can be seen in the quality of the diffraction patterns (Fig. 5.1). The data collected in this way showed peaks down to ~0.6 Å d-spacing all of which are fitted quite closely by the Rietveld refinement procedure and afforded a precise structure determination of both AgF_3 and AuF_3.

Both structures were refined with the package GSAS[16] using neutron diffraction data collected at both ±153° 2θ for d-spacings >0.6 Å. The results are given in Table 5.3. In both cases Fourier Series were used for the background and absorption coefficients were refined for each data set. For AgF_3 an extinction coefficient was also refined; the value, 38(8)μm^2, indicates that the average grain size was ~6μm. No extinction effects were observed for AuF_3. The peak profiles were considerably broadened and thus some of the coefficients of the peak shape function were also refined. Their values indicate that both materials exhibit a substantial degree of microstrain particularly perpendicular to the hexagonal axis.

Table 5.2. Details of the Neutron Diffraction Data Collection for AgF_3 and AuF_3

Instrument employed	Los Alamos National Laboratory Manuel Lujan, Jr. Neutron Scattering Center High Intensity Powder Diffractometer (HIPD)
Sample	100 mg AgF_3 contained in two 2.0mm diameter quartz capillaries, sample length ~35mm. 100mg AuF_3 contained in a 2.0mm diameter quartz capillary, sample length ~35mm.
Diffraction geometry	9.0m initial flight path, 1.25m secondary flight paths to 4 each 1/2 x 12" 10atm ^3He detectors at ± 153° 2θ.
Data collection	0.6 Å ≤ d ≤ 4.8 Å in ~3800 constant _t/t steps for 10.85 hrs. at 71.2μA beam current for AgF_3 and for 4.19 hrs. at 70.19μA for AuF_3. Range included 275 reflections for AgF_3 and 298 reflections for AuF_3.

Table 5.3. Final models from Neutron Diffraction Structure Refinements for AgF_3 and AuF_3.

	AgF_3[a]	AuF_3
Space Group	$P6_122$	$P6_122$
a/Å	5.0782(2)	5.1508(1)
c/Å	15.4523(8)	16.2637(7)
abs,+153°	-0.023(5)	0.291(14)
abs,-153°	-0.028(5)	0.265(13)
ext/μm^2	38(8)	0
profile coefficients		
σ_1^2/$\mu s/Å)^2$,+153°	77(4)	50(3)
σ_1^2/$\mu s/Å)^2$,-153°	119(5)	91(4)
σ_{1a}^2/$\mu s/Å)^2$,+153°	-17(9)	-26(5)
σ_{1a}^2/$\mu s/Å)^2$,-153°	-18(12)	-45(8)
A in 6(b):x,2x,1/4; x	0.2694(4)	0.2399(3)
$U_{iso}/Å^2$	0.0112(9)	0.0111(8)
F(1) in 6(a):x,0,0; x	0.2176(8)	0.1639(8)
$U_{iso}/Å^2$	0.0233(12)	0.0215(12)
F(2) in 12(c):x,y,z; x	0.8401(7)	0.7761(6)
y	0.3186(10)	0.3099(7)
z	0.0054(2)	0.0053(2)
$U_{iso}/Å^2$	0.0350(11)	0.0328(10)
R_{wp}	6.21%	11.21%
R_p	3.83%	7.58%
χ^2	1.327	1.175

[a] The lattice constants for AgF_3 are slightly larger from the neutron experiment than from the synchrotron experiment. This difference is probably due to the slightly higher temperature in the neutron case and to the difficulty in estimating the exact scattering center in a time-of-flight experiment. As we are mainly interested in comparing AgF_3 and AuF_3, we have used the neutron data for calculating distances and angles.

Interaction of AgF_3 with AsF_5 in AHF AgF_3 (708.9 mg, 4.30 mmole) in AHF (~ 3 ml was exposed to AsF_5 (>>4.30 mmole) at ~20°C, rapid dissolution of the AgF_3 occurred, to produce a deep blue solution, this being accompanied by the evolution of gas which was not condensable at -196°C. This gas was shown to be F_2 by its quantitative interaction with clean Hg. Removal of AHF under vacuum yielded a deep blue solid. The

X - ray powder data of this material was indexed completely on the of basis the cell obtained by Gantar et al. (see Chapter 6) for $AgFAsF_6$.[17]

Preparation of $Ag(II)Ag(III)F_5$: $KAgF_4$ and $AgFAsF_6$ in AHF. $KAgF_4$ (238 mg,1.07 mmole) dissolved in AHF(5 mL) contained in one leg of the FEP T apparatus, was poured, at 20°C, slowly into a solution of $AgFAsF_6$ (346 mg, 1.10 mmole) in AHF(~ 5 mL) in the leg at right angles to it. A maroon solid precipitated immediately. Some of the AHF was back distilled into the $KAgF_4$ leg to wash any remaining $KAgF_4$ into the mixture. When the transfer of that salt was complete the supernatant AHF solution was colorless. This colorless supernatant AHF was then decanted into the empty leg of the T and the AHF back vacuum distilled on to the maroon residue to wash that solid free of $KAsF_6$. The washing cycle was repeated 10 times and the AHF was then removed under vacuum at 20°C. An X-Ray powder photograph of the maroon solid showed a sharp strong-line pattern of a new phase. Lines of $KAsF_6$, AgF_3 and AgF_2 were absent. Data are given in Table 5.4. The weight of the solid (326 mg) was appropriate for an almost quantitative yield of Ag_2F_5 (1.05 mmole).

Table 5.4. X-Ray Powder Data for $Ag^{II}Ag^{III}F_5$ (CuK<α> Ni Filter) at 293K

I/I_o	$(1/d^2) \times 10^4$(obsd)	I/I_o	$1/d^2) \times 10^4$(obsd)
vw	512		
s	670	ms	2882
vs	755	m	3049
s	896	vvw	3129
m	979	vw	3204
vvw	1068	vw	3294
s	1128	vvw	3366
ms	1245		

Table 5.4. cont.

I/I_o	$1/d^2 \times 10^4$(obsd)	I/I_o	$1/d^2 \times 10^4$(obsd)
ms	1295	ms(br)	3573
m	1445	ms	3729
m	1575	vvw	3912
ms	1737	vvw	4101
vvw	1915	vvw	4217
vw	1956	vvw	4319
w	2109	vvw	4498
s	2199	vw	4790
vvw	2340	vvw	4982
vw	2470	vvw	5234
vvw	2646	vvw	5424
vw	2732		

Preparation of $Ag(II)Ag(III)_2F_8$: (a) $KAgF_4$ with $AgFAsF_6$ and BF_3. $KAgF_4$ (412 mg, 1.85 mmole) dissolved in AHF (~ 3 mL) in one leg of an FEP T apparatus, was added slowly to a blue solution of $AgFAsF_6$ (313 mg, 0.99 mmole) dissolved in AHF (~ 5 mL). Immediate precipitation of a maroon solid (probably Ag_2F_5) occurred, the supernatant AHF solution retaining the orange coloration of dissolved AgF_4^-. To this mixture was then slowly added BF_3 with brisk stirring. The suspended solid rapidly became deep red-brown in color, as the AgF_4^- in the AHF was replaced by BF_4^-, and at the end-point the supernatant AHF was colorless. This AHF solution (containing $KAsF_6$ and KBF_4) was decanted into the other leg of the FEP T, and the washing of the precipitate was carried out, as in the preparation of Ag_2F_5. X-Ray powder photography showed that the well-washed solid was free of $KAsF_6$ and KBF_4. There were no traces of Ag_2F_5, AgF_3 or AgF_2 and the pattern matched that of the product of the decomposition of AgF_3 in AHF and is given in Table 5.5. The yield of washed Ag_3F_8 was 400 mg (0.84 mmol) 91%. **(b) Ag_2F_5 and AgF_3 in AHF.** A sample of Ag_2F_5 (180 mg, 0.57 mmole) was mixed with an equimolar quantity of AgF_3 (93 mg, 0.57 mmole) in an FEP tube and AHF (6 mL) was vacuum distilled on to the mixture, which was then briskly stirred at ~20°C. The color quickly changed to deep red-brown characteristic of Ag_3F_8 and the AHF was removed

under dynamic vacuum after 1 hr. X-Ray powder photography (see Table 5.5) established that this material was identical with that formed in preparation (a) and in the decomposition of AgF_3 in AHF. No other silver fluorides were present. The stoichiometry of this preparation and that of preparation (a) confirmed that the composition must be Ag_3F_8.

Table 5.5. X-Ray Powder Data for Ag_3F_8 (CuK<α>, Ni Filter) at 293K

I/I_o	$(1/d^2) \times 10^4$(obsd)	I/I_o	$(1/d^2) \times 10^4$(obsd)
w	321	vw	2410
ms	482	vw	2477
mw	673	ms	2706
m	694	s(br)	2944
vvs	740	m	3269
m	839	m	3457
ms	920	m	3524
mw	985	ms	3682
vs	1087	m	3785
mw	1142	s(br)	3830
w	1322	m	3924
m	1382	ms	4180
w	1477	ms	4340
ms(br)	1603	m	4555
m(br)	1706	m	4686
ms	1840	m(br)	4891
s(br)	1940	vw	5296
vw	2038	vw	5504
m	2215		
mw	2301		

Interaction of AgF_2 with AgF_3 In a reaction designed to remove AgF_3 from a sample of Ag_3F_8, 245mg of the Ag_3F_8/AgF_3 mixture was loaded into a one armed teflon/FEP reactor along with 45mg (mmol) AgF_2. The reactor was attatched to the teflon manifold of the vacuum line, evacuated, and charged with 5ml AHF at -196 °C. On warming to room temperature, the reactor was agitated for 1 hour, the sample becoming noticeably

more brown during this time. The solvent was evacuated through the soda - lime scrubber and the sample dried for several hours under dynamic vacuum. No weight change was observed in the products. X - Ray powder photographs showed largely Ag_3F_8 and a small amount of AgF_2. No lines attributable to Ag_2F_5 were observed.

Preparation of $Pd(AuF_4)_2$: In the DRILAB, one trap of a set of two pyrex traps in series was loaded with a 1:2 (0.8 mmol) mixture of $PdBr_2$ and Au metal. The traps were fitted with Whitey valves and removed to a stainless steel vacuum line where an excess of BrF_3 was condensed on to the reactants under static vacuum by cooling the trap to -196 °C. On warming to room temperature, a vigorous reaction ensued with Br_2 evolution. The reaction was heated with a heat gun, the Br_2 formed being condensed into the second trap by intermittant cooling with liquid N_2. After 10 min, the second trap was held at -196 °C while the heating of the first trap was continued in order to remove excess BrF_3. Final traces of BrF_3 were removed from the heated lime - green product under a dynamic vacuum. The trap containing the product was sealed off under vacuum using a gas/oxygen flame. X - Ray powder photographs were indexed on the basis of the orthorhombic cell given by Müller for[18] $Pd(AuF_4)_2$. Although the X - ray powder pattern for this material exhibited some similarities to that for Ag_3F_8 the structures are evidently not closely related.

Magnetic Susceptibility of Ag_3F_8. A sample of Ag_3F_8 (181 mg 0.380 mmole), prepared by route (a), was encapsulated in a Kel-F capsule previously passivated with F_2 and AsF_5. Magnetic susceptibility measurements made, at both 5 and 40 kGauss, over the temperature range 6 to 280°K, obeyed the Curie-Weiss law, with a Weiss Constant θ = -4.2(5)°, the susceptibility being field independent. The data are shown in Fig. 5.2. The effective magnetic moment μ_{eff} = 1.924(3) B.M.

Results and Discussion

Bright red, diamagnetic AgF_3 has now been obtained via fluoride ion capture from tetrafluoroargentate salts according to the equation

$$AgF_4^- + A \xrightarrow{AHF} AgF_3 + AF^- \qquad (1)$$

where A = AsF_5, BF_3

The material is thermodymically unstable at room temperature and loses fluorine according to the equation

$$3AgF_3 \xrightarrow{AHF} Ag_3F_8 + 1/2F_2 \qquad (2)$$

This decomposition in AHF, occurs quantitatively in less than 24 h, but dry samples of AgF_3 exhibit considerable kinetic stability, no noticeable decomposition occuring over several months in the DRILAB, nor over several hours of intense synchrotron X - Ray radiation. The decomposition product, Ag_3F_8, is a red - brown solid which gives an X - Ray powder pattern identical to that obtained for the material described by Bougon as AgF_3.

The ability of BF_3 to carry out reaction (1) suggests that AgF_3, like other transition metal trifluorides, is a relatively weak Lewis acid, particularly when compared with the pentafluorides and tetrafluorides. Žemva et al.[8], however, have observed an equilibrium in reaction (1) when PF_5 is used in conjunction with $XeF_5^+AgF_4^-$

$$XeF_5^+AgF_4^- + PF_5 \xleftrightarrow{AHF} AgF_3 + XeF_5^+PF_6^- \qquad (3)$$

which only favors AgF_3 production in the presence of an overpressure of PF_5. Thus AgF_3 must be comparable with PF_5 in acidity and must be a significantly stronger acid than AuF_3 which can be produced merely by the solvolysis of $XeF_5^+AuF_4^-$ in the weaker acid AHF:

$$XeF_5^+AuF_4^- + y\,HF \longrightarrow XeF_5^+F(HF)_y^- + AuF_3\downarrow \qquad (4)$$

Curiously, AgF_3 also appears to behave as a stronger base than AuF_3. This is suggested by the remarkable reduction of AgF_3 by strong Lewis acids, including AsF_5, which is itself a powerful oxidizer

$$AgF_3 + AsF_5 \xrightarrow{AHF} AgF^+AsF_6^- + 1/2F_2 \qquad (5)$$

A plausable mechanism for reaction (5) involves F^- capture from AgF_3 by AsF_5 to form $AgF_2^+AsF_6^-$. Such a reaction would place the Ag(III) in a cation. The electronegativity of Ag(III) in such a cation must be extremely high; so high, that it undergoes reductive elimination of fluorine to form the cationic Ag(II) salt, $AgF^+AsF_6^-$, which is itself, a powerful oxidizer (Chapter 7). There is some indication that AuF_3 reacts with very strong Lewis acids, however such reactions are very slow and have proven difficult to characterize. It is possible that the difference in reactivity of these trifluorides with strong acids is not a function of the basicity of the materials, but is due to the rapid decomposition, in acid solution, of any Ag(III) cation formed to very soluble cationic Ag(II) in AHF, from which Ag(III) cannot be regenerated. An Au(III) cation is certain to be much more stable with respect to fluorine elimination than the Ag(III) cation. No such decomposition has been observed for AuF_3.[19]

X - Ray powder photographs of AgF_3 obtained from reaction (1) indicated that

authentic AgF_3 was indeed isomorphous with AuF_3, the data being completely indexable on the basis of a hexagonal AuF_3 type cell . The subsequent structure determination of AgF_3 and redetermination of AuF_3 from neutron powder data confirmed that the two trifluorides have essentially the same structure Fig. 5.3. The structure consists of roughly square planer units which are joined by *cis* related F ligands to make helical chains of 6_1 symmetry, the unit cell containing 6 MF_3 formula units. The comparable interatomic distances (Table 5.6) within the MF_4 unit are not significantly different in the trifluorides. Similarly, the M - F - M bridges are significantly bent to $\approx 120°$, the angle in AgF_3 being slightly larger than that in AuF_3. The absence of any π bonding interaction (the antibonding π orbitals are completely filled) coupled with the near removal of the axial F ligands which allows for close approach of the canted MF_4 units, accounts for the very small bridging angle.

Table 5.6. Selected distances (Å) and angles (Deg.) for AgF_3 and AuF_3

	Ag	Au		Ag	Au
A(1)-F(1)x2	2.000(6)	2.04(3)	F(1)-A(1)-F(1)	88.5(5)	88(2)
A(1)-F(2)x2	1.883(8)	1.91(4)	F(1)-A(1)-F(2)x2	90.8(3)	90(2)
A(1)-F(2)x2	2.526(8)	2.69(4)	F(1)-A(1)-F(2)x2	179.21(1)	178(2)
			F(2)-A(1)-F(2)	89.9(5)	92(2)
A(1)-F(1)-A(1)	121.8(6)	116(3)	A(1)-F(2)-A(1)	139.7(5)	148(3)

The most remarkable difference in the two structures involves the weak linkages of adjacent helical chains. Unique F ligands of a chain are nearly normal to MF_4 planes of adjacent chains and serve to complete the grossly distorted octahedral arrangement of F ligands about each metal, Fig. 5.4. In AgF_3 this interatomic distance, termed M - F_{axial}, is 2.540(4)Å. This is significantly shorter than for the comparable weak bonding in AuF_3

where Au - F_{axial} = 2.761(3)Å. The closer approach of chains might be expected to hinder the approach of MF_4 units, and thus increase the M - F - M bridge angle in AgF_3.

The shorter M - F_{axial} bonds in AgF_3 and the reduction of its formula unit volume with respect to AuF_3 indicate much tighter binding of the remaining valence electrons in the Ag(III) compound. A comparison of formula unit volumes of Ag(III) and Au(III) compounds in Table 5.7 indicates smaller volumes for Ag(III) compounds in general. The difference is a constant 5Å^3 in the fluorides. These differences are in contrast to the effective volumes of Ag and Au atoms in the metallic elements, which are 17.05Å^3 and 16.97Å^3 respectively,[20] and nicely illustrate the impact of relativistic effects on gold. These effects result in significant stabilization and contraction of all s orbitals in Au with respect to the s orbitals in Ag, thus metallic Au is observed to be smaller than metallic Ag since the binding in the metal is primarily of s orbital character. The relativistic contraction of the s orbitals and to a lesser extent, the p orbitals, provides greater shielding for the d and f orbitals, thereby having the secondary effect of enhancing the size increase of the Au 5d orbitals over the 4d orbitals of Ag.[21] In the Ag(III)/Au(III) compounds the valence shell s electrons have been removed , so that it is this latter effect which is observed. The $4d_z^2$ electron pair in Ag(III) is much more contracted and hence much more tightly bound than in Au(III). These electrons are expected to be much more difficult to involve in bonding than the $5d_z^2$ electrons of Au(III) and in fact the most potent oxidative fluorinators known do not react with Ag(III), while they readily generate Au(V) complexes. The greater acidity observed above for AgF_3 can be accounted for along these lines as well. The vacant LUMO available for donation by a Lewis base, F^-, in these trifluorides is the $d_{x^2-y^2}$ orbital. The $4d_{x^2-y^2}$ orbital in AgF_3 is significantly contracted and hence of relatively lower energy, than the $5d_{x^2-y^2}$ orbital of AuF_3.

Table 5.7. Comparison of Formula Unit Volumes ($Å^3$) of Ag(III) and Au(III) Compounds

A	XeF_5AF_4	KAF_4	AF_3	$AO_{3/2}$
Ag	159.4[a]	97.0[b]	57.4[c]	61.9[e]
Au	164.5[a]	102.1[b]	62.2[d]	64.7[f]

ref. a = 7; b = 5; c = this work, d = 14; e = 22; f = 23

The final structural determination of AgF_3 was carried out using samples prepared with BF_3 because it was found that samples prepared with AsF_5 always contained small amounts of an insoluble paramagnetic impurity. It was believed that this material was associated with the reduction of AgF_3 to Ag(II) by AsF_5, since small amounts of blue material indicative of cationic Ag(II) were observed, which subsequently disappeared when excess AgF_4^- was present. In a separate experiment, shown in reaction (6), which was designed to mimic these conditions

$$2KAgF_4 + AgFAsF_6 + BF_3 \xrightarrow{AHF} Ag^{(II)}Ag^{(III)}{}_2F_8 + KAsF_6 + KBF_4 \quad (6)$$

two equivalents of $KAgF_4$ were reacted with one equivalent of cationic Ag(II) in the form of $AgFAsF_6$ in AHF acidified with BF_3. The insoluble red - brown solid which was produced gave an X-Ray powder pattern which was identical to those obtained for the material described by Bougon as AgF_3. It was also identical with the Ag_3F_8 decomposition product obtained by reductive elimination of fluorine from authentic AgF_3 in AHF. This material could also be obtained from a 1:2 mixture of AgF_2/AgF_3 in AHF according to the overall reaction:

$$AgF_2 + 2AgF_3 \xrightarrow{AHF} Ag_3F_8 \qquad (7)$$

Interestingly a 1:1 mixture of AgF_2:AgF_3 failed to give the 1:1 acid/base adduct $AgF^+AgF_4^-$ analogous to $AgF^+AsF_6^-$:

$$2AgF_2 + 2AgF_3 \xrightarrow{AHF} AgF_2 + Ag_3F_8 \qquad (8)$$

The 1:1 adduct, $Ag^{II}Ag^{III}F_5$ was obtained from $AgFAsF_6$ and $KAgF_4$ in AHF via

$$AgF^+AsF_6^- + KAgF_4 \xrightarrow{AHF} Ag^{II}Ag^{III}F_5 + KAsF_6 \qquad (9)$$

It appears that this salt, $AgF^+AgF_4^-$, is thermodynamically unstable with respect to AgF_2 and Ag_3F_8.

The ability of AgF_2 to act as a pseudo alkaline earth fluorobase, combined with the relatively good Lewis acidity of AgF_3 suggest a composition of $Ag^{II}(Ag^{III}F_4)_2$ for Ag_3F_8. The similarity in X - Ray powder data of this phase and $Pd^{II}(Au^{III}F_4)_2$, for which the structure is known also supports such a composition. More convincing, however, is the magnetic data. As expected Ag_3F_8 is paramagnetic. Moreover the variable temperature magnetic susceptibility data shown in Fig. 3 indicate that the material is a simple paramagnet, obeying the Curie law. The small Weiss constant, $\theta = -4.2(5)°$, indicates that the material is magnetically dilute and supports a composition of a single paramagnetic d^9 Ag(II) cation well separated from other Ag(II) cations by two diamagnetic AgF_4^- anions as in $Ag(AgF_4)_2$. The observed magnetic moment of 1.95(8) μ_β is identical to that reported by Bougon when "AgF_3" is adjusted to the Ag_3F_8 formula. The identical X-Ray and magnetic data prove that AgF_3 as described by Bougon et al. is in fact the lower fluoride Ag_3F_8.

Conclusions

The synthesis of high purity AgF_3 by fluoride ion capture from the anion demonstrates the primary utility of the Lewis acid displacement of binary fluorides, namely the synthesis of thermally unstable, high oxidation state systems. Because AgF_3 is thermally unstable at room temperature or any temperature sufficiently high to activate the known oxidative fluorinators, it cannot be synthesized by oxidation of a lower fluoride. However, by obtaining the high oxidation state first as the more stable fluoroanion, in this case AgF_4^-, heretofore inaccessible oxidation states in neutral systems can be obtained.

As expected authentic AgF_3 is isostructural with AuF_3. A comparison of structural data on these as well as other Ag(III)/Au(III) suggest the impact of relativistic effects on gold, which in turn help to explain the abundance of Au(V) chemistry in the absence of any such chemistry for silver.

The existence of two mixed valence silver fluorides has been demonstrated, with 1:1 and 1:2 Ag(II):Ag(III) ratios. The 1:2 compound, Ag_3F_8, is identical to that described previously by Bougon et al as AgF_3.

References

1. Müller, B.G. *Angew. Chem. Int. Ed. Eng.* **1987**, *26*, 1081.
2. Bartlett, N.; Leary, K. *Rev. Chim. Minér.***1976**, *13*, 82.
3. Edwards, A.J.; Falconer, W.E.; Griffith, J.E.; Sunder, W.A.; Vasile, M.J. *J.Chem. Soc. Dalton Trans.* **1974**, 1129.
4. Hoppe, R., *Z. Anorg. Chem.* **1957**, *292*, 28.
5.Hoppe, R.; Homann, R., *Naturwissenschaften* **1966**, *53*, 501.
6. Hoppe, R.; Homann, R., *Z. Anorg. Chem.* **1970**, *379*, 193.

7. Sorbe, P.; Grannec, J.; Portier, J.; Hagenmuller, P. *C.R. Hebd. Séances Acad. Sci. Ser. C282* **1976**, 663.

8. Lutar, K.; Jesih, A.; Leban, I.; Žemva, B., and Bartlett, N., *Inorg. Chem.* **1989**, *28*, 3467.

9. Bougon, R.; Lance, M., *Comptes Rendus, Acad. Sci., Ser. 2* **1983**, *297*, 117.

10. Bougon, R.; Bai Huy, T.; Lance, M.; Abazli, H., *Inorg. Chem.* **1984**, *23*, 3667.

11.Kiselev, Yu M.; Popov, A. I.; Timakov, A.A.; Bukharin, K.V.; Sukhoverkhov, V.F., *Zhurnal Neorganicheskoi Khimii*, **1988**, *33*, 1252.

12. Einstein, F.W.B.; Rao, P.R.; Trotter, J.; and Bartlett, N., *J. Chem. Soc. (A)*, **1967**, 478.

13. R.P. Rao, Ph.D. Thesis, University of British Columbia, 1965.

14. Gruner, E.; Klemm, W. *Naturwissenschaften* **1937**, *25*, 59.

15. Žemva, B.; Lutar, K.; Jesih, A.; Casteel, Jr., W.J.; Wilkinson, A.P.; Cox, D.E.; Von Dreele, R.B.; Bormann, H.; Bartlett, N. *J. Am. Chem. Soc.* **1991**, *113*, 4192.

16. Larson, A.C.; Von Dreele, R.B. Los Alamos Laboratory Report No. LA - UR - 86 - 748, 1987.

17. Gantar, D.; Frlec, B.; Russell, D.R.; Holloway, J.H. *Acta Crystallogr.* **1987**, *C43*, 618.

18. Müller, B.G. *Z. Anorg. Allg. Chem.* **1987**, *555*, 57.

19. K. Leary, Ph.D. Thesis, University of California, Berkeley, .

20. R.W.G. Wyckoff, "Crystal Structures", Interscience Publishers, London/Sydney, 1963, Vol. 1.

21. Pitzer, K., *Accounts of Chemical Research* **1982**, *12*, 271.
Pyykko, P.; and Desclaux, J.P.; *Accounts of Chemical Research* **1982**, *12*, 276.

22. Standke, B.; Jansen, M. *Z. anorg. allg. Chem.* **1986**, *535*, 39.

23. Jones, P. G.; Rumpel, H.; Schwarzmann, E.; Sheldrick, G. M. *Acta. Crystallogr.* **1979**, *B35*, 1435.

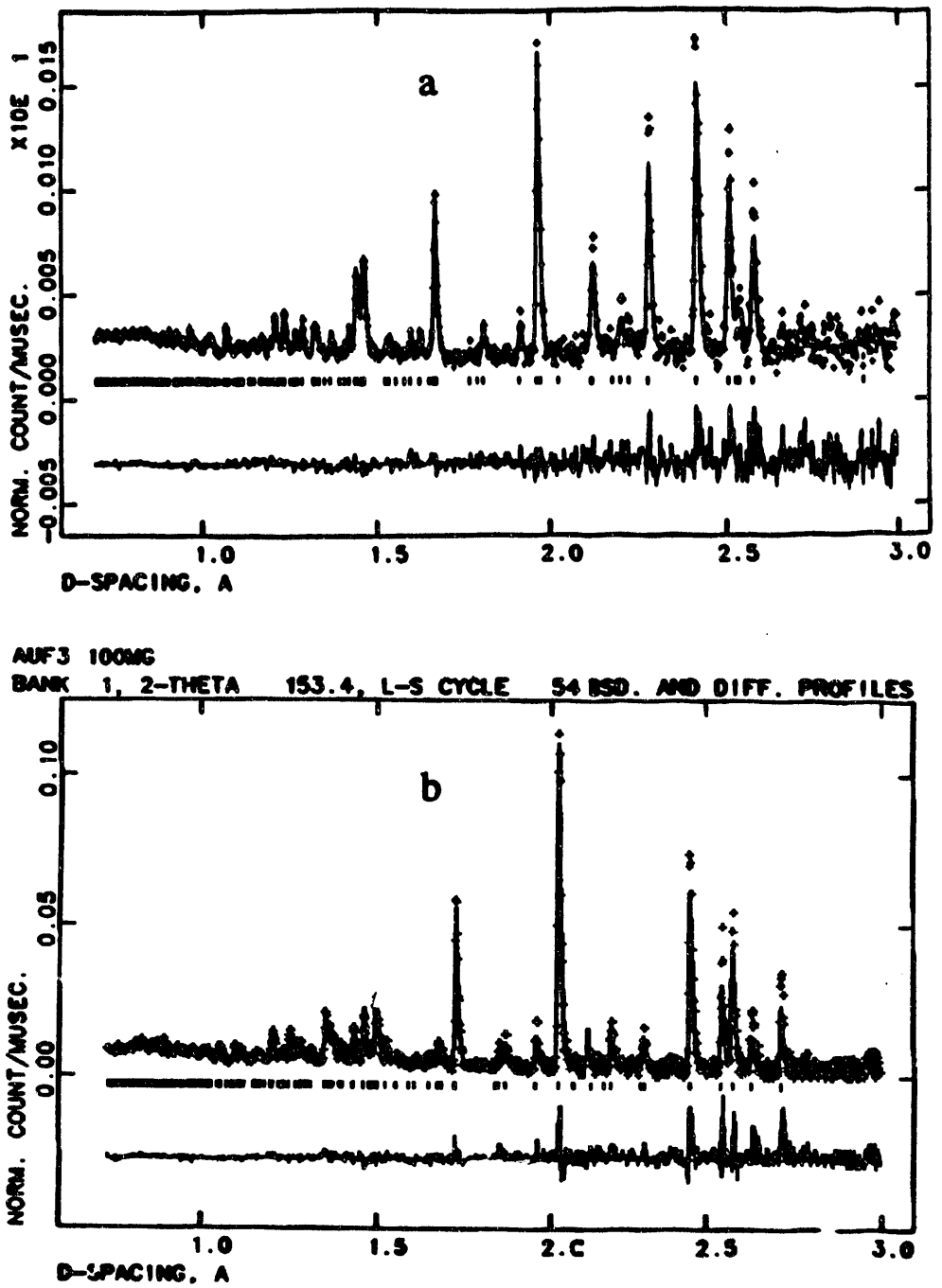

Figure 5.1. Portions of the fitted neutron time - of - flight powder diffraction patterns for data taken on the + 153 ° 2 θ bank on HIPD for (a) AgF_3 and (b) AuF_3. The observed values are shown as (+) and the calculated values from the best fit are shown as a curve. A difference (I_{obs} - I_{calc}) curve and the reflection positions are also shown. All intensity values are normalized by a previously measured incident spectrum.

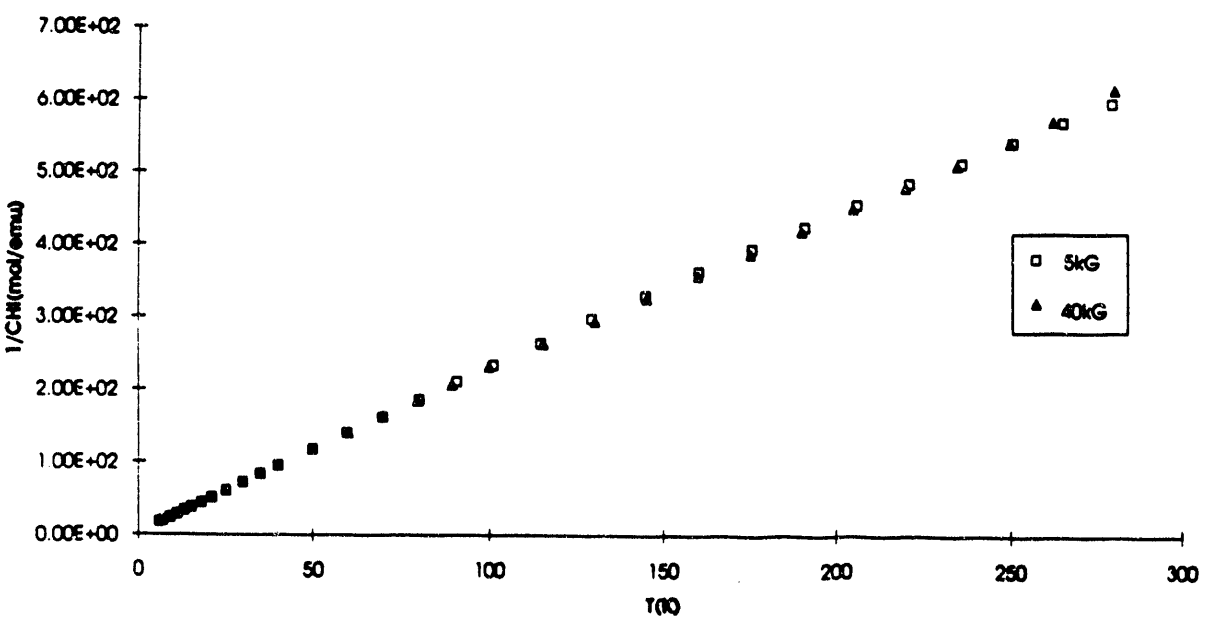

Figure 5.2. Curie - Weiss plot for Ag_3Fg:

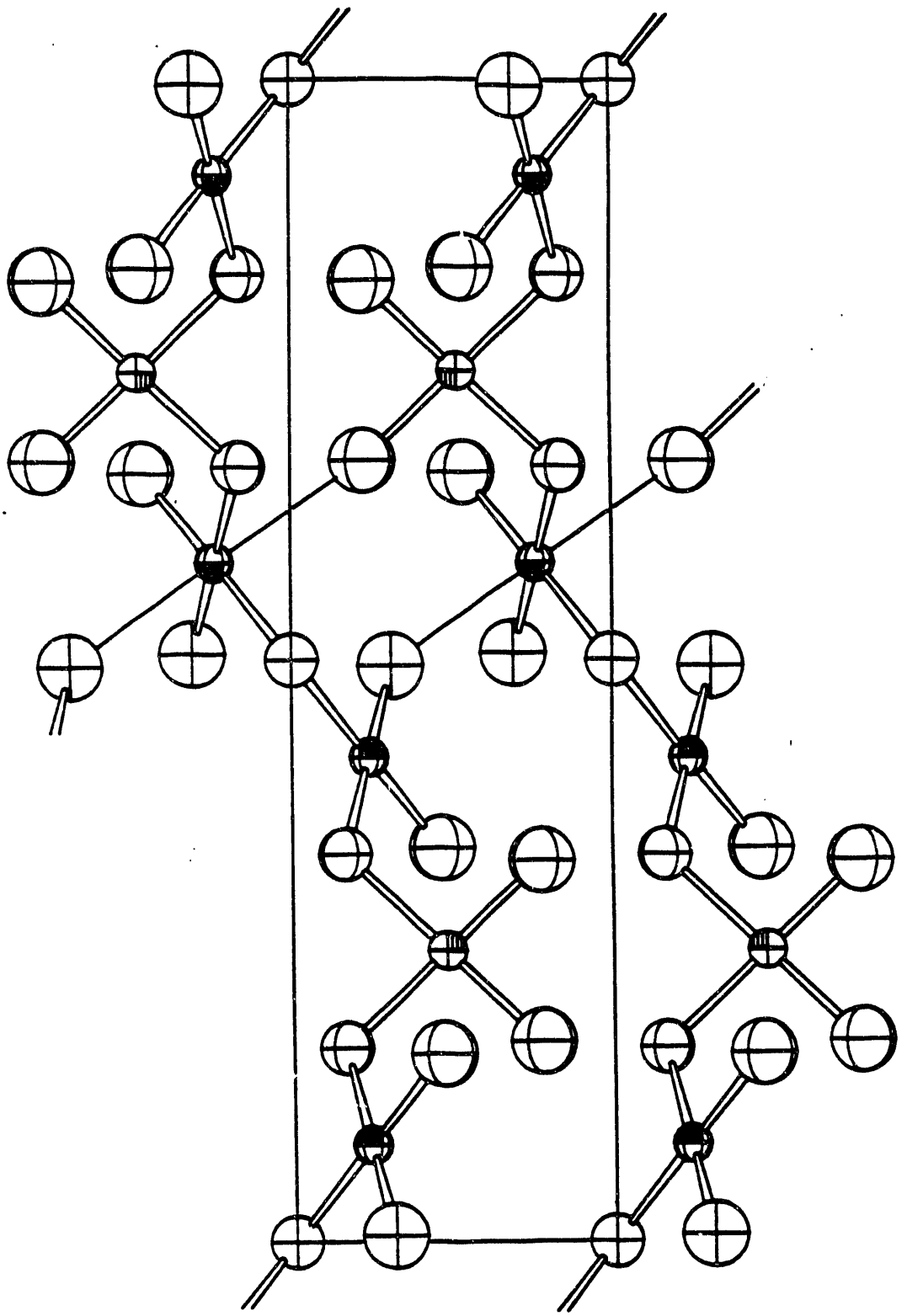

Figure 5.3. View down *a* showing unit cell contents and the F(2) interchain bridging in AgF_3 and AuF_3.

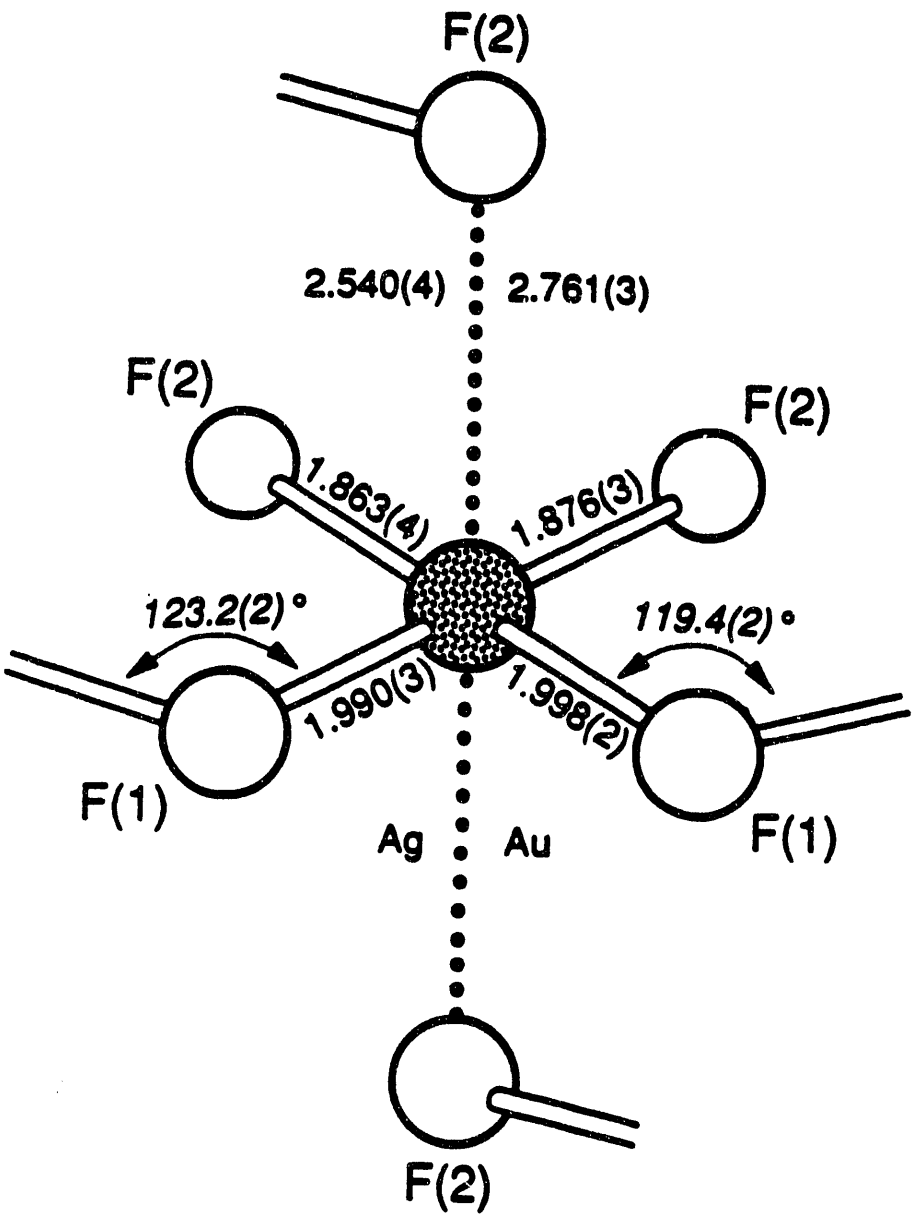

Figure 5.4. Interatomic distances (Å) for the elongated octahedral F ligand arrangement about the metal atom in AgF_3 and AuF_3 (estimated standard deviations in parenthesis)

Chapter 6

The Synthesis, Structural Characterization, and Magnetic Properties of AgF^+ Salts

Introduction

The fluorine chemistry of silver is remarkably diverse, involving the metal in oxidation states ranging from +1/2 in Ag_2F to +3 in the thermally unstable trifluoride. Even Ag(V) has been claimed to exist under extraordinary conditions.[1] Ag(I)fluoride is readily prepared in high purity and is a sufficiently strong base to form a bifluoride, $AgHF_2$, akin to those of the alkali - matels. In contrast Cu(I)fluoride and Au(I)fluoride are not known. The difluoride of silver, is a true Ag(II) material, the d^9 species being antiferromagnetically coupled. A canting of the spins in the puckered sheet structure of AgF_2 however, results in an observed ferromagnetism. This contrasts with the oxide "AgO" which is the mixed oxidation state material, $Ag^{I}Ag^{III}O_2$ in the oxide.[2]Indeed, there is yet no structural evidence for any mixed valence Ag(I)/Ag(III) fluoride.

In recent years, with the improved techniques for handling AHF, AgF_2 has been shown to behave as a fluorobase, exhibiting some similarity to the alkaline - earth fluorides in combination with strong Lewis acids. Two compounds, $Ag(SbF_6)_2$[4] and $Ag(TaF_6)_2$,[5] have been synthesized and structurally characterized prior to this work which contain isolated Ag(II) cations. A third cationic Ag(II) compound, $AgF^+AsF_6^-$, had also been prepared from AsF_5 and AgF_2 and the structure showed[6] that it contained Ag(II) as the endless chain cation $(AgF)_n^{n+}$. The $Ag(MF_6)_2$ compounds were reported to be paramagnetic, but little else was known about the physical properties of the cationic Ag(II) materials.

The finding that AsF_5 interacts with AgF_3 to produce $AgFAsF_6$ also led to its identification as a powerful oxidizer (see Chapter 7). This prompted a further investigation

of this Ag(II) salt, including its structure and magnetic properties, and a systematic effort to generate additional AgF^+ salts. In chapter 5, $AgFAsF_6$ was used as a reagent in the synthesis of the first mixed valence Ag(II)/Ag(III) compounds, Ag_2F_5 and Ag_3F_8. The fair solubility of $AgFAsF_6$ suggested that it could be useful in the synthesis of other cationic Ag(II) salts. It has subsequently been used to synthesize a variety of AgF^+ salts. The relatively weak Lewis acids BF_3, AgF_3 and AuF_3 have all proved to be capable of stabilizing the chain cation, $(Ag - F)_n^{n+}$. Remarkably, AgF_3 and AuF_3 even stabilize 1:2 compounds $Ag(MF_4)_2$, the simple Curie paramagnetism of which indicate that they are Ag^{2+} salts.

Experimental.

Materials. Commercial AgF (Ozark - Mahoning - Pennwalt, Tulsa, OK) was purified by recrystallization from AHF. $AgSbF_6$ (Aldrich, Milwaukee, WI) was recrystallized from AHF, a final purity check being made by X-Ray powder photography before use.[7] $AgBF_4$ was prepared by addition of excess BF_3 to a solution of AgF in AHF. $KAuF_4$[8], $KAuF_6$[9], O_2AuF_6[9], and AgF_2[10] were prepared by literature methods. $Ag(SbF_6)_2$ was prepared by the method of Ganter et al.[4], F_2 being added to insure complete oxidation of Ag(I).

Preparation of $AgFBF_4$. In the DRILAB a one armed Teflon/FEP reactor was loaded with 1.37 mmol AgF. The reactor was evacuated and charged with 5ml AHF. The solution was treated with BF_3 and immediately a copious white precipitate of $AgBF_4$ formed. The pressure of BF_3 was maintained above 1300 Torr until no further uptake was observed. On addition of F_2, to a total pressure of 2 atm, an immediate blue coloration of the sediment occured. The F_2 pressure was maintained near 2 atm until after 3 hr gas uptake was no longer observed. A deep blue precipitate remained in a pale blue supernatant

solution. Removal of volatile materials under vacuum through a soda - lime scrubber left 0.270 g (1.30 mmol) of deep blue solid for a 93% yield based on $AgFBF_4$. X - Ray powder data for $AgFBF_4$ were indexable on the basis of a tetragonal unit cell and are given in Table 6.1.

Preparation of $AgFBF_4$ from AgF_2 and BF_3. In the DRILAB 2.03 mmol AgF_2 was loaded into a one armed Teflon/FEP reactor. The reactor was charged with 5 ml AHF and 2atm BF_3 were admitted at room temperature. Over 30 min with intermittant agitation, there was no observable reaction, or BF_3 uptake. The reactor was cooled to near the freezing point of AHF (≈ -80 °C) and allowed to warm slowly to room temperature to facilitate the uptake of BF_3. During warming, the AgF_2 began to dissolve giving a royal blue solution and a blue green precipitate. Vigorous gas evolution was observed as the solution approached room temperature, but the final pressure indicated significant BF_3 uptake. Thermal cycling of the reaction between ≈ -80 °C and room temperature was repeated until AgF_2 was no longer visible, a blue - green solid, in a pale blue supernatant remaining. Volatile materials were removed leaving a green - blue solid. X - Ray powder photographs of this solid indicated that it was largely $AgFBF_4$, however, they also revealed the presence of AgF_2.

Table 6.1. X - Ray Powder Data for $AgFBF_4$ (CuKα Ni Filter)[a]

I/I_0	$1/d^2 x 10^4$ obsd	$1/d^2 x 10^4$ calcd	*hkl*
s	442	446	110
m	623	624	001
vs	845	847	101,011
vs	889	893	200,020
---	---	1070	111
w	1520	1517	201,021
s	1738	1740	211,121
m	1792	1786	220
vs	2239	2232	310,130
vvw	2427	2410	221
m	2506	2495	002

Table 6.1. cont.

I/I_O	$1/d^2 \times 10^4$ obsd	$1/d^2 \times 10^4$ calcd	*hkl*
s	2637	2633	301,031
m	2718	2718	102,012
w	2871	2856	311,131
m	2944	2941	112
m	3393	3388	202,022
sb	3532	3526	321,231
wb	3604	3572	400,040
		3611	212,122
w	4036	4018	330
		4195	401,041
w	4304	4281	222
mb	4441	4419	141,411
		4465	420,240
s	4730	4727	312,132
vvw	5098	5088	421,241
s	5399	5397	322,232
vw	5613	5614	003
mb	5822	5804	510,150
		5837	103,013
m	6068	6060	113
		6067	402,042
m	6221	6205	501,051
		6205	431,341
w	6300	6290	412,142
		6427	511,151
m	6522	6507	203,023
		6513	332
w	6723	6730	213,123
mb	6988	6960	422,242
		7079	521,251
mb	7144	7143	440
wb	7411	7400	223
mb	7615	7590	530,350
		7623	303,033
		7766	441
mb	7847	7846	313,133
		8036	600,060
wb	8077	8076	502,052
		8076	432,342
		8213	531,351

Table 6.1. cont.

I/I_O	$1/d^2 \times 10^4$ obsd	$1/d^2 \times 10^4$ calcd	*hkl*
wb	8317	8299	512,152
vwb	8534	8516	323,233
		8659	601,061
m	8891	8883	611,161
m	8961	8929	620,260
		8969	522,252
		9184	403,043
		9408	413,143
		9552	621,261
w	9654	9632	333
		9637	442
w	9794	9776	541,451
		9979	004
w	10110	10078	423,243
		10085	532,352
m	10202	10203	104,014
		10425	114
		10530	602,062
		10668	631,361
w	107471	10755	612,162
		10871	204,024
m	11089	11096	214,124
m	11144	11162	710,170
		11162	550
		11193	503,053
		11193	433,343
		11416	513, 153
		11423	622,262
		11561	701,071
mvb	11632	11608	640,460
		11648	542,452
		11764	224
		11784	711,171
		11784	551
m	$11995\alpha_1$	11989	304,034
	$11984\alpha_2$	11989	
		12086	523,253
		12211	314,134
		12231	641,461
w	$12508\alpha_1$	12455	721,271

Table 6.1 cont.

I/I_0	$1/d^2 \times 10^4$ obsd	$1/d^2 \times 10^4$ calcd	*hkl*
	$12503\alpha_2$	12540	632,362
		12756	443
m	$12902\alpha_1$	12882	324,234
	$12913\alpha_2$		
		12948	730,370
w	$13207\alpha_1$	13204	533,353
	$13194\alpha_2$		

[a] Tetragonal unit cell with (20 °C) $a_o = 6.693(3)$ Å; $c_o = 4.004(3)$ Å; V = 179.4 $Å^3$; Z = 2; possible space group, P4/n.

$AgFAsF_6$ from fluorination of $AgAsF_6$ in AHF with excess AsF_5. (A) In the DRILAB, (1301mg, 10.25mmol) AgF was loaded into a 1/2 in. O.D. FEP tube fitted with a teflon valve. AHF (6ml) was condensed under vacuum onto the AgF and this gave a colorless solution at room temperature. AsF_5 was allowed to dissolve in the solution and immediately produced a colorless precipitate of $AgAsF_6$. When no further AsF_5 uptake was observed at 1.5 atm, the AsF_5 supply was closed and the reactor was pressurized with F_2 to 2atm. The mixture was vigorously agitated and uptake of F_2 was observed, the HF solution simultaneously becoming blue. After 24 hrs F_2 uptake had ceased and a deep, royal-blue solution free of solid remained. The excess F_2, AsF_5, and HF were removed at room temperature in a dynamic vacuum to leave a dark, blue-green solid. The solid (3160mg, 10.01mmol $AgFAsF_6$) was held under vacuum for another 2 hrs with no color change. X-Ray powder photographs showed $AgFAsF_6$ lines only (based on an indexing from single crystal data given by Gantar et al)[6]. Variable temperature magnetic susceptibility measurements showed temperature independent paramagnetism above 63K with a small paramagnetic impurity evident at temperatures below 63K. No field dependence was observed from 6 to 280K on switching from a 5 to 40 kGauss field. The data are shown as A in Fig.6.1.

$AgFAsF_6$ crystallized from AHF with excess AsF_5 at low temperature. In an identical experiment, a solution of $AgFAsF_6$ was made up in AHF with a 5 fold excess of AsF_5. The solution was cooled to -60 °C at which time removal of the AsF_5/AHF solution was begun. After 24 hrs a blue - green solid remained. X - Ray powder photographs were identical to those observed above for $AgFAsF_6$. Variable temperature magnetic susceptibility data are not significantly different from those obtained above.

$AgFAsF_6$ from stoichiometric AsF_5 addition. (B). Several preparations were carried out in the following way. In the DRILAB, AgF (usually 300 mg, 2.4mmol) was loaded into an FEP T-reactor fitted with a Teflon valve. When the AHF (3ml) which had been transferred in a dynamic vacuum was warmed to room temperature, a small amount of dark, insoluble material (perhaps AgF_2 from the fluorine used to passivate the reactor) precipitated out of the colorless solution. The solution was decanted into the free leg of the T and AsF_5 was admitted as above. On complete conversion of AgF to $AgAsF_6$ as judged by no further uptake of AsF_5, the AHF and any excess AsF_5 were removed in a dynamic vacuum, which was maintained for 3 hrs. The colorless solid, $AgAsF_6$, which remained, was washed twice with AHF (4ml) by decantation to remove any unreacted AgF. This washed $AgAsF_6$ in AHF (4ml) was pressurized with F_2 to 2 atm and the mixture was agitated. A deep blue solid formed as F_2 was taken up. F_2 uptake ceased after 8 hrs. Removal of F_2 and AHF left a dark blue solid (usually 700 mg, 2.2mmol $AgFAsF_6$). X-Ray powder data for this material could be indexed completely on the basis of the $AgFAsF_6$ phase. However, a few weak reflections which were not visible in the $AgFAsF_6$ material prepared by route (A), were observed. The results of variable temperature magnetic susceptibility measurements varied somewhat from sample to sample, however, a representative set is shown as B in Fig.6.1.

In sample B, the appearance of a small field dependence below 163K signifies a

small AgF_2 impurity (see Fig. 6.5 for the susceptibility temperature profile for a dilute AgF_2 sample). Even with the AgF_2 impurity the paramgnetism appears to be temperature independent down to 63K where a drop in susceptibility occurs. The susceptibility of the AgF_2 impurity and perhaps a paramagnetic impurity eventually offset this decrease in chi as the temperature falls.

$AgFAuF_4$. In the DRILAB, $AgFAsF_6$ (453mg, 1.43 mmol) prepared by method (A) and $KAuF_4$ (402mg, 1.29mmol) were loaded into an FEP T-reactor fitted with two 3/8 in. O.D. FEP tubes and a Teflon valve. The reactor was exposed to vacuum (better than 0.05 torr) and anhydrous HF (4ml) was condensed onto the solid mixture. On warming to room temperature an insoluble green precipitate formed, the supernatant solution being colorless. The reactor was then pressurized with F_2 to 2 atm. No F_2 uptake was observed over several hours. The insoluble green product was washed free of $KAsF_6$ and excess $AgFAsF_6$ by decantation and back distillation of the AHF, this being repeated 10 times. X-Ray powder photographs of the green material were indexed on the basis of a $CuFAuF_4$ type cell[11] as given in Table 6.2. Magnetic susceptibility data are shown in Fig. 6.2.

Table 6.2. X - Ray powder data for $AgFAuF_4$ (CuKα, Ni Filter)[a]

$1/d^2x10^4$ obsd	$1/d^2x10^4$ calcd	I/I_o obsd	I/I_o calcd[b]	*hkl*
293	296	w	90	100
479	483	w	75	010
725	730	vs	1000	010
	730		906	$1\bar{1}0$
826	828	s	753	110
---	858	---	19	$01\bar{1}$
---	862	---	52	$10\bar{1}$
939	---	vvw	---	imp
1038	1039	s	493	$11\bar{1}$
1183	1184	s	414	200
	1189		44	101
1256	1268	m	231	$1\bar{1}1$

Table 6.2. cont.

$1/d^2x10^4$ obsd	$1/d^2x10^4$ calcd	I/I_0 obsd	I/I_0 calcd	*hkl*
1487	---	vvw	---	imp
	1567		98	011
1578	1569	mbr	33	$2\bar{1}0$
	1586		138	$20\bar{1}$
1652	1650	m	280	$1\bar{1}\bar{1}$
---	1765	---	2	210
---	1813	---	11	$21\bar{1}$
1947	1931	sbr	193	020
	1952		155	$02\bar{1}$
2080	2075	m	182	111
---	2129	---	1	$1\bar{2}0$
	2182		51	$12\bar{1}$
2233	2240	sbr	201	201
	2270		37	$2\bar{1}1$
	2313		5	$1\bar{2}1$
2329	2325	vvw	11	120
	2326		13	$2\bar{1}\bar{1}$
2477	---	vvw	---	imp
2565	---	vvw	---	imp
---	2663	---	5	300
---	2692	---	1	$01\bar{2}$
2716	2710	m	206	$11\bar{2}$
	2887	---	4	$10\bar{2}$
---	2903	---	10	$30\bar{1}$
2917	2918	s	119	002
	2919		163	$2\bar{2}0$
3000	2999	m	180	$3\bar{1}0$
3020	3004	m	134	$22\bar{1}$
	3176		2	211
3191	3178	m	104	$31\bar{1}$
3246	3265	m	82	$1\bar{1}2$
	3266		91	$2\bar{2}1$
	3293		112	310
3302	3311	m	108	220
	3320		9	$21\bar{2}$
3376	3370	w	85	021
---	3405	---	5	$1\bar{2}\bar{1}$
3442	3431	mbr	104	$02\bar{2}$
	3448		77	$20\bar{2}$
---	3498	---	11	$12\bar{2}$

Table 6.2. cont.

$1/d^2x10^4$ obsd	$1/d^2x10^4$ calcd	I/I_o obsd	I/I_o calcd	*hkl*
---	3541	---	1	102
3583	3593	mbr	86	$3\bar{1}\bar{1}$
3858	3864	mbr	92	$3\bar{1}1$
---	3883	---	15	301
---	3928	---	5	121
---	3956	---	6	$1\bar{2}2$

[a] Triclinic cell with a_o = 5.906(6) Å; b_o = 4.769(6) Å; c_o = 3.933(5) Å; α = 107.01(5) °; β = 99.46(4) °; γ = 90.75(4) °; V = 104.3 Å^3.

[b] The calculated intensities were based on parameters given by B.G. Müller[11] for the structure of $CuFAuF_4$. Calculations were performed using the program LAZY[12].

$AgFAuF_6$: In the DRILAB, (683mg, 1.95mmol) $KAuF_6$ and (810mg, 2.56mmol) $AgFAsF_6$, prepared by method (A), were loaded into one leg of an FEP T-reactor as described above. AHF (5ml) was transferred into the reactor under static vacuum and warming to room temperature provided a dark, green-blue precipitate, the supernatent solution being pale blue. The solid proved to be insoluble and was washed free of $KAsF_6$ and excess $AgFAsF_6$ by decantation and back distillation of the AHF. After 6 washings the AHF over the solid was colorless. The AHF was removed in a dynamic vacuum, and the solid was dried under vacuum overnight. X-Ray powder photographs of the solid showed it to be isomorphous with $AgFAsF_6$. The X-Ray data are given in Table 6.3. Variable temperature magnetic susceptibility measurements (Fig.6.1, C) showed behavior very similar to those for $AgFAsF_6$. Again a small AgF_2 impurity appears to be present, otherwise the susceptibility exhibits temperature-independent paramagnetism above 63K, with a sharp drop just below that temperature. The apparent field-dependence, even at temperatures above the Curie temperature for AgF_2 (163K), is puzzling and could arise from a ferromagnetic contaminent, e.g. nickel metal.

Table 6.3. X - Ray powder data for $AgFAuF_6$ (CuKα, Ni Filter)

$1/d^2x10^4$ obsd	$1/d^2x10^4$ calcd	I/I_0 obsd	I/I_0 calcd	*hkl*
268	270	w	119	101
286	293	w	41	011
---	389	---	8	002
425	---	vw	---	imp
463	466	vs	1000	111
562	562	m	263	102
665	---	w	---	imp
689	692	wbr	131	200
---	758	---	19	112
782	781	sbr	381	020
	790		193	201
---	888	---	0.2	210
976	985	vw	20	211
---	1049	---	4	103
---	1052	---	29	121
1070	1071	s	391	013
	1082		64	202
---	1170	---	1.5	022
1250	1244	vvw	56	113
1287	1277	m	213	212
1350	1344	m	173	122
1473	1474	vwbr	41	220
	1557		17	004
	1568		1	203
1571	1571	wb	59	221
1653	1655	w	35	301
---	1730	---	18	104
1774	1764	w	92	213
	1830		27	123
1854	1851	w	63	311
	1855		12	031
1857	1863	m	23	222
---	1925	---	8	114
---	1947	---	0.2	302
2045	2028	wbr	54	131
2142	2143	wbr	52	312
---	2250	---	0.1	204
	2320		0.1	132
2321	2338	vvw	24	024
	2349		1	223

Table 6.3. cont.

$1/d^2x10^4$ obsd	$1/d^2x10^4$ calcd	I/I_0 obsd	I/I_0 calcd	*hkl*
	2434		0.1	303
	2437		41	321
2451	2445	w	32	214
	2450		2	230
2513	2511	w	99	124
---	2547	---	11	231
---	2606	---	1	105
---	2628	---	0.5	015
	2629		9.5	313
2636	2633	mbr	151	033
---	2728	---	12	322
---	2770	---	3	400
	2801		22	115
	2806		22	133
2826	2839	m	103	232
2852	2867	w	13	401
2963	2965	vw	29	410

[a] Orthorhombic unit cell with a_o = 7.600(4) Å; b_o = 7.156(4) Å; c_o = 10.137(5) Å; V = 551.3 $Å^3$. Probable space group, *Pnma*.

[b] The calculated intensities are based on parameters given by Gantar et al.[6] for the structure of $AgFAsF_6$.

$Ag(AuF_4)_2$. In the DRILAB, $AgFAsF_6$ from preparation (A) (1.6 mmol) and $KAuF_4$ (3.2 mmol) were loaded into separate legs of a Teflon T-reactor, described above. AHF (4ml) was condensed into each leg of the reactor under static vacuum, resulting in yellow and blue solutions of $KAuF_4$ and $AgFAsF_6$, respectively. Pouring the $KAuF_4$ solution onto the $AgFAsF_6$ solution produced an olive-green precipitate, the supernatent solution being yellow. The reactor was pressurized with 2 atm of BF_3 until the supernatant solution became colorless. The light green precipitate was washed 10 times by decantation and back distillation of the AHF to remove $KAsF_6$ and KBF_4 side products. AHF was removed and the light green solid was dried in a dynamic vacuum overnight. X-Ray powder photographs showed a new phase similar to $Ag(AgF_4)_2$ (chapter 5) and are given in Table 6.4. No lines attributable to $AgFAuF_4$, or AuF_3 were

observed. Variable temperature magnetic susceptibility measurements from 6 to 280K at 5 and 40kGauss obeyed the Curie-Weiss law for a dilute one-electron paramagnet with μ_{eff} = 1.82 B.M. and θ = -2 ° The Curie - Weiss plots of $AgAu_2F_8$ and $Ag(SbF_6)_2$ are shown as (A) and (B) in Fig. 6.3.

Table 6.4 . X - Ray powder data for $AgAu_2F_8$ (CuKα, Ni Filter)

I/I_o	$1/d^2 \times 10^4$ obsd
vw	544
vvw	664
s	708
s	727
w	756
s	850
s	1067
vw	1105
m	1330
vw	1459
w	1505
vw	1559
wb	1674
w	1769
s	1818
m	1905
w	2017
m	2136
m	2176
m	2388
m	2467
w	2567
w	2699
s	2904
m	2962
m	3120
w	3249
m	3361
w	3526
m	3583
m	3980
m	4277
m	4462

Table 6.4. cont.

I/I_o	$1/d^2 \times 10^4$ obsd
m	4681
m	4767
s	6594
s	6732

$Ag^{I}SbF_6$ with Fluorine in AHF. In the DRILAB $AgSbF_6$ was loaded into a two armed Teflon/FEP reactor. After charging with 5 ml AHF the system was pressurized with 2 atm F_2. Immediately the poorly soluble $AgSbF_6$ took on a tan color which quickly changed to blue. Fluorination over several hours left deep blue crystals in a pale blue supernatant solution. When no further F_2 uptake was observed, the AHF solution was slowly evacuated. Removal of the AHF resulted in a destruction of the crystals, however, and a finely divided dark blue powder remained. X - Ray powder photographs indicated a new phase of very poor crystallinity. Magnetic suceptibility measurements show TIP down to 163K where onset of a large field dependence indicative of AgF_2 (10%) was observed.

Reaction of $O_2^+AuF_6^-$ with AgF. In the DRILAB, 0.23 g (0.68 mmol) O_2AuF_6 and 0.096 g (0.76 mmol) AgF were loaded into a one armed Teflon/FEP tube reactor which had been passivated with 2 atm F_2 for several hours. The reactor was attatched to the teflon manifold of a S.S. vacuum line, evacuated, and charged with 4ml of AHF. On warming to room temperature vigorous gas evolution was observed, while the solids became dark brown. When gas evolution had ceased, a black solid remained in a pale yellow solution. Volatile materials and AHF were removed under dynamic vacuum through a soda - lime scrubber leaving 0.30 g of black, solid product. X - Ray powder photographs of the black solid revealed a fairly simple, broad lined pattern.

$O_2^+AuF_6^-$ and $AgFBF_4$. Under identical conditions to those above, 0.30 g

(0.88 mmol) O_2AuF_6 and 0.19 g (0.88 mmol)$AgFBF_4$ were allowed to react in AHF. Vigorous gas evolution was again observed, which on ending left a dark blue solid in a yellow solution. Evacuation of volatile materials and AHF left 0.4200 g of dark blue, solid product. X - Ray powder photographs revealed O_2AuF_6 and lines attributable to the black phase observed in the O_2AuF_6/AgF reaction. The crystallinity of the material was greatly improved, however, and the data are shown in Table 6.5.

Table 6.5. X - Ray Powder Data for O_2AuF_6/ $AgFBF_4$ Phase (CuKα, Ni Filter)

I/I_o	$1/d^2 \times 10^4$ obsd
m	675
vs	686
s	1233
w	1268
s	1463
vvw	1703
vvw	1884
m	2126
vw	2186
w	2684
s	2720
s	3123
s	3159
m	3224
w	3471
w	3533
sb	3610
mb	4138
wb	4270
sb	4398
mb	4927
vwb	5056
wb	5190
wb	5873
wb	6126
wb	6330

Interaction of $AgFAsF_6$ with AHF. In a reaction originally designed to produce $AgFAuF_4$, $KAuF_4$ was loaded into one arm of a two armed Teflon/FEP reactor and $AgFAsF_6$ from preparation (A) was loaded into the other arm. Both arms of the reactor were charged with AHF on the vacuum line. Decantation of the blue "$AgFAsF_6$" solution on to the yellow $KAuF_4$ solution and solid, produced a lime - green solid. This AHF was distilled back into the tube containing the $AgFAsF_6$ which had been cooled to -196 °C. The decantation and back distillation procedure was repeated until colorless AHF was left in the tube originally containing the $AgFAsF_6$. A small amount of insoluble black solid remained in this tube, while an insoluble lime green solid had been produced in the other tube. AHF was removed under dynamic vacuum through the soda - lime scrubber. X - Ray powder photographs of the black solid revealed a pattern which was isomorphous with the blue and black phase obtained from the O_2AuF_6 reactions. Subsequent washing of the green solid (to remove $KAsF_6$) left $AgAu_2F_8$ as evidenced by the X - Ray powder data. Magnetic susceptibility data for the black phase are given in Fig. 6.4.

Results and Discussion

Three different methods have been used in the synthesis of a variety of new AgF^+ salts. The first simply involves the acid - base interaction of AgF_2 with strong fluoroacids in AHF in a manner similar to that used by Gantar et al. in the synthesis of $AgFAsF_6$ and $Ag(SbF_6)_2$, eq 1

$$AgF_2 + A \xrightarrow{AHF} AgF^+AsF_6^- \qquad (1)$$

$$A = AsF_5, BF_3$$

While this procedure allows the synthesis of members of this class of salts from commercially available starting materials, thus avoiding the use of elemental F_2, the

resulting products are inevitably contaminated with the Ag(I) fluoroacid salt and, or AgF_2. The quantities of these contaminents can be large if the quality of AgF_2 is inferior. Recently Žemva has shown that reaction (1) is in equilibrium even for the strong acid AsF_5 unless the acid concentration is high.[13] Indeed, he has shown that, in the presence of a large amount of AsF_5 free AHF, $AgFAsF_6$ is solvolyzed to AgF_2 provided the AsF_5 produced in the back reaction is effectively removed. This equilibrium was far more obvious when the weaker acid, BF_3 was used, this being in part due to the low solubility of this acid in AHF at room temperature. Cooling of the BF_3/AHF/AgF_2 reaction mixture to -20° was required to achieve a BF_3 concentration in solution high enough to drive the forward reaction.On allowing the insoluble solid $AgFBF_4$ to stand in AHF at room temperature, partial decomposition to AgF_2 occurs, BF_3 being effectively removed from solution by its low solubility.

A much more effective synthesis for high purity AgF^+ salts, is by the direct fluorination of the available Ag(I)fluorometallate salts, eq 2

$$Ag^{I}MF_6 + 1/2\,F_2 \xrightarrow{AHF} AgF^{+}MF_x^{-} \qquad (2)$$

$$MF_x^- = AsF_6^-, BF_4^-, SbF_6^-$$

This method has resulted in the first high purity synthesis of $AgFBF_4$. On the other hand, the product of the interaction of $AgSbF_6$ with F_2 has remained difficult to characterize due to poor crystallinity of the final deep blue solid. The production of a seemingly crystalline product in AHF perhaps indicates that HF molecules contained in the crystal lattice are removed during the final evacuation of solvent AHF from it. X - Ray powder photographs, however, show no traces of the $Ag(SbF_6)_2$ salt, which is light blue and sufficiently soluble to provide well developed crystals from AHF.

The purest samples of $AgFAsF_6$ and $AgFBF_4$, as judged by X-Ray powder data

and variable temperature magnetic susceptibility data, have been obtained by a combination of reactions (1) and (2), that is direct fluorination of the Ag(I) fluorometallate salt in the presence of the conjugate acid. X - Ray powder photographs for samples of $AgFBF_4$ prepared in this way indicated that the material was free of both $AgBF_4$ starting material and AgF_2 and was of good crystallinity. These data were indexed readily on the basis of a tetragonal unit cell (Table 6.1). The tetragonal symmetry of the cell and the unit cell volume which required 2 AgF^+ chain fragments per cell provided for a correct deduction of the structure prior to the availability of single crystals.[14] This was possible, because the chains had to be parallel to the shortest axis, the c axis. Since $c_o = 4.013$Å and the chain Ag - F interatomic distance is expected to be nearly 2.00Å based on the $AgFAsF_6$ structure, it was concluded that the Ag - F^+ chain had to be linear. This result has been confirmed from a single crystal structure determination carried out in these laboratories by Dr. Horst Bormann from single crystals prepared by Mr. George Lucier.[15]

That reaction (2) proceeded at all without the addition of small amounts of added acid was initially somewhat surprising given the inability of molecular F_2 to oxidize pure AgF in AHF at room temperature.[16]

$$AgF + 1/2\,F_2 \;\not\longrightarrow\; AgF_2 \qquad (3)$$

The AgF^+ salts are much more powerfully oxidizing (chapter 7) than the neutral difluoride and are therefore expected to be much more difficult to obtain by direct fluorination. Catalytic amounts of BF_3 were found to bring reaction (3) to completion very quickly[16], however, suggesting that the Ag(I) fluorometallates must undergo some solvolysis in AHF to produce this catalytic amount of acid. Once a small amount of the AgF^+ salt is formed solvolysis can provide enough acid to catalyze the further fluorination.

A final preparative method, which has significantly increased the number of these

salts, involves the metathesis of $AgFAsF_6$ with potassium fluorometallate salts.

$$AgF^+AsF_6^- + KMF_x \xrightarrow{AHF} AgF^+MF_x^- + KAsF_6 \qquad (4)$$

$$MF_x = AgF_4^-, AuF_4^-, AuF_6^-$$

In all cases the reaction is driven to completion by the formation of an insoluble AgF^+ salt. Thus far, the only structural information available for these materials comes from X - Ray powder data, which are, however, very informative. X - Ray powder data for $AgFAuF_4$ (Table 6.2) can be indexed completely on the basis of the triclinic $CuFAuF_4$ type cell, known from single crystal data.[11] Rough intensities from the $AgFAuF_4$ powder data correlate well with the intensities anticipated on the basis of a $CuFAuF_4$ structure,with Ag substituted for Cu. This indicates that the two salts are isostructural. This structure contains a nearly linear $(M - F)_n^{n+}$ chain. The $P\bar{1}$ symmetry of the cell does not allow for non - linearity of the chain, however the large thermal parameter observed for the chain F atoms in the structure of Müller et al.[11] suggests slight deviations of the chain from linearity, so P1 may be the true symmetry of the cell. If in fact the chain is parallel to the c axis as described, the known chain Ag -F interatomic distance from the $AgFAsF_6$ and $AgFBF_4$ structures which are barely significantly different from 2.000Å would need a bridging M - F - M angle of 159° based on c_o = 3.933Å in the $AgFAuF_4$ cell. X - Ray data for Ag_2F_5 (Chapter 5) have not yet been indexed, owing to impurity lines which include those of Ag_3F_8. However, when known impurity lines are subtracted from the data (Table 5.5) the remaining data are markedly similar to those of $AgFAuF_4$, again suggesting the $AgFAgF_4$ formulation and a structural relationship to $CuFAuF_4$.

Under acidic conditions a 1:2 ratio of $AgFAsF_6$ to $KAgF_4$ was observed to give Ag_3F_8 (see chapter 5). A similar set of conditions using $KAuF_4$ produces a phase distinct from that of $AgFAuF_4$ which is akin to Ag_3F_8. Indeed the magnetic data are similar to

those for $Ag(AgF_4)_2$ (q.v.) and indicate the formulation $Ag^{2+}(AuF_4^-)_2$. Under these synthetic conditions it was realized that the oxidation of AuF_4^- to AuF_6^- cationic Ag(II) was also a possibility. No soluble AuF_6^- salt was observed, however, and basic solvolysis of the insoluble, olive - green product, $AgAu_2F_8$, with KF in AHF, produced only $KAuF_4$ and AgF_2, eq 5

$$AgAu_2F_8 + 2\,KF \xrightarrow{AHF} AgF_2 + 2KAuF_4 \qquad (5)$$

In order to synthesize the Au(V) AgF^+analogue, Au(V) starting materials were required. X-Ray powder data for insoluble, aqua colored $AgFAuF_6$ is nearly identical to that observed for $AgFAsF_6$[17] and can be indexed completely on the basis of the $AgFAsF_6$ type cell (Table 6.3). Again rough intensity data indicate that these two AgF^+ salts are probably isostructural. The Ag - F - Ag bridging angle determined by Gantar et al.[6] to be 143° in $AgFAsF_6$ must be nearly the same in the Au(V) analog.

In the metathesis, reaction (4), generally either the solid reagents were mixed, followed by the addition of AHF, or the potassium fluorometallate salt dissolved in AHF was poured on to $AgFAsF_6$ in AHF. Reactions were carried out in this manner to avoid local excesses of the fluorometallate salts which would favor formation of $Ag(MF_x)_2$ salts. It was subsequently found that when solutions of $AgFAsF_6$ were repeatedly decanted, an insoluble black solid eventually remained. X - Ray powder photographs of this material revealed that it was identical to a black solid obtained by Žemva and his coworkers[13] when less than one equivalent of AsF_5 was added to pure AgF_3 in AHF. Interestingly, the material was clearly isomorphous with the dark blue product observed when a large excess of $O_2^+AuF_6^-$ was reacted with $AgFBF_4$, eq 6

$$1 - x\ O_2^+AuF_6^- + AgFBF_4 \xrightarrow{AHF} \text{dark blue solid} + O_2 + BF_3 + x\ O_2^+AuF_6^- \qquad (6)$$

Reaction (6) was originally proposed as a means to make $AgFAuF_6$. In a subsequent experiment by Žemva, it was discovered that $AgFAsF_6$ could be completely solvolyzed in AHF to the black solid and $AgAsF_6$ by adding adding successive aliquots of AsF_5 free AHF to it.[13] Apparently the total solvolysis is normally prevented by the increasing concentration of free AsF_5 in solution. Only by effectively removing this AHF could the solvolysis go to completion.

In our studies of the AgF^+ salts, it was discovered that the solubility of $AgFAsF_6$ in AHF was greatly enhanced by the addition of AsF_5. This probably means that the Ag(II) is then present as AHF solvated Ag^{+2} species. A puzzling feature was the seemingly significant solubility of $AgFAsF_6$ which produces dark blue solutions in AHF, in contrast to all other AgF^+ salts, which are nearly insoluble in AHF. Since it is now apparent that addition of AHF to $AgFAsF_6$ releases some "free" AsF_5, the solubility of $AgFAsF_6$ in AHF can now be interpreted as due to the solvolysis of this material producing black solid, $AgAsF_6$ and AsF_5, the last of which aids in the dissolution of the remaining $AgFAsF_6$. It is expected that in the absence of AsF_5 the solubility would be comparable with other AgF^+ salts.

A closer inspection of the X - ray powder data revealed that $AgFAsF_6$ prepared by reaction (2) contained a small amount of the black solid, the strongest lines of that impurity being barely visible in the $AgFAsF_6$ data. $AgFAsF_6$ prepared using excess AsF_5, however, showed no traces of this impurity. Still, all $AgFAsF_6$ used in metatheses, reaction (4), was dissolved in AsF_5 free AHF and therefore must have been tainted with the black solid, as a consequence of the solvolysis. It was expected that each product from these reactions might contain traces of this material. Indeed, X - ray powder photographs of $AgFAuF_6$ and Ag_2F_5 do contain the strongest lines of the pattern of the black solid. Interestingly, the $AgFAuF_4$ data, which was indexable, shows no signs of the black solid phase. It is possible that the black solid which must contain some Ag(III), since Ag(I) is

also formed in its production from the solvolysis of $AgFAsF_6$, is reduced by $KAuF_4$ in eq (3) to produce $KAuF_6$ which is washed away in the $AgFAuF_4$ synthesis. Subtracting the lines due to the black solid from the Ag_2F_5 pattern subsequently revealed a much closer relationship to the $AgFAuF_4$ pattern, suggesting a similar cell and structure. Unfortunately, removal of all the lines which could be attributable to the black solid, including those which are probably coincident with authentic Ag_2F_5, leaves too few data to index the cell.

Magnetic Measurements

Variable temperature magnetic susceptibility measurements have proven to be extremely sensitive to the environment about the d^9 Ag(II) species and readily distinguish AgF_2, AgF^+, and Ag^{+2} species. AgF_2 is paramagnetic with a ferromagnetic transition below 163K.[18] The sudden onset of field dependence at 163K serves as a very sensitive test for AgF_2 impurities in Ag(II) salts, the effect being pronounced in a sample diluted to 15% with CaF_2 (see Fig. 6.5). Salts containing isolated Ag(II) cations such as $Ag(SbF_6)_2$, "$Ag(AgF_4)_2$", and "$Ag(AuF_4)_2$" have room temperature moments similar to that of AgF_2. However, like Ag_3F_8, these materials show no field dependence and obey the Curie law as magnetically dilute systems to very low temperatures, Fig. 6.3. This behavior was anticipated, as in these salts, the paramagnetic Ag(II) ions must be well separated by the two diamagnetic anions. Interestingly, it is the hexafluoroantimonate salt, containing the largest diamagnetic anions among the the Ag^{+2} salts, which shows the most significant deviation from Curie behavior at low temperatures, but this is indicative of only weak antiferromagnetic coupling, evidently fostered by the anions.

In contrast to these materials, with their relatively large susceptibilities, the AgF^+ salts containing Ag(II) in a 2 - D chain, are only weakly paramagnetic with room temperature χ_g measurements nearly two orders of magnitude smaller than those of other

Ag(II) materials. Remarkably, the observed paramagnetism in all of the AgF^+ salts studied thus far appears to be temperature independent at least down to temperatures below 60K where the impact of small amounts of paramagnetic Ag^{+2} or ferromagnetic AgF_2 becomes large.

Unfortunately there was great variability in the magnetic data, the presence of impurity phases having large effect on the small AgF^+ susceptibilities. Certainly there was much difficulty in obtaining $AgFAuF_4$ and $AgFAgF_4$ free from the 1:2 complexes $AgAu_2F_8$ and Ag_3F_8, which probably contribute to the increased magnetization observed at lower temperatures for these AgF^+ salts. Even so, these materials exhibit small, roughly temperature independent paramagnetism, further supporting their formulation as AgF^+ salts. The scatter seen in Fig. 6.2 below 163K may also indicate the presence of some AgF_2. The variances in susceptibility data for $AgFAsF_6$ and $AgFAuF_6$ are somewhat more difficult to rationalize. All samples, regardless of the method of preparation show increased magnetization at low temperatures, this in spite of the instability of the corresponding 1:2 complex $Ag(AsF_6)_2$ in the absence of AsF_5 rich AHF. As expected preparations using a large excess of AsF_5 were free of AgF_2, as indicated by the lack of any field dependence below 163K. In contrast samples prepared by reaction 2 involving a stoichiometric quantity of AsF_5, show a field dependence below 163K, the presence of 1% AgF_2 being suggested by comparison with the 15% diluted AgF_2/CaF_2 measurement. $AgFAuF_6$ data indicated a field dependence over the entire range of temperatures, this possibly arising from ferromagnetic NiF_2 impurity in the original $KAuF_6$ starting material which was made in a Monel bomb.

With the exception of $AgFAsF_6$ prepared under AsF_5 rich conditions, all $AgFAsF_6$ and indeed all AgF^+ salts prepared from $AgFAsF_6$ showed a significant drop in susceptibility below 63K before rising again at ≈30K. The absence of such a drop in susceptibility in the purest samples of $AgFAsF_6$, suggests that an impurity common to the

remaining AgF+ salts is responsible for this susceptibility drop. Since the new black phase was known to be present in all of these samples, it was anticipated that susceptibility data on the pure material would show a large drop at 63K. However, as the data shown in Fig. 6.4 indicate, no such drop is observed. In fact the data are very similar to those for pure $AgFAsF_6$, i.e., a small temperature independent paramagnetism from 280 to 50K with an increase in susceptibility below 50K. The identity of the impurity phase which is producing this ubiquitous drop in susceptibility at 63K is unclear, however, the absence of any effect of the fluorometallate anion on the temperature of this transition in the different samples, suggest that the impurity may simply be a binary silver fluoride. It is possible that pure Ag_2F_5, in the absence of any paramagnetic Ag_3F_8 impurity would exhibit a more substantial drop in suceptibility at 63K, such that a small amount of it interposed on the already weakly paramagnetic AgF^+ salts would produce the observed impurity behavior.

Nevertheless, the low, temperature - independent susceptibilities observed to be general for the AgF^+ salts are intriguing, as they are indicative of a partially filled band, obeying Fermi - Dirac, rather than Boltzmann statistics.[19] Apparently there is a high degree of electron mobility in the $(Ag - F)_n^{n+}$ chains. The Ag - F interatomic distances in these chains appear to be nearly 2.00Å in all cases and compared to the nearest Ag anionic F contacts which are closer to 2.35Å, indicate considerable covalent bonding and overlap of the Ag(II) valence $4d_z2$ orbitals and F $2p_z$ orbitals in the chains. The chemistry of the cationic Ag(II) systems (Chapter 7) indicates that these materials are powerful electrophilic oxidizers comparable with F atoms. This suggests that the Ag(II) $4d_z2$ and the F $2p_z$ orbitals must be very close in energy. This would provide the basis for the metallic magnetic properties observed here, since the conduction band would be half filled. Direct conductivity measurements on the AgF^+ salts are extremely difficult owing to oxidation of electrode materials by these compounds. It remains to be proved that crystals of these salts do indeed carry electricity.

Conclusions

A number of fluorometallate anions, of varying acidity are capable of stabilizing cationic Ag(II) either as Ag^{+2}, or as AgF^{+}. The available structure data suggest that all AgF^{+} salts contain the Ag(II) in chains, $(Ag - F)_n^{n+}$, which may be linear as in $AgFBF_4$ and possibly $AgFMF_4$ (M = Ag, Au), or bent as in $AgFMF_6$ (M = As, Au). All AgF^{+} salts exhibit very low, temperature independent paramagnetism to low temperatures. This contrasts the behavior of the $Ag^{+2}(MF_x^{-})_2$ (MF_x^{-} = AgF_4^{-}, AuF_4^{-}, and SbF_6^{-}) which obey the Curie law as simple one electron paramagnets.

References

1. Sorbe, P.; Grannec, J.; Portier, J.; Hagenmuller, P. *J. Fluor. Chem.* **1978**,*11*, 243.
2. Yvon, K.; Betzinge, A.; Tissot, P.; Fischer, J. *J. Solid State Chem*, **1986**, *60*, 225.
3. Jesih, A.; Lutar, K.; Žemva, B.; Bachmann, B.; Becher, St.; Müller, B.G.; Hoppe, R. *Z. Anorg. allg. Chem.* **1990**, *588*, 77.
4. Gantar, D.; Leban, I.; Frlec, B.; Holloway, J.H. *J.Chem. Soc. Dalton Trans.* **1989**, 2379.
5. Müller, B. G. *Angew. Chem., Int. Ed. Eng.* **1987**, *26*, 689.
6. Gantar, D; Frlec, B.; Russell, D.R.; Holloway, J. *Acta Crystallogr. Sect. C Cryst. Struct. Commun.* **1987**, *43*, 618.
7. Kemmitt, R.D.W.; Russell, D.R.; Sharp, D.W.A. *J. Chem. Soc.* **1963**, 4408.
8. Sharpe, A.G. *J.Chem. Soc.* **1949**, *613*, 2901.
9. Bartlett, N.; Leary, K. *Rev, Chim. Minér.* **1976**, *13*, 82.
10. Gruner, E.; Klemm, W. *Naturwissenschaften* **1937**, *25*, 59.
11. Müller, B.G. *Angew. Chem. Int. Ed. Eng.* **1987**, *26*, 688.

12. Yvon, K.; Jeitschko, W.; Parthe, E. "LAZY PULVERIX, A Program to Calculate Theoretical X - ray and Neutron Diffraction Powder Patterns," **1977**.

13. B. Žemva, unpublished results.

14. Žemva, B.; Hagiwara, R.; Casteel, Jr., W.J.; Lutar, K.; Jesih, A.; Bartlett, N. *J. Am. Chem. Soc.* **1990**, *112*, 4846.

15. Casteel, Jr., W.J.; Lucier, G.; Hagiwara, R.; Bormann, H.; Bartlett, N. *J. Solid State Chem.* **1992**, *96*, 84.

16. R. Hagiwara, unpublished result.

17. S. Mayorga, Ph.D. Thesis, U.C. Berkeley **1988**.

18. Chapin, P.; Dianoux, A.J.; Marquet - Ellis, H.; Nguyen - Nghi *C.R. Acad. Sci. Paris* **1967**, *264*, 1108.

19. Kittel, C. "Introduction to Solid State Physics," p.413, Wiley, New York, **1986**.

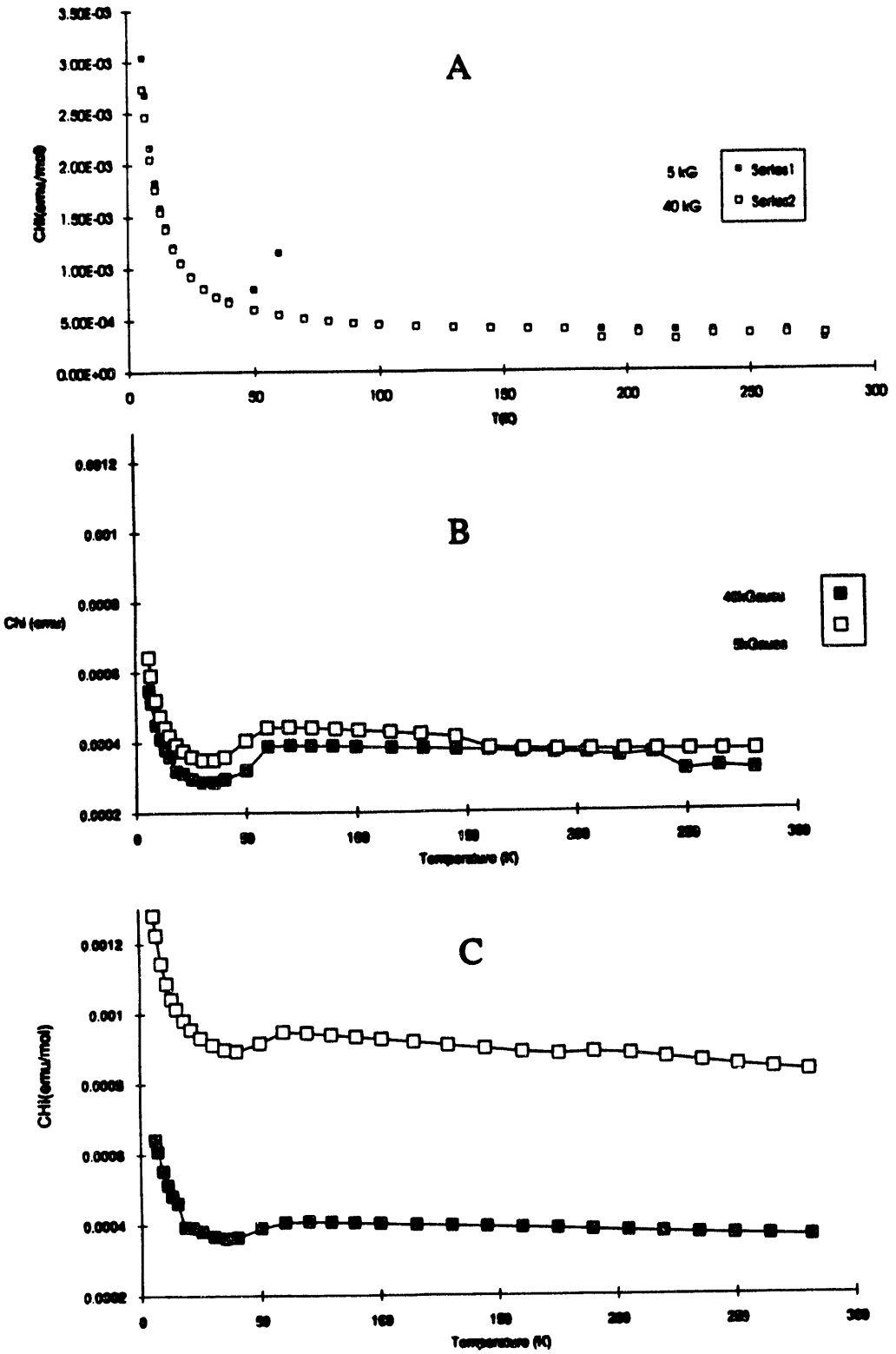

Figure 6.1. Magnetic susceptibility data for $AgFAsF_6$ (A,B) and $AgFAuF_6$ (C). 5kG(□), 40kG (■).

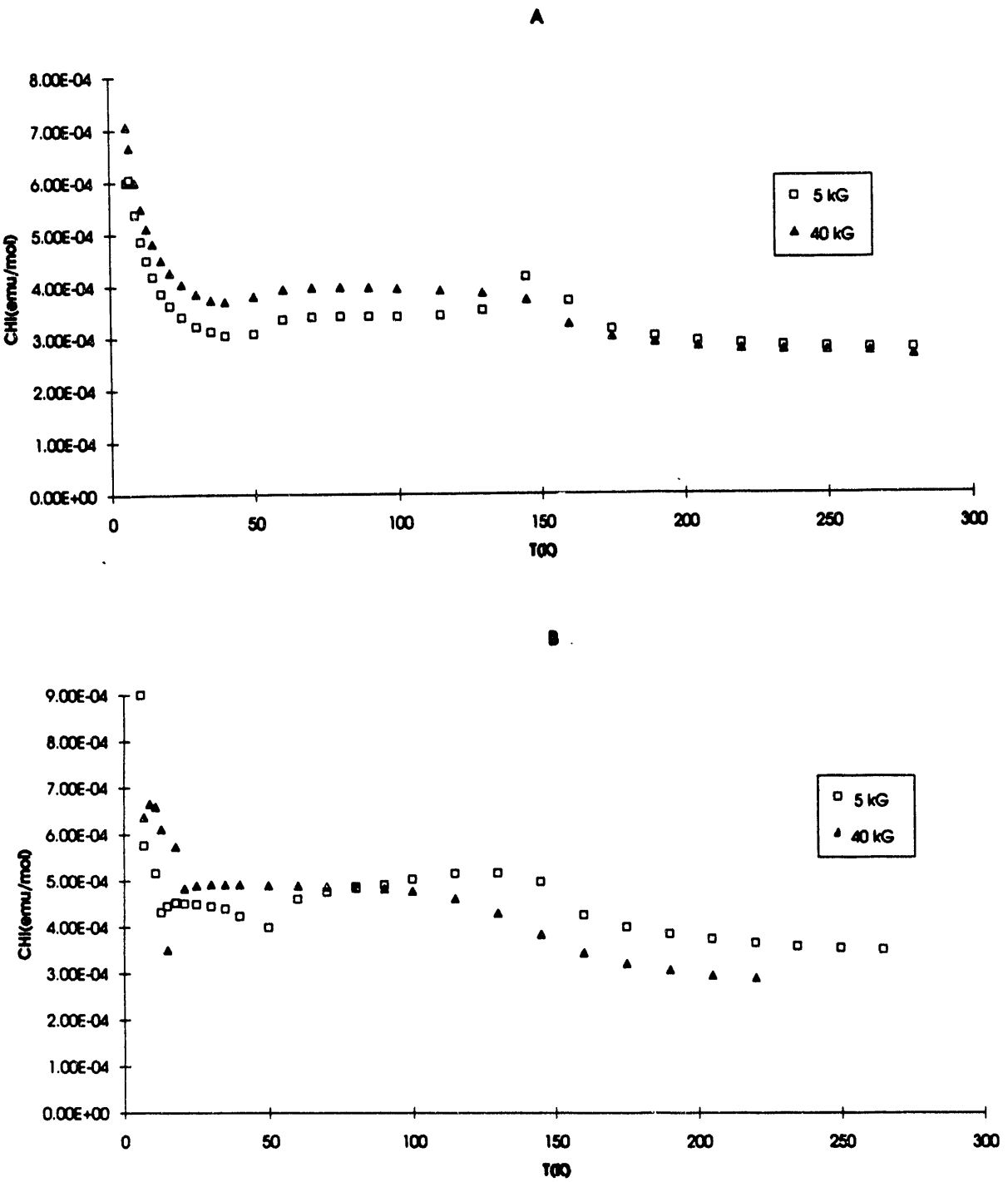

Figure 6.2. Magnetic susceptibility data for Ag_2F_5 (A) and $AgFAuF_4$ (B). 5kG(□) 40kG (▲).

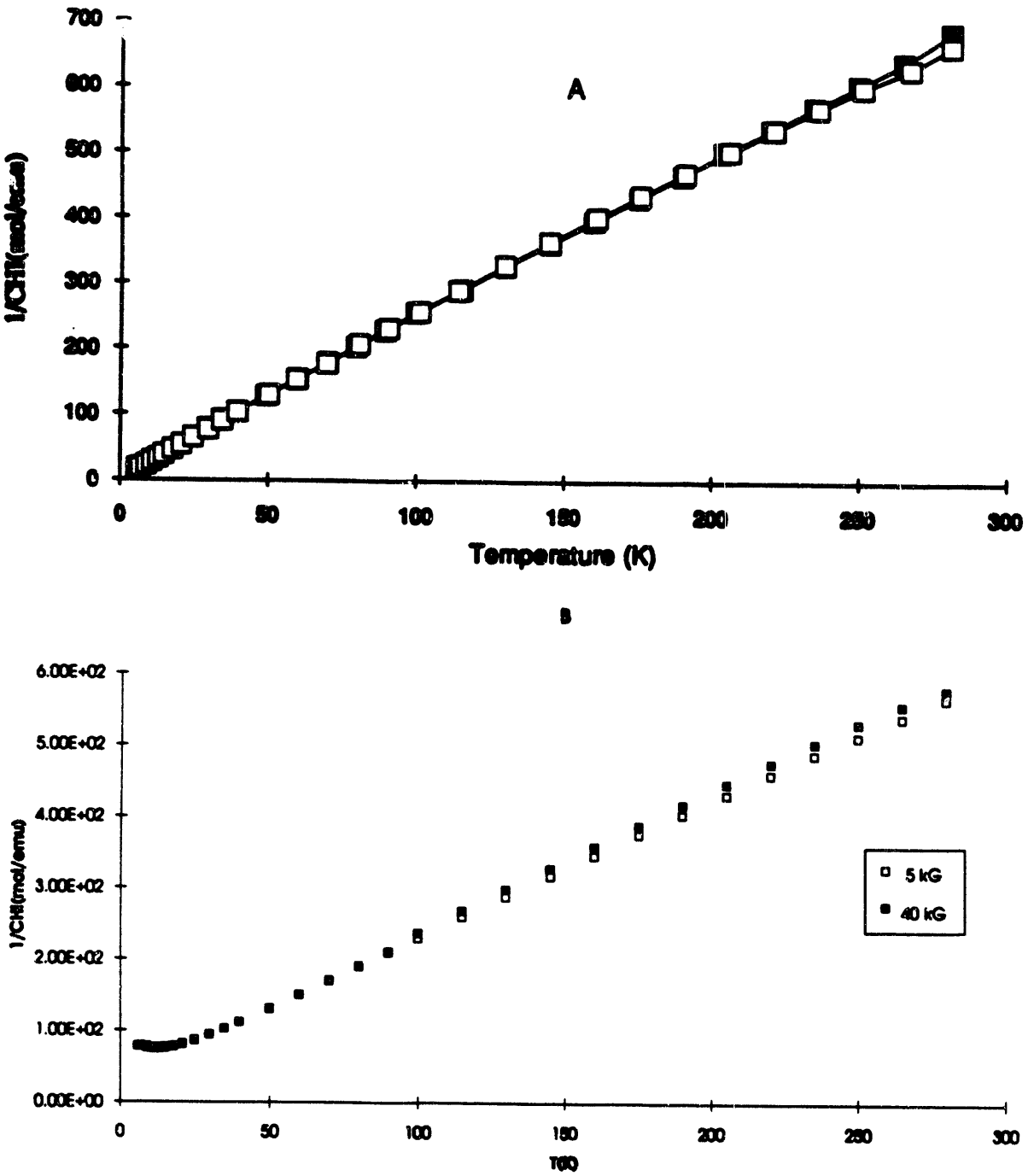

Figure 6.3. Curie - Weiss Plots for $AgAu_2F_8$ (A) and $Ag(SbF_6)_2$ (B). 5kG(□) 40kG (■).

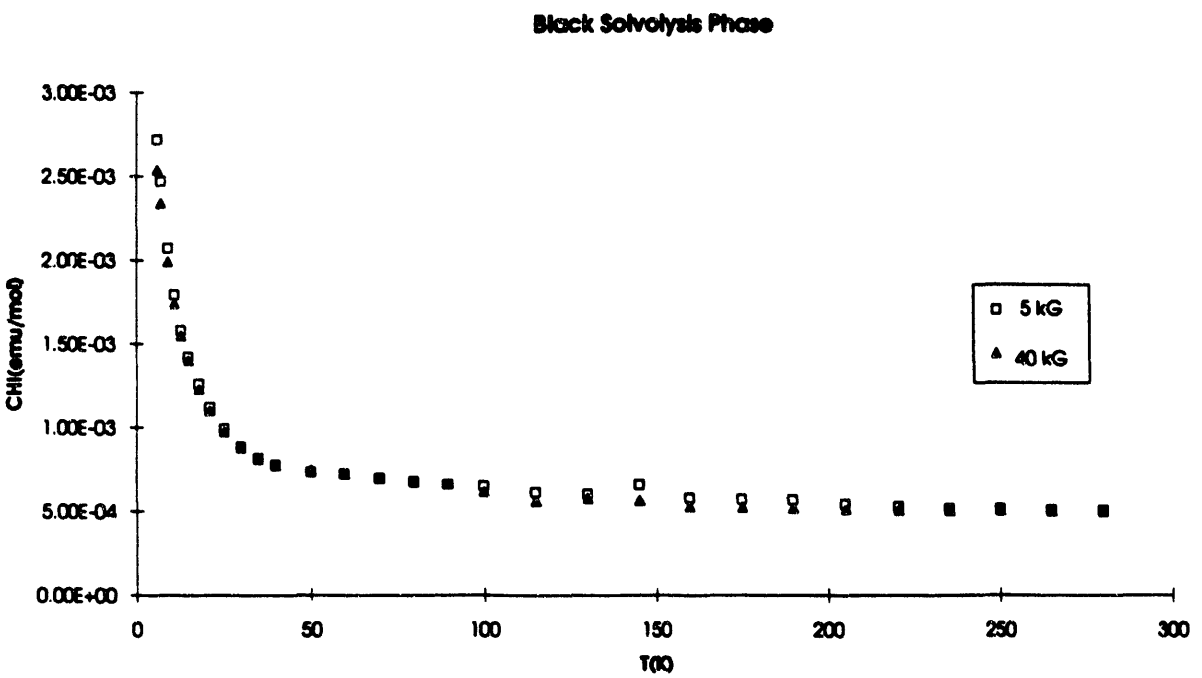

Figure 6.4. Magnetic susceptibility data for the black solvolysis product of $AgFAsF_6$. 5kG(□) 40kG (▲).

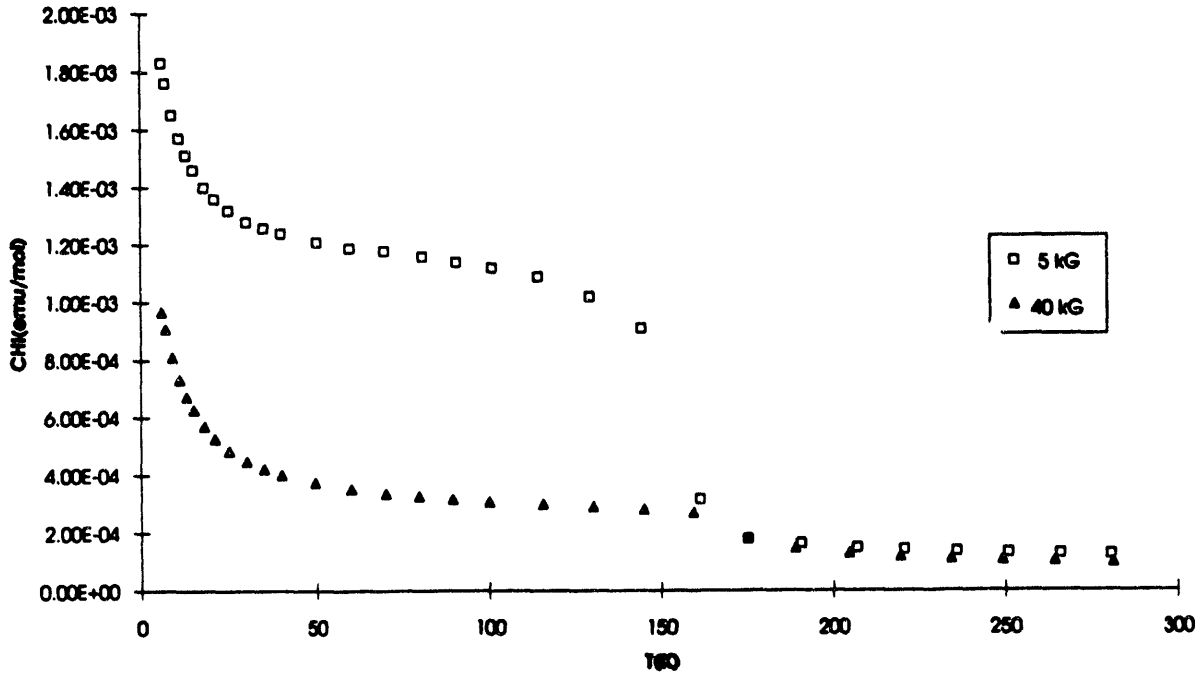

Figure 6.5. Magnetic susceptibility data for dilute AgF_2 (15% AgF_2, 85% CaF_2). 5kG(□) 40kG (▲).

Chapter 7

The Oxidizing Properties of Cationic Ag(II) and a Comparison with Ag(III)

Introduction

Subsequent to its discovery,[1] AgF_3 was observed to be, as anticipated, an extremely powerful oxidizer. Indeed Žemva and his coworkers have demonstrated that it is capable of oxidizing Xe to XeF_6 at room temperature.[2] It was conjectured that the loss of F_2 from the thermally unstable trifluoride was under strongly acidic conditions:

$$AgF_3 + AsF_5 \xrightarrow{AHF} AgF^+AsF_6^- + 1/2\,F_2 \qquad (1)$$

occuring through a cationic Ag(III) species, AgF_2^+. If this were so, it was believed that such a cation, would be more powerfully oxidizing than neutral AgF_3 alone. In fact dissolution of AgF_3 in acidified HF was observed to oxidize Xe at ordinary temperatures and pressures but, remarkably, Ag(I) in the form of $AgAsF_6$ was observed in the products[3]

$$2AgF_3 + 3AsF_5 + 2Xe \xrightarrow{AHF} Xe_2F_3^+AsF_6^- + 2AgAsF_6 \qquad (2)$$

This indicated that even Ag(II), in cationic form, was capable of oxidizing xenon.

The remarkable oxidizing power of cationic Ag(II) has been further exemplified in these studies, by employing as reducing agents C_6F_6 and C_3F_6. The products of these reactions indicate that the first step is transfer of an electron from the substrate to cationic Ag(II). An attempt has been made to evaluate the upper limits of the oxidizing power of cationic Ag(II). In addition, reaction (1) as a potential source of AgF_2^+ has been

investigated to assess the upper limits of its oxidizing power.

Experimental

Materials. AgF_3 was prepared as described in Chapter 5. $AgFAsF_6$ and $AgFBF_4$ were prepared as described in Chapter 6. NF_3 was prepared by the room temperature direct fluorination of N_2F_4(Airco, Riverton, NJ), and checked for impurities by infrared spectroscopy before use.[4] House O_2 was dried by passing through a coil cooled to -196 °C before use. The purity of C_3F_6, and C_6F_6 (PCR,inc., Gainesville, FL) was checked by I.R. spectroscopy[5], C_3F_6 being used without further purification while C_6F_6 was kept dry by storing it over P_2O_5. Xenon and krypton (Airco, Riverton, NJ) were used as received.

Cationic Ag(II) from $AgFBF_4$ and BF_3 with Xe in AHF. In the DRILAB 0.179 g, (0.839mmol) $AgFBF_4$ was loaded into a one armed Teflon/FEP reactor. On the vacuum line 5ml AHF was condensed into the reaction vessel by cooling it to -196 °C. Warming to room temperature resulted in no visible dissolution of $AgFBF_4$, the blue solid remaining in colorless AHF. The reactor was pressurized to 2 atm with Xe and agitated for 2 hrs. No Xe uptake and no change in appearence of the reactants was observed. The Xe pressure was reduced 200 torr by opening to a ballast volume on the line and BF_3 was now admitted to the reactor until a pressure of 1500 Torr had been restored. Still, no change in the reactants was observed. In order to saturate the AHF with BF_3 and Xe the solution was frozen and warmed slowly back to room temperature. At lower temperatures ($\leq$ -30 °C) a blue solution was observed. The solution became paler and vigorous gas evolution was observed on warming to room temperature, the final pressure, however being lower than 1500 Torr. The pressure was restored to 1500 Torr with Xe and the cooling - warming cycle was repeated. After 5 thermal cycles between the freezing point

of AHF and room temperature, a colorless solid remained in a colorless solution. Volatile materials were removed at -45 °C in a dynamic vacuum for 5 hr. XeF_2 was evacuated for 15 min at 40 °C into a FEP U - trap cooled to -78 °C. and was shown to be XeF_2 by X - ray powder photography and its intense Raman band[6] at 498cm^{-1}. The combined yield of XeF_2 and $AgBF_4$, characterized by X - Ray powder photography,[7] was 235.3mg (theoretical 234.3 mg): yield of recovered XeF_2, 46.8 mg, 66.0%.

Interaction of Cationic Ag(II) with C_3F_6 in AsF_5 rich AHF. In a one - armed Teflon tube reactor $AgFAsF_6$ was synthesized in situ from 0.238 g $AgAsF_6$ (0.795 mmol) and in a greater than two fold molar excess of AsF_5. The procedure (A) in Chapter 6 was followed. An overpressure of 2 atm of fluorine was maintained until a royal blue solution with no colorless precipitate was obtained. The solution was frozen at -196 °C and opened to a dynamic vacuum through the soda - lime scrubber to remove residual fluorine. With the reactor still at - 196 °C, C_3F_6 (0.36 mmol; 220 Torr x 30 ml) was added to the frozen mixture in 3 separate aliquots of 0.2, 0.1, and 0.06 mmol. The reaction mixture was allowed to warm to - 70 °C after the addition of each aliquot. A colorless precipitate was observed to form at the first signs of melting of the AHF. Each successive aliquot resulted in a paler blue supernatent solution over larger quantities of colorless solid. In the end (the entire reaction took ≈ 5min) a pale blue supernatent solution and a copious colorless solid remained. Volatile materials were condensed, under static vacuum, into a tube filled with NaF, which had been cooled to -196 °C. The volatile materials were allowed to remain in this tube for 15 min at room temperature in order trap AHF and AsF_5 and then were condensed, at -196 °C, into a 5ml stainless steel tube reactor which was sealed at one end and equipped with a SS-KS4 Whitey valve at the other. The weight of collected volatile compound was 70 mg which corresponds to 0.35 mmol of C_3F_8, this being the only material observed in the I.R.[8] of the collected volatiles. No traces of CF_4, C_2F_6, or residual C_3F_6 were observed.

Interaction of Cationic Ag(II) with C_6F_6 in AsF_5 rich AHF. A solution of cationic Ag(II) was made up in the same way as above from 0.190 g (1.31 mmol) AgF_2. After freezing the solution at -196 °C to remove residual fluorine under vacuum, 1 ml (8.6 mmol) C_6F_6 was condensed on to the frozen solution. As soon as the AHF began to melt a bright yellow solid began to form, the reaction being completed in less than one minute, as judged by the disappearance of blue color characteristic of cationic Ag(II), at temperatures below -50 °C. Even at -60 °C the yellow solid appeared to have significant solubility in AHF and was washed by several decantations into the free arm of the reactor. In the end a colorless solid in colorless AHF was left in the original reaction arm, bright yellow solid remaining in the second. AHF and excess C_6F_6 were removed under vacuum through a soda - lime scrubber, while holding the arm containing the yellow solid at 0 °C. The total weight of products in both arms of the reactor was 0.4311 g. Assuming product formation follows reaction (5), the anticipated yield of $AgAsF_6$ is 0.387 g and of $C_6F_6AsF_6$ is 0.491 g. It is likely that much of the $C_6F_6AsF_6$ formed was evacuated as the thermal decomposition products[9] C_6F_6 and 1, 4 C_6F_8 (see reaction 6). The yield of $C_6F_6AsF_6$, assuming 0.387 g of the product is $AgAsF_6$, is 44 mg (0.09 mmol), 7%. X - Ray powder photographs revealed that the yellow product contained $C_6F_6^+AsF_6^-$ and $AgAsF_6$.[10] The colorless solid in the other arm was $AgAsF_6$.

Interaction of Cationic Ag(II) and O_2 in AsF_5 rich AHF. In the DRILAB 0.68g (2.2 mmol) $AgFAsF_6$ was loaded into one arm of a two armed Teflon/FEP reactor. On the vacuum line 5ml AHF and 2.0 g (12 mmol) AsF_5 were condensed on to the solid at -196 °C. Warming to room temperature resulted in a royal blue solution free of solids. The reactor was cooled again to -196 °C and evacuated under dynamic vacuum to ensure the absence of molecular F_2. The royal blue solution was allowed to equilibrate at -70 °C for 15 min. No sediment appeared during this time. Opening the reactor to the vacuum

line, which had been pressurized with 1600 Torr of dry O_2, produced an immediate drop due to expansion into the reactor volume. This was followed by a further steady, slow decrease in pressure accompanied by the formation of a colorless solid and a near disappearance of the blue solution color. Within 15 min O_2 uptake had ceased and the colorless precipitate was copious. Warming the reaction mixture slightly to -60 °C resulted in an increase in line pressure, an increase in intensity of the blue color in the solution, and a decrease in the quantity of colorless solid. At -40 °C, no solid remained in the royal blue solution and the line pressure had returned to the level observed immediately after opening the line to the reactor. Warming to room temperature and removing the AsF_5/AHF solution under vacuum left only $AgFAsF_6$ which was identified by X - ray powder photography. Restoring the AsF_5/AHF solution and cooling to -70°C again, resulted in O_2 uptake and again produced the colorless solid. To facilitate removal of the AsF_5/AHF solution under vacuum the mixture was warmed to -60 °C and in consequence of this, the colorless solid diminished in quantity. On drying under dynamic vacuum 0.80 g of light blue solid product remained for a yield of ≈ 0.16 g (0.79 mmol; 37%) O_2AsF_6 based on the anticipated formation of 0.64 g of $AgAsF_6$. X - Ray powder photographs of the solid indicated that it contained $O_2^+AsF_6^-$ and $AgAsF_6$.[11] The blue tint indicates that some $AgFAsF_6$ was also present, but this was not revealed by the X - Ray powder photographs.

Interaction of AgF_3 with O_2 in AsF_5 rich AHF. In the DRILAB 0.147 g (0.893 mmol) AgF_3 was loaded into one arm of a two armed Teflon/FEP reactor which had been passivated for several hours with 2 atm F_2. The reactor was evacuated and charged with 3ml AHF and 1.5 g (8.8 mmol) AsF_5 by cooling the tube containing the AgF_3 to -196 °C. While warming this tube to -70°C, the entire vacuum system and reactor (125ml) was pressurized to 1500 Torr (10 mmol) with dry O_2. The pressure of the system

increased slightly until the AsF_5/AHF mixture began to melt. Then the pressure in the line immediately began to drop, and a coloress solid and pale blue solution began to form. The reaction arm was allowed to warm to -60 °C and held at that temperature for 20 min with intermittent agitation until all traces of the red solid, AgF_3, had disappeared. A voluminous colorless solid and a blue solution remained and the latter appeared to become more intensely colored as the solution was warmed. The pressure fell approximately 200 Torr during the reaction for an O_2 uptake of ≈ 1.0 mmol. The pressure varied considerably, however, with fluctuations in temperature.With the colorless solid held at - 60 °C, the blue solution was decanted into the free arm of the reactor. Volatile materials were removed from the reaction vessel as it was allowed to warm to room temperature. The colorless solid was identified as $O_2^+AsF_6^-$ based on its X - Ray powder pattern and its characteristic O_2^+ Raman stretch[11] at 1857 cm^{-1}. The weight of 0.13 g corresponds to (0.64 mmol); 72 % yield based on AgF_3.

AgF_3 with NF_3 in AsF_5 rich AsF_5. In the DRILAB 0.14 g (0.84 mmol) AgF_3 was loaded into one arm of a two armed teflon/FEP reactor. The reaction was set up identically to that for the interaction of AgF_3 with O_2 in acidified AHF. Following the transfer of the AHF/AsF_5 mixture on to the AgF_3 by cooling this arm of the reactor to -196 °C the reactor was pressurizerd to 1100 Torr with NF_3 as it was allowed to warm to -60 °C. The reactor was left open to the Helicoid gauge to monitor the pressure.The solution was cycled between -90 °C and -60 °C several times in an effort to saturate it with NF_3. No significant pressure change was observed as the AgF_3 began to dissolve in the AsF_5/AHF solution. Within 15 min all AgF_3 had dissolved (the dissolution of AgF_3 in acidified AHF being much more rapid at -60 °C than at temperatures only slightly cooler). The mixture was allowed to stand at -60 °C with occasional agitation for another hour. NF_3 and the AsF_5/AHF solution were removed under dynamic vacuum through a soda -

lime scrubber as the reaction tube was warmed to room temperature. The solid blue products were dried under vacuum for 1 hr at room temperature. X -Ray powder photographs revealed $AgFAsF_6$ and an additional uncharacterized phase. Raman spectroscopy revealed a weak band at 1125 cm^{-1}, which is in a region where N - F stretches are known to occur, however, it does not correspond to that of any NF_4^+ species.[12]

AgF_3 with Kr in AsF_5 rich AHF. In a similar reaction 0.15 g (0.91 mmol) AgF_3 was allowed to interact with 1500 Torr (10 mmol) Kr at -70 °C as it was dissolved in AsF_5 (5:1 molar excess of AgF_3)/AHF solution. Thermal cycling between -90 and -70 °C resulted in Kr uptake. At -70 °C, the AgF_3 took several hours to dissolve (in contrast to the relatively rapid dissolution at -60 °C), eventually leaving a deep blue solution and a small amount (≈ 5mg) of white precipitate which readily dissolved at higher temperatures. Because of the thermal instability of $KrF^+AsF_6^-$ and the volatility of KrF_2, at temperatures which would permit the removal of the AsF_5/AHF solution under vacuum, efforts were made to obtain Raman spectra on the colorless solid and the frozen solution at -196 °C, still in the FEP tube reactor. No frequencies characteristic[13] of KrF^+, KrF_2, or $Kr_2F_3^+$ were observed either from the colorless solid, or the frozen blue solution. However, bands attributable to AsF_6^- as well as FEP were observed.

Results and Discussion

AgF_2 has long been an important oxidative fluorinator in organo - fluorine chemistry and has been desribed as the most oxidizing of the divalent metal fluorides.[14] The Ag(II) in the positively charged $(Ag - F)_n^{n+}$ cation is expected to be more electronegative, and hence more oxidizing than in the neutral species and Ag^{+2} solvated with neutral HF molecules might be expected to be an even more potent oxidizer than $(Ag - F)_n^{n+}$.

The oxidation of Xe by $AgF^+AsF_6^-$ as described by Žemva et al.[3] proceeds very slowly in neutral AHF solution, the reactivity being greatly enhanced by the addition of AsF_5 to the solution

$$4AgFAsF_6 + 2Xe + AsF_5 \xrightarrow{AHF} Xe_2F_3^+AsF_6^- + 4AgAsF_6 \quad (3)$$

The presence of additional AsF_5 certainly facilitates oxidation of Xe and its presence may be necessary for any oxidation of Xe to occur at all. In Chapter 6, it was pointed out that dissolution of $AgFAsF_6$ in AHF was always accompanied by a solvolysis reaction releasing AsF_5 into the solution. Recently in these laboratories[15] it has been established that a large molar excess of AHF leads to precipitation of AgF_2.

That additional acid is a necessary component of Xe oxidation by Ag(II) is more clearly demonstrated in the oxidation of Xe by $AgFBF_4$. The poorly soluble $AgFBF_4$ exhibited no signs of interaction with Xe in AHF over several hours. Even in the presence of an overpressure of BF_3, at room temperature, no signs of reaction were observed. However, under these conditions there was no hint of blue color in the solution, either, probably indicating the absence of Ag(II) in solution. Cooling solutions of AHF had been observed to greatly enhance the solubility of BF_3 in them, this being utilized in the synthesis of $AgFBF_4$ from AgF_2 and BF_3 (Chapter 6). Indeed, cooling AHF containing $AgFBF_4$ resulted in considerable uptake of BF_3 as judged by tensimetry and the production of a royal blue supernatent solution over the dark blue solid. When Xe was added to this blue solution at -40 °C a slow reaction did proceed as judged by the gradual lightening of the solid materal in equilibrium with the solution. The speed of the reaction was significantly increased by thermal cycling of the solution between the freezing point of AHF and 0 °C. It is probable that at lower temperatures the solution becomes more saturated with Xe and BF_3 the latter facilitating the dissolution of $AgFBF_4$. Warming the

solution must provide greater activation energy for the oxidation and coupled with the short lived supersaturation of the AHF solution with BF_3 and Xe, makes for more favorable reaction kinetics.

Because BF_3 is a weaker acid than AsF_5,[16] and unlike the latter is incapable of stabilizing Xe(II) fluorocations out of solution, the isolated Xe product from its oxidation by $AgFBF_4$ is XeF_2

$$2AgFBF_4 + Xe + BF_3 \xrightarrow{AHF} 2AgBF_4 + XeF_2 + BF_3 \quad (4)$$

The effect of additional fluoroacid in facilitating the reaction of cationic Ag(II) species is not established, but it probably involves the formation of an $Ag^{+2}(AF^-)_2$ species (where A = BF_3 or AsF_5), the cation and anion being solvated with neutral HF molecules. Such salts are known (Chapter 6), and although, in the case of the BF_4^- and AsF_6^- salts, are not derivable from AHF solution, they are suggested by the greatly increased solubilities of $AgFBF_4$ and $AgFAsF_6$ when additional acid is provided. The formation of a more charged Ag(II) cation by effectively removing the covalently bound bridging F ligands of the $(Ag - F)_n^{n+}$ chain, is expected to increase the electron affinity (EA) of the cationic Ag(II) making it a more powerful oxidizer than $(Ag - F)_n^{n+}$.

The remarkable oxidizing power of Ag(II) correlates with the high second ionization potential of silver. That is compared with those of other coinage metals and that of xenon in Table 7.1

Table 7.1. The 2nd Ionization Potentials of the Coinage Metals and Xenon[17]

M	2nd I.P (eV)
Cu	20.29
Ag	21.49
Au	20.5
Xe	21.21

The 2nd I.P. of Ag is higher than those of Cu or Au, and, in fact is higher than that of any non - alkali metal. Because the d^9 configuration is strongly antibonding (both sigma and pi), the binding of the solvent molecules (such as HF) must be weak. The electron affinity of $Ag(HF)_x^{+2}$ must therefore be high. It is therefore plausible to postulate that the first step in the oxidation by cationic Ag(II) is the transfer of an electron from the species to be oxidized to that cation.

The behavior of the reducing agents C_6F_6 and C_3F_6 in the presence of $AgFAsF_6/AsF_5$ in AHF strongly suggest that such electron transfer is, in fact, occuring. In reactions with additional AsF_5, C_6F_6 in combination with $AgFAsF_6$ gave the radical cation salt $C_6F_6^+AsF_6^-$, the acid reaction proceeding via

$$Ag^{2+}_{(solv)} + C_6F_6 \xrightarrow{AHF/AsF_5} C_6F_6^+{}_{(solv)} + Ag^+_{(solv)} \quad (5)$$

This salt is unstable[9] at room temperature and decomposes to C_6F_6 and the fluorinated product, which is the specific diene, 1,4 C_6F_8

$$2\ C_6F_6^+AsF_6^- \longrightarrow C_6F_6 + 1,4\ C_6F_8 \quad (6)$$

The initial formation of the radical cation salt rather than the fluorinated cyclic olefin demonstrates the electron transfer. The relative ease of this reaction, which proceeds rapidly near the melting point of AHF (≈ - 80 °C) is in accord with the relatively low 1st I.P. of C_6F_6 (9.97 eV).[18]

That $AgFAsF_6/AsF_5$ solutions are not behaving simply as F atom sources, is further borne out in their reaction with the fluorinated olefin, C_3F_6. Again the reduction of Ag(II) is observed to proceed rapidly at low temperatures , C_3F_6 (1st I.P. = 10.62 eV),[19] C_3F_8 being the only observed fluorinated organic product. By analogy with reaction 5, a radical cation, $C_3F_6^+$, is probable, but in this case not isolable as a salt.

$$Ag^{+2}_{(solv)} + C_3F_6 \xrightarrow{AHF/AsF_5} [C_3F_6^+]_{(solv)} + Ag^+_{(solv)} \quad (7)$$

This may be attacked by F^- to yield the C_3F_7 radical, which in turn is oxidized by a second equivalent of $Ag^{+2}_{(solv)}$ to the cation $C_3F_7^+$, this then yielding C_3F_8. If the Ag(II) cation in AHF were simply acting as a F atom sources, fluorination with C - C bond cleavage to create CF_4 and C_2F_6 would have been expected.[20] No such fragmentation was detected in these cationic Ag(II) oxidations.

Fig 7.1. Electron Oxidation by Cationic Ag(II)

1. $Ag^{+2}(AF^-)_2 + Xe \longrightarrow Xe^+AF^- + Ag^+AF^-$

2. $Xe^+ A - F^- \longrightarrow \cdot Xe\text{-}F + A$

3. $Ag^{+2}(AF^-)_2 + \cdot Xe\text{-}F \longrightarrow XeF^+AF^- + Ag^+AF^-$

4.(opt) $XeF^+A - F^- \longrightarrow XeF_2 + A$

net reaction: $2Ag^{+2}(AF^-)_2 + Xe \longrightarrow XeF_2 + 2Ag^+AF^-$

where A = BF_3 and AsF_5

As indicated in Fig 7.1, the oxidation of Xe probably begins with the removal of an electron from Xe. The Xe^+ cation is a strong acid since the XeF radical is bound (ΔH° $Xe_{(g)} + F_{(g)} \rightarrow XeF_{(g)}$ = 3.5 kcal mol^{-1})[21]. As Bartlett and Sladky[22] point out in their outline of the thermochemical series for the formation of XeF_2 and XeF^+ from Xe and F atoms, the I.P. of XeF radical is equal to the I.P of Xe less the difference in bond energies of XeF and XeF^+. A number of independent studies place the bond dissociation energy of XeF^+ at 2.0 eV,[23] while Tellinghuisen[21] finds that a reasonable estimate for XeF is ≈ 0.15 eV. This means that the I.P of the XeF radical is nearly 2 eV lower than that of Xe atoms. Hence, oxidation by a second Ag(II) species readily occurs to form XeF^+ in step 3. This cation is also an extremely strong acid. This is indicated by the crystal structure of $FXe - F - AsF_5$, where the bridging F ligand is making a strong interaction with the cationic XeF species.[24] The XeF^+ cation readily abstracts a F^- to form XeF_2

from BF_4^- since BF_3 is a weaker fluoroacid (step 4). The situation with AsF_5 is more complex. $XeF^+AsF_6^-$ is stable, but in AHF[25], partial solvolysis occurs to yield $Xe_2F_3^+AsF_6^-$. Formation of the last product results from a combination of steps 3 and 4.

This reaction scheme is helpful for understanding the ineffectiveness of AgF^+ salts alone in oxidizing Xe. The F^- ligand donates electrons more effectively than the HF molecule. The electron affinity of any monocation $AgF(HF)_y^+$ is therefore likely to be lower than that of the dication $Ag(HF)_x^{+2}$.

Attempts to oxidize O_2 with $AgFAsF_6/AsF_5$ initially failed at room temperature even though the 1st I.P. of O_2 is measured to be the same as that of Xe.[26] While step 1 in the electron oxidation scheme is expected to be energetically similar for both Xe and O_2, fluorine ligation to generate XeF^+, significantly differentiates the two cases. The observed O - O stretching frequencies for O_2, O_2^+, and O_2F shown in Table 7.2 indicate that F ligation weakens the O - O bond of O_2. This is expected since the electron density from the F atom must flow into an O - O antibonding π orbital on O - F bond formation.[27] Thus formation of an $O_2\cdots F$ bond simultaneously with electron removal does not significantly lower the ionization energy.

Table 7.2. Observed O - O Stretching Frequencies

	υ O - O (cm^{-1})
O_2F	1490[28]
O_2F_2	1210[29]
O_2	1555[30]
(O_2^+)	1857[11]

If Xe, which is readily oxidized, is reacting via a first step which is energetically similar to that expected for O_2, then Ag(II) under acidic conditions must be very close to oxidizing O_2. Indeed, in subsequent experiments it was found that lowering the temperature of $AgFAsF_6/AsF_5$ solutions in the presence of O_2 below -50 °C, induced O_2 uptake with the formation of $O_2^+AsF_6^-$. Nearly complete conversion to O_2AsF_6 and $AgAsF_6$ was observed at -78 °C as evidenced by the formation of large quantities of colorless O_2AsF_6 and $AgAsF_6$ in a nearly colorless solution. By itself, $AgFAsF_6$ is extremely soluble in AsF_5 rich AHF even at these low temperatures, giving an intensely blue solution.

The reaction

$$O_2 + Ag^{+2}_{(solv)} \xleftrightarrow{AHF/AsF_5} O_2^+AsF_6^- + Ag^+_{(solv)} \qquad (8)$$

is certainly in equilibrium as warming above -50 °C brought about a complete reversal of reaction (8). Apparently the reaction is sufficiently close thermally that the negative entropy term encountered on going from gaseous O_2 to O_2^+ in a lattice ($\Delta S \approx -75$ cal deg^{-1} mol^{-1})[31] makes the forward reaction unfavorable at higher temperatures. The enthalpy change for the forward reaction must be exothermic and approximately independent of temperature.

Yields in reaction (8) were usually low, because the AsF_5/AHF solution could not be completely evacuated below -70 °C. The higher temperatures required for that favored the reverse reaction. As expected yields were greatly increased when AgF_3 was used as the starting material in AsF_5 rich AHF

$$AgF_3 + O_2 + AsF_{5(excess)} \xrightarrow{AHF} O_2AsF_6 + AgFAsF_6 \qquad (9)$$

for now the O_2AsF_6 is formed in the presence of a comparable oxidizer, cationic Ag(II).

If a cationic Ag(III) species, such as AgF_2^+, is formed it is perhaps not sufficiently long - lived to act as an oxidizer, for there is no conclusive evidence that the acidic AgF_3 system reacts with the more difficult to oxidize NF_3 (1^{st} I.P. = 13.20 eV)[32] and Kr(1^{st} I.P. = 13.99 eV)[33]. It is possible that solid AgF_3 in AHF is simply providing F atoms to refluorinate the Ag(I) as it is formed by Ag(II) oxidation of O_2. At -70 °C reaction (9) appears to go slightly faster than reaction (8), however O_2AsF_6 is being formed very rapidly in both. A rate increase for reaction (8) is to be expected, however, because a large concentration of cationic Ag(II) is always maintained in reaction (9), until the AgF_3 is depleted, while it is diminishing from the start of reaction (8).

A comparison of the chemistry of cationic Ag(II) with anionic Ag(III) highlights the remarkable nature of this oxidizer. In a reaction with Xe it was observed that a solution of $KAgF_4$ rapidly produced XeF_2 and AgF_2. A comparable oxidation of O_2, however, has not been demonstrated. In fact Mr. Byron Shen has shown[34] that O_2AsF_6 will actually oxidize a mixture of KF and AgF to Ag(III) as $KAgF_4$. At low temperatures, therefore cationic Ag(II) appears to be a stronger oxidizer than even certain Ag(III) systems.

References

1. Žemva, B.; Lutar, K.; Jesih, A.; Casteel, Jr., W.J.; Bartlett, N. *J. Chem. Soc., Chem. Commun.* **1989**, 346.
2. B. Žemva and coworkers, unpublished results.
3. Žemva, B.; Hagiwara, R.; Casteel, Jr., W.J.; Lutar, K.; Jesih, A.; Bartlett, N. *J. Am. Chem. Soc.* **1990**, *112*, 4846.
4. Nakamato, K. Infrared Spectra of Inorganic and Coordination Compounds, " p.86, Wiley, New York, **1963**.

5. Hall, K.R.; Wilholt, R.C.; Fergusson, A.M.; Boyd, B. "Thermodynamic Research Center Data Project," Ser. # 1010, Austin, TX, **1983**.

6. Agron, P.A.; Begun, G.M.; Levy, H.A.; Mason, A.A.; Jones, G.; Smith, D.F. *Science*, **1963**, *139*, 842.

7. Sharp, D.W.A.; Sharpe, A.G. *J. Chem. Soc.* **1956**,1855.

8. Hall, K.R., Ser. # 981

9. Richardson, T.J.; Tanzella, F.L.; Bartlett, N. *J. Am. Chem. Soc.* **1986**, *108*, 4937.

10. Cox, *J. Chem. Soc.* **1956**, 876.

11. Shamir, J.; Binenboym, J.; Stringham, R.S.; Hill, M.E. *Inorg. Chim. Acta.* **1968**, *2*, 37.

12. Christe, K.O.; Guertin, J.P.; Pavlath, A.E.; Sawodny, W. *Inorg. Chem.* **1967**, *6*, 533.

13. Gillespie, R.J.; Schrobilgen, G.J. *Inorg. Chem.* **1976**, *15*, 22.

14. Meshri, D.T. "The Modern, Inorganic Fluorochemical Industry," *J. Fluor. Chem.* **1986**, *33*, p.211.

15. B. Žemva, unpublished results.

16. For the evaluation of the fluoride ion affinities of BF_3, AsF_5, and other fluoroacids see Mallouk, T. E.; Rosenthal, G. L.; Muller,G; Brusasco, R; Bartlett, N. *Inorg. Chem.*, **1984**, *23*, 3167.

17. Ionization Potentials and Ionization Limits for Atomic Spectra. Moore, C.E. *Natl. Stand. Ref. Data Ser., Natl. Bur. Stand.* **1970**, 34.

18. Ionization Potentials, Appearance Potentials, and Heats of Formation of Positive Ions. Levin, R.D.; Lias, S.G *Natl. Stand. Ref. Data Ser., Natl. Bur. Stand.* **1982**, 273.

19. Ibid., 272

20. Banks, R.E.; Tatlow, J.C. "Synthesis of C - F Bonds: The Pioneering Years, 1835 - 1940," *J. Fluor. Chem.* **1986**, *33*, 81 - 89.

21. Tellinghuisen, P.C.; Tellinghuisen, J.; Coxon, J.A.; Velazco, J.E.; Setser, D.W.; *J. Chem. Phys.* **1978**, *68*, 5187.

22. Bartlett, N.; Sladky, F.O "The Chemistry of Krypton, Xenon, and Radon," *Comprehensive Inorganic Chemistry* p.250 - 254, Pergamon Press, Oxford, **1973**.

23. Berkowitz, J.; Chupka, W.A *Chemical Physics Letters* **1970**, *7*, 447.

24. Žemva, B.; Jesih, A.; Templeton, D.H.; Zalkin, A.; Cheetham, A.K.; Bartlett, N. *J. Am. Chem. Soc.* **1987**, *109*, 7420.

25. Morrison, J.D.; Nicholson, A.J.C.; O'Donnell, T.A. *J. Chem. Phys.* **1968**, *49*, 959.

26. Levin, R.D.; Lias, S.D, 170

27. Walsh, A.D. *J. Chem. Soc.* **1953**, *467*, 2266.

28. Kim, K.C.; Campbell, G.M *Chem. Phys. Letters* **1985**, *23*, 236.

29. Kim, K.C.; Campbell, G.M. *J. Molec. Struct.* **1985**, *129*, 263.

30. Nakamoto, K., p. 72.

31. T.E. Mallouk, Ph.D. Thesis, University of California, Berkeley, 1984.

32. Levin, R.D.; Lias, S.D., 279.

33. Ibid., 481.

34. C. Shen, Ph.D. Thesis, University of California, Berkeley, **1992**.

END

DATE FILMED

1/11/93